

Experiments on oblique transition in wall bounded shear flows

Per Elofsson

Doctoral Thesis Stockholm, 1998

Royal Institute of Technology Department of Mechanics

Experiments on oblique transition in wall bounded shear flows

by

Per Elofsson Department of Mechanics

April 1998 Technical Reports from Royal Institute of Technology Department of Mechanics S-100 44 Stockholm, Sweden

Typsatt i $\mathcal{A}_{\mathcal{M}}\mathcal{S}\text{-}\text{L}^{2}\text{T}_{\text{E}}\text{X}$ med KTHs thesis-stil.Akademisk avhandling som med tillstånd av Kungliga Tekniska Högskolan i Stockholm framlägges till offentlig granskning för avläggande av teknologie doktorsexamen torsdagen den 28 maj kl 10.15 i Kollegiesalen, Administrationsbyggnaden, Kungliga Tekniska Högskolan, Valhallavägen 79, Stockholm. ©Per Elofsson 1998 Högskoletryckeriet, Stockholm 1998

Elofsson, P. 1998 Experiments on oblique transition in wall bounded shear flows.

Department of Mechanics, KTH S-100 44 Stockholm, Sweden

Abstract

This thesis considers laminar-turbulent transition in wall bounded shear flows, with a focus on transition emanating from a pair of oblique disturbance waves. The oblique waves interact nonlinearly and transfers disturbance energy into streamwise vortices, which generate streamwise streaks through a linear mechanism that operates also at conditions where stability theory predicts decay of all eigenmodes. If the strength of this transient growth is sufficient to produce streaks with an amplitude exceeding a threshold value, the streaks break down through what is described as a secondary instability operating on the streaks, which is not to be confused with the traditional secondary instability operating on finite amplitude waves.

A survey of transition in plane Poiseuille and Blasius flows is presented together with a description of different methods for generating disturbances in a flow experiment. Details about the specific methods for disturbance generation used in the present investigations are also given.

Experimental investigations of oblique transition in plane Poiseuille and Blasius flow have been made using hot-wire measurements and flow visualisations. The main effort in the experimental work has been in describing the structure of the flows, but also to determine the amplitude of individual frequency-spanwise wavenumber modes and their development during the transition process. During an initial stage of each experiment, measurements on the stability characteristics of single waves were compared to results from linear stability calculations.

Spatial direct numerical simulations (DNS) together with numerical modelling of the vibrating ribbons used in the plane Poiseuille flow experiments helped to clarify the reason for symmetry properties observed in the measurements.

A model experiment is also reported which was designed to study the last stage in the oblique transition scenario. Stationary streamwise streaks of large amplitudes were generated and the breakdown of the streaks was investigated both at unforced conditions and by forcing with phase controlled time-dependent disturbances. Most of the experimental results were found to be in agreement with previous theoretical and numerical work.

Descriptors: laminar-turbulent transition, oblique wave, oblique transition, nonlinear interaction, transient growth, streak instability, Tollmien-Schlichting wave, hot-wire measurement, flow visualisation, linear stability, numerical simulation

Preface

This study considers laminar-turbulent transition initiated by a pair of oblique waves. The thesis is based on the following papers:

- **Paper 1:** ELOFSSON, P. A. & ALFREDSSON, P. H. 1998 An experimental study of oblique transition in plane Poiseuille flow. *J. Fluid Mech.* **358**, 177–202.
- **Paper 2:** ELOFSSON, P. A. 1998 An experimental study of oblique transition in a Blasius boundary layer flow. TRITA-MEK, Technical Report 1998:4, Dept. of Mechanics, KTH, Stockholm, Sweden
- Paper 3: ELOFSSON, P. A. & LUNDBLADH, A. 1994 Ribbon induced oblique transition in plane Poiseuille flow. In *Bypass Transition Proceedings from a Mini Workshop* (HENNINGSON, D. S., editor). TRITA-MEK, Technical Report 1994:14, 29–41, Dept. of Mechanics, KTH, Stockholm, Sweden
- **Paper 4:** ELOFSSON, P. A., KAWAKAMI, M. & ALFREDSSON, P. H. 1997 Experiments on the stability of streamwise streaks in plane Poiseuille flow. *Phys. Fluids* (submitted).

Contents

Preface Introduction Stability theory		iv
		1
		4
2.1	Stability theory for linear waves	5
2.2	Linear growth mechanisms	7
2.3	Secondary instability and nonlinear breakdown	9
Transition in plane Poiseuille and Blasius flows		13
3.1	Methods for generating disturbances	13
3.2	Transition studies in plane Poiseuille flow	17
3.3	Transition studies in Blasius flow	20
Oblique transition		24
4.1	Studies on oblique transition	24
4.2	The different stages in oblique transition	27
4.3	Oblique transition in relation to other scenarios	30
Summary of papers		31
Acknowledgments		34
Bibliography		35
Paper	· 1	
Paper	· 2	
Paper	· 3	
Paper	• 4	

v

CHAPTER 1

Introduction

Traditionally, transition from laminar to turbulent flow has been studied by investigating under which conditions infinitesimal two-dimensional waves (also known as Tollmien-Schlichting waves or TS-waves) can grow in amplitude. Since the growth of two-dimensional waves could not always explain experimental observations, researchers turned their interest towards the possibility for finite amplitude two-dimensional waves to become unstable with respect to low amplitude three-dimensional disturbances. This so-called secondary instability has been successful in describing transition initiated by artifically generated two-dimensional waves. Direct numerical simulations of the governing equations and theoretical work have both resulted in close agreement with data obtained from measurements. The obvious question then follows: How relevant is it to assume the presence of finite amplitude two-dimensional waves in a general flow situation? In an environment with a low level of background disturbances, such as exists at free flight conditions, growing two-dimensional waves can be of importance. However, there are many other situations where two-dimensional waves cannot be amplified from background disturbances or with such high disturbance levels that transition occurs on a time scale much faster than it takes for two-dimensional waves to amplify enough to become unstable to three-dimensional disturbances.

In 1993 a paper by Trefethen et al. was published in Science summarizing work on the stability of flows made by a few research groups during the previous ten years. The paper discussed the role of linear mechanisms in disturbance growth and described how large transient growth can be obtained at conditions for which traditional stability theory predicts exponentially decaying disturbances. These results also suggest that the concept of transient growth may explain experimental observations where transition from laminar to turbulent flow is obtained at Reynolds numbers much below theoretically predicted values.

Laminar-turbulent transition is usually described as a process involving three stages: the receptivity problem, the stability problem and the breakdown. During the receptivity stage external disturbances are transformed to instability waves inside the boundary layer. This important stage is, however, not treated in the present thesis, which instead focuses on the growth of disturbances and the breakdown of the flow. Usually the stability problem considers

1

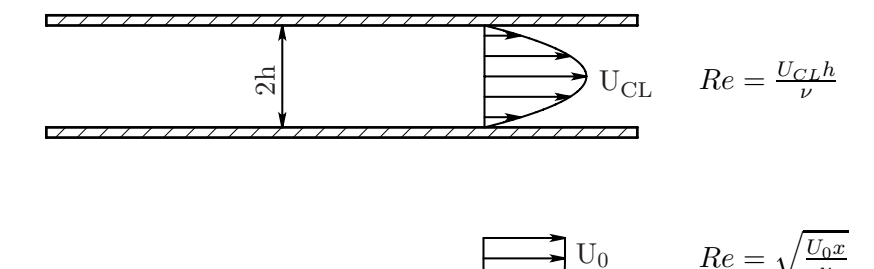


FIGURE 1.1. Geometry of the investigated flows. The top figure shows plane Poiseuille flow and the bottom a Blasius boundary layer flow.

the growth of low amplitude two-dimensional waves but we will start from a pair of oblique waves of small, but finite amplitude. The waves will interact with each other and form streamwise oriented vortices. An interaction between these vortices and the mean flow will result in regions of high- and low-speed fluid alternating in the spanwise direction. If the structures grow in amplitude and break down, this scenario will in the following be referred to as 'oblique transition'.

Transient growth of three-dimensional structures, which is an important part of the oblique transition scenario, may occur whenever a three dimensional disturbance is introduced into a boundary layer. Such disturbances have been studied in several experiments over the last decade by e.g. disturbing the flow through a small hole or a membrane at the wall or from the free stream. For such experiments transient growth of the disturbance is usually observed.

A complication in these studies is that it is hard to get a complete and accurate description of the initial disturbance. The control of the resulting disturbance is also limited. Therefore the possibility to use two oblique waves to study transiently growing disturbances is attractive since the initial disturbance in this case can be well described both mathematically and experimentally.

Oblique transition does, however, not only occur in model experiment but has probably significance in a number of natural situations. For instance in supersonic flows where the most unstable linear waves are oblique and one would expect that interaction between various oblique modes would give rise to the oblique transition scenario. For low levels of free stream turbulence the disturbances give rise to wave packets and the interaction among such wave packets may also give rise to oblique transition. Also for higher levels of free stream turbulence where generation of streaky structures occur oblique waves may play an important role for the breakdown.

The thesis is based on four papers (I-IV) which describe results obtained from experiments on oblique transition in two of the canonical shear flows, namely plane Poiseuille flow (paper I) and Blasius flow (paper II). A sketch of the flow geometries and a definition of Reynolds numbers related to the flows are shown in figure 1.1. The experiments consisted of measurements of the disturbance field resulting from a forcing with deterministic wave disturbances (so-called controlled forcing). Two methods to force the oblique waves have been used; in the plane Poiseuille flow case vibrating ribbons were used, whereas for the boundary layer the waves were introduced through periodic (both in time and in the spanwise direction) suction and blowing through a slit. Direct numerical simulations (paper III) were also used to clarify some features observed in the experiments, whereas one experiment was especially designed to investigate the secondary instability and breakdown of the streaky structures (paper IV).

CHAPTER 2

Stability theory

This chapter covers some useful issues in stability theory that will be used later in this thesis as well as in some of the included papers.

The Navier–Stokes equations together with the continuity equation describe the flow of a fluid. For an incompressible Newtonian fluid they read

$$\frac{\partial u_i}{\partial t} + u_j \frac{\partial u_i}{\partial x_j} = -\frac{1}{\rho} \frac{\partial p}{\partial x_i} + \nu \frac{\partial^2 u_i}{\partial x_j \partial x_j} + f_i \tag{1}$$

$$\frac{\partial u_i}{\partial x_i} = 0 \tag{2}$$

where u_i , p are the velocity and pressure fields, ρ and ν the density and kinematic viscosity and f_i describes the action of body forces. A right-handed coordinate system is used where $(x_1, x_2, x_3) = (x, y, z)$ are the streamwise, wall normal and spanwise axes. The corresponding velocities are denoted (u, v, w). For the flat plate boundary layer the origin is located on the centreline at the leading edge, whereas for the channel flow the origin is on the centreline half-way between the lower and upper wall (different streamwise positions are used for the origin).

By assuming the absence of body forces and a base flow in the streamwise direction with a variation in the wall-normal direction and by considering linear disturbances (squared disturbance quantities are neglected), the following equations can be derived

$$\left[\left(\frac{\partial}{\partial t} + U \frac{\partial}{\partial x} \right) \nabla^2 - U'' \frac{\partial}{\partial x} - \frac{1}{Re} \nabla^4 \right] v = 0, \tag{3}$$

$$\left[\left(\frac{\partial}{\partial t} + U \frac{\partial}{\partial x} \right) - \frac{1}{Re} \nabla^2 \right] \eta = -U' \frac{\partial v}{\partial z}$$
 (4)

The equations describe the evolution of any linear disturbance (the derivation of the equations can be found in e.g. Hallbäck *et al.* 1996). U is the laminar base flow, ∇ is the nabla-operator and the normal (perturbation) vorticity is given by

$$\eta = \frac{\partial u}{\partial z} - \frac{\partial w}{\partial x}$$

2.1 Stability theory for linear waves

Equations describing the behaviour of individual wave disturbances with infinitesimal amplitudes can be derived from equations (3) and (4) by introducing normal-modes of the form

$$v(x, y, z, t) = \text{Real}\left[\tilde{v}(y)e^{i(\alpha x + \beta z - \omega t)}\right]$$
 (5)

$$\eta(x, y, z, t) = \text{Real}\left[\tilde{\eta}(y)e^{i(\alpha x + \beta z - \omega t)}\right]$$
(6)

where α and β are the streamwise and spanwise wave numbers and ω is the angular frequency of oscillation. The result is the following pair of equations

$$\left[(-i\omega + i\alpha U)(D^2 - k^2) - i\alpha U'' - \frac{1}{Re}(D^2 - k^2)^2 \right] \tilde{v} = 0$$
 (7)

$$\left[(-i\omega + i\alpha U) - \frac{1}{Re} (D^2 - k^2) \right] \tilde{\eta} = -i\beta U' \tilde{v}$$
 (8)

in which D = d/dy and $k^2 = \alpha^2 + \beta^2$. The equations are known as the Orr–Sommerfeld and Squire equations, respectively. Together with boundary conditions, these equations form eigenvalue problems for the normal velocity and vorticity. The horizontal velocity components can be determined from

$$\tilde{u} = \frac{i}{k^2} (\alpha \frac{\partial \tilde{v}}{\partial y} - \beta \tilde{\eta}) \tag{9}$$

$$\tilde{w} = \frac{i}{k^2} (\beta \frac{\partial \tilde{v}}{\partial y} + \alpha \tilde{\eta}) \tag{10}$$

If only two-dimensional waves are considered (so-called Tollmien–Schlichting or TS-waves), it is sufficient to solve (7) and (9) together with appropriate boundary conditions to get \tilde{v} and \tilde{u} . However, if oblique waves ($\beta \neq 0$) are of interest the complete set of equations (7)-(10) need to be solved in order to get all velocity components. The boundary conditions for plane Poiseuille flow are

$$\tilde{v} = \frac{\partial \tilde{v}}{\partial u} = \tilde{\eta} = 0 , \quad y = \pm 1$$

whereas for a boundary layer flow they are

$$\tilde{v} = \frac{\partial \tilde{v}}{\partial y} = \tilde{\eta} = 0 , y = 0$$

$$\tilde{v} = \frac{\partial \tilde{v}}{\partial y} = \tilde{\eta} \to 0 , y \to \infty$$

Wave disturbances can either be considered to evolve in time or in space, and the corresponding stability problems are known as the temporal or the spatial problem. The temporal problem is solved for the complex eigenvalue ω with α , β and Re appearing as real parameters. In this case the sign of the imaginary part of the angular frequency ω_i determines if the disturbance

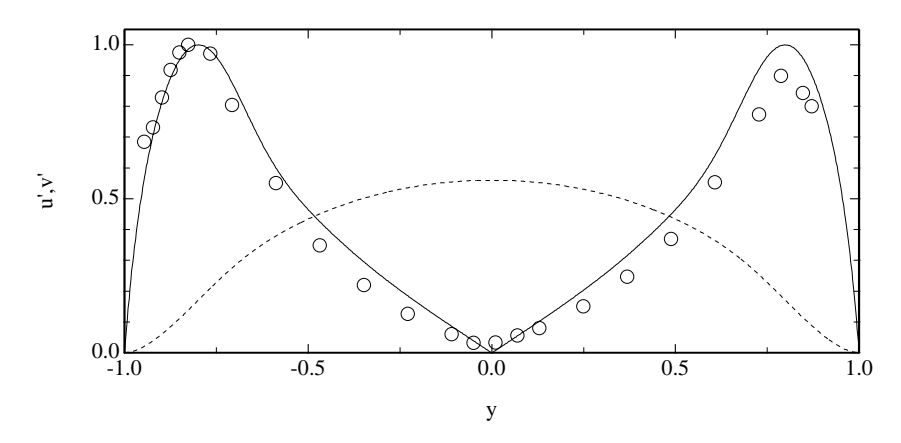


FIGURE 2.1. Amplitude profiles for plane Poiseuille flow at Re=1600 and $\omega=0.42$. Comparison between measurements (by Elofsson & Alfredsson) of the streamwise disturbance velocity (\circ) and eigenfunctions of u (——) and v (---) normalized by the maximum of u.

decays or grows with time. For $\omega_i < 0$ the disturbance decays whereas growth occurs for $\omega_i > 0$. A disturbance with $\omega_i = 0$ is said to be neutral. For the spatial problem the streamwise wave number α is complex and the angular frequency appears as a real parameter. In this case growth occurs in space if $\alpha_i < 0$.

Figure (2.1) shows examples of eigenfunctions for a Tollmien–Schlichting wave in plane Poiseuille flow. The numerical results, obtained by solving the spatial Orr–Sommerfeld equation with a shooting method, are compared with measurements of the streamwise disturbance velocity.

Squire's transformation and oblique waves

By using the transformation proposed by Squire (1933) it is possible to obtain information about oblique waves by solving the disturbance equations for two-dimensional waves. The transformation is as follows

$$\alpha_{2D}^2 = \alpha_{3D}^2 + \beta_{3D}^2 = k^2$$
 $Re_{2D} = \frac{\alpha_{3D}^2}{k^2} Re_{3D}$

where the subscripts 2D and 3D refers to Tollmien–Schlichting and oblique waves, respectively. The effect of the transformation is illustrated in figure 2.2 which shows neutral stability curves (contours of $\omega_i = 0$) for plane Poiseuille flow. Squire's transformation was derived for temporally growing waves in a parallel basic flow. For the spatial case it can be applied at neutral conditions. From the last of these equations one can see that a two-dimensional wave becomes unstable at a lower Reynolds number than the corresponding oblique

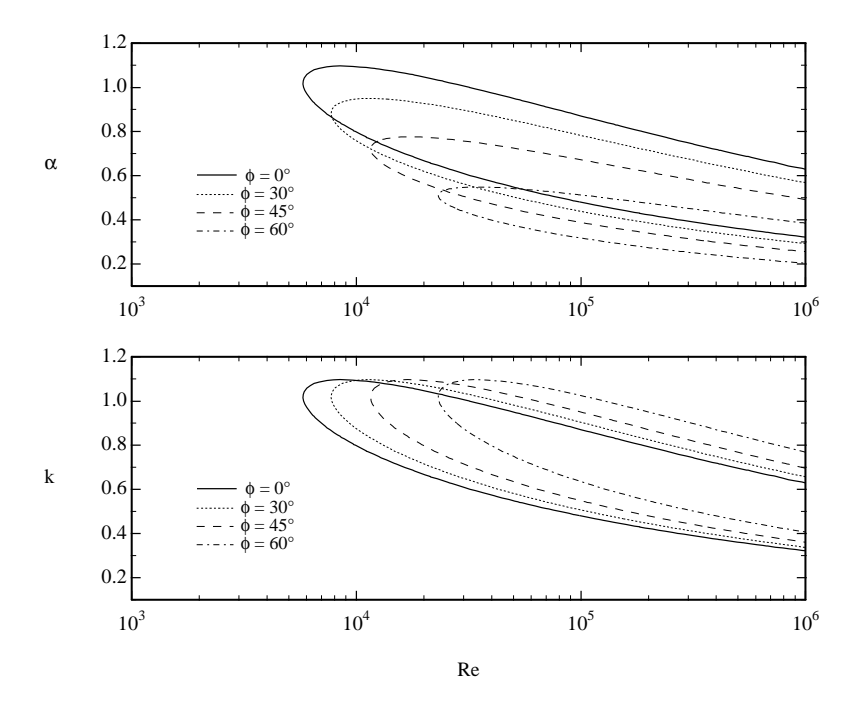


FIGURE 2.2. Curves of neutral stability for different wave angles $(\phi = \arctan(\beta/\alpha))$ in plane Poiseuille flow.

wave. This observation is known as Squire's theorem and is probably the main reason why three-dimensional disturbances for a long time were neglected in studies of laminar-turbulent transition.

An example of eigenfunctions for oblique waves in plane Poiseuille flow is given in figure 2.3. The calculated eigenfunctions are plotted together with a measured distribution of the streamwise disturbance velocity. When comparing with a two-dimensional wave it is seen that the positions where maximum \boldsymbol{u} occurs have moved closer to the centreline for the oblique wave.

2.2 Linear growth mechanisms

Recently there has been an increased awareness of the importance of linear growth of three-dimensional disturbances in the transition process, especially at subcritical Reynolds numbers. The need for linear growth mechanisms can be motivated by considering the so-called Reynolds-Orr equation, which describes the evolution of the disturbance kinetic energy. In the equation there are only terms that correspond to linear terms in the disturbance equations

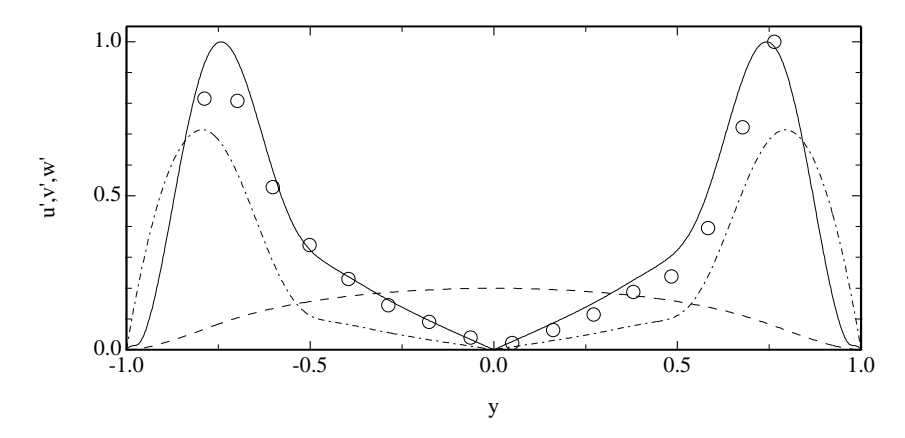


FIGURE 2.3. Amplitude profiles for an oblique wave ($\varphi = 45^{\circ}$) in channel flow at Re = 2000 and $\omega = 0.33$. Comparison between measurements (by Elofsson & Alfredsson) of the streamwise velocity (\circ) and eigenfunctions of u (——), v (- - -) and w (- \cdot -) normalized by the maximum of u.

and therefore it has been concluded that a linear mechanism is necessary for disturbance growth (see Henningson 1995).

For the inviscid case Ellingsen & Palm (1975) showed that streamwise independent three-dimensional disturbances would lead to a linear growth of the streamwise disturbance amplitude with time. Landahl (1980) investigated localized disturbances and demonstrated that the disturbance energy grows at least linearly with time as the disturbed region elongates in the streamwise direction. The studies mentioned above both describe a growth that is linear in time with no damping effects due to viscosity and can therefore be referred to as an algebraic instability.

The mechanism behind the described growth is the *lift-up* effect (see Landahl 1977), which is the generation of horizontal velocity perturbations by the upward or downward movement of fluid elements in a region with mean shear. By essentially conserving the horizontal velocity, the fluid elements will create a defect in the velocity profile at their new position.

The *lift-up* effect is also of great importance in viscous flows. Instead of the algebraic instability seen in the inviscid case the flow will rather experience a transient algebraic growth, since viscosity will eventually limit the growth. Mathematically, the transient growth can be explained as a result of decaying non-orthogonal eigenfunctions (see e.g. Trefethen *et al.* 1993).

One of the first studies which demonstrated the existence of transient growth in a viscous flow was the work by Hultgren & Gustavsson (1981). They investigated the temporal development of three-dimensional disturbances in a parallel boundary layer flow and found an initial linear growth followed by

a viscous decay. Later investigations of transient growth have been able to describe and quantify the growth in a number of flow situations. Studies in plane Poiseuille and Blasius flows will be presented in chapter 3, references to investigations of transient growth in other flows can be found in the review by Henningson (1995).

The structures that show the largest transient growth are streamwise independent disturbances ($\alpha=0$) with a fairly narrow spanwise scale. As an example we can consider plane Poiseuille flow, for which the amplitude of a streamwise independent disturbance with a spanwise wave length near 3h can grow to a value of 28 times its initial value at Re=2000 (see Trefethen et al. 1993¹). This growth is quite large especially if one considers that it occurs for a subcritical Reynolds number where all individual wave disturbances decay ($Re_{cr}=5772$ for plane Poiseuille flow). One can further note that by only using the least damped mode as in the study by Gustavsson (1991), almost the same growth will be obtained as found by solving the variational problem for the optimal growth.

Transient growth is a strong candidate to explain why transition observed in an experiment usually occurs at a lower Re than what is predicted for the least damped eigenmode. However, at supercritical Re there will be a competition between exponentially growing eigenmodes and linear growth mechanisms in determining the onset of transition.

As described above, viscous damping will eventually cause disturbances to decay in many situations. However, as pointed out by Luchini (1996), this is not the situation in a growing boundary layer where the weak viscous damping is insufficient to damp the algebraic growth. For a parallel flow the viscous decay is exponential and will eventually be larger than the algebraic growth, but for a growing boundary layer, both the viscous decay and the growth is algebraic and there are situations for which the growth can be larger than the decay.

2.3 Secondary instability and nonlinear breakdown

2.3.1 Nonlinear interactions and conditions for resonance. Nonlinear interactions involving three waves can occur if the wave number vectors of the waves satisfy

$$\mathbf{k}_1 = \mathbf{k}_2 + \mathbf{k}_3$$
 where $\mathbf{k}_i = (\alpha_i, \beta_i)$

The amplitude of the resulting wave will then be the product of the amplitudes of the two other waves. If in addition the angular frequencies of the waves match

$$\omega_{r,1} = \omega_{r,2} + \omega_{r,3}$$

 $^{^1 \}text{They showed that the maximum transient growth scales as } Re/71.5 and occurs for <math display="inline">\alpha=0$ and $\beta=2.04.$

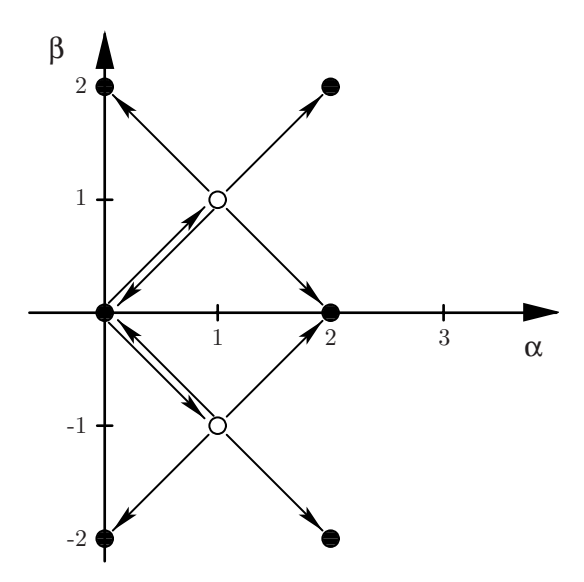


FIGURE 2.4. Figure illustrating nonlinear interactions occurring in the oblique transition scenario.

a resonance is said to occur. Provided that the individual waves have amplitudes of similar order they will force each other at resonance conditions, resulting in large growth rates.

Figure 2.4 illustrates nonlinear interactions involved in the oblique transition scenario. Initially only the two modes marked with open symbols contain energy, but nonlinear interactions redistribute energy among other wave number components. Wave number modes that receive energy in the first generation are marked by filled symbols, and the nonlinear interactions are shown by the arrows which indicate addition or subtraction of wave number vectors. In the next generation of nonlinear interactions, all energy containing modes will participate. We will in the following make use of a notation where modes are expressed as a pair of integers multiplying the streamwise and spanwise wave numbers of the initial oblique waves. The initial oblique waves are then denoted the $(1,\pm 1)$ modes and a TS-wave with the same frequency as the oblique waves will be noted a (1,0) mode.

2.3.2 Secondary instability of waves. Transition starting from Tollmien-Schlichting waves (two-dimensional waves) proceeds through a stage where vortices dominate. Flow visualisation studies and hot-wire measurements have indicated the appearance of two different vortical patterns at this stage. One structure consists of aligned Λ -shaped vortices and the other of Λ -vortices arranged in a staggered pattern. The former is denoted K-type transition after Klebanoff, and the case with a staggered pattern is usually called subharmonic

transition since a spectrum obtained by a hot-wire positioned in the flow would indicate a subharmonic frequency. There have been many investigations on these transition scenarios and several alternative names have appeared. K-type transition is also called fundamental, aligned and peak-valley splitting. Alternative names for subharmonic transition are C-type, H-type, N-type and staggered and we will usually refer to it as N-type transition.

Which of the scenarios that will be observed in a transitional flow is mainly governed by the amplitudes of the individual waves. N-type transition is generally observed at lower disturbance amplitudes of the two-dimensional wave. However, in plane Poiseuille flow experiments, K-type transition is usually observed (as opposed to theoretical predictions and observations from direct numerical simulations).

Several models have been proposed to explain the different vortex patterns. The models found to be of most relevance will be described below.

Subharmonic transition

Two main models are associated with the subharmonic secondary instability. The model by Craik (1971) uses weakly nonlinear theory, whereas the secondary instability theory (Orszag & Patera 1983, Herbert 1983) makes use of Floquet theory to investigate the linear stability of a modified baseflow with respect to three-dimensional disturbances. This modified baseflow is the combination of the undisturbed flow and a two-dimensional wave of finite amplitude.

Craik's model was originally put forward to explain the rapid growth of three-dimensional disturbances observed in experimental investigations of K-type transition, but the strongest growth occurred for subharmonic instead of fundamental frequencies. The model considers nonlinear interactions between a two-dimensional wave of fundamental frequency and a pair of oblique waves

$$Ae^{i(\alpha_1x-\omega_1t)}$$
 and $Be^{i(\alpha_2x\pm\beta_2z-\omega_2t)}$

Rapid growth occurs at resonance conditions

$$\alpha_1 = 2\alpha_2$$
 , $\omega_1 = 2\omega_2$

i.e. if the oblique waves have a subharmonic frequency. These conditions also imply that the phase velocities of the waves should be equal. The resonance conditions are rather strict and can only be fulfilled for some specific spanwise wave numbers.

A more general model which explains subharmonic transition was presented by Herbert (1983). This model also involves a two-dimensional wave and a pair of subharmonic three-dimensional disturbances, but the three-dimensional disturbances are now Squire modes, whose phase speed is independent of the spanwise wave number. This allows an instability to occur for a range of spanwise wave numbers.

K-type transition

The flow structures associated with K-type transition has been recognized since

the beginning of the 1960's. However, several observed features are still not fully understood. These features involve the question whether there exists a preferred spanwise wavelength or not, and also which of the proposed resonances is of greatest importance?

Characteristic for K-transition is the appearance of so-called spikes (large-amplitude fluctuations) seen in the streamwise velocity. These are now believed (see Kachanov *et al.* 1985) to result from local phase synchronization of three-dimensional disturbances with frequencies which are harmonics to the fundamental wave.

The wave-resonance concept by Kachanov (1987) explains the growing harmonics with a cascade of four-wave resonances involving waves of type

$$(\omega_1,0)$$
 , $(2\omega_1,0)$ and $(\omega_1,\pm\beta)$

Waves involved in this series of resonances have been observed in measurements at the spike stage (see the review by Kachanov 1994 for a description).

Examples of other models describing K-transition are the fundamental resonance by Herbert, which involves

$$(\omega_1, 0)$$
 , $(0, \pm \beta)$ and $(\omega_1, \pm \beta)$,

or a combination of Herbert's resonance and the wave-resonance concept.

The models described above for K- and N-type transition all involve a finite amplitude TS-wave, which later distorts as three-dimensional disturbances gain in amplitude. However, the oblique transition scenario (see chapter 4) does not need to rely on two-dimensional waves but rather starts directly from a nonlinear interaction between a pair of oblique waves.

CHAPTER 3

Transition in plane Poiseuille and Blasius flows

This chapter concentrates on describing the first stages of the transition process, occurring before the formation and growth of turbulent spots. Further information on the late transition stages in plane Poiseuille and Blasius flows can be found in Henningson, Johansson & Alfredsson (1994) and Riley & Gadel-Hak (1985). Oblique transition is not treated in this chapter, but a detailed description is given in chapter 4.

The chapter starts with a survey of methods for the generation of controlled disturbances in an experiment and it also gives some information on how disturbances can be modelled in a direct numerical simulation.

3.1 Methods for generating disturbances

In order to get accurate and detailed information about the complicated process of transition from laminar to turbulent flow, controlled disturbances are usually introduced in experiments. The idea is to generate deterministic disturbances and then study their behaviour. If studies of this kind are to be of any wider interest, it is of course important that the generated disturbances resemble those that are observed for transition at unforced conditions (also known as natural transition). By prescribing specific disturbances as initial or inflow conditions in a direct numerical simulation, one can also make use of 'controlled disturbances' in such investigations.

3.1.1 Experimental disturbance generation. Numerous methods for the generation of disturbances have appeared since the study by Nikuradse (1933), who used periodic suction through the surface of a flat plate model in order to experimentally verify the stability theory of Tollmien and Schlichting. Methods for disturbance generation differ in the way they were designed to effect the flow and in their degree of control. There are methods which only allow the amplitude to be controlled whereas other make it possible to control the complete disturbance spectrum. According to Gaponenko & Kachanov (1994), the general requirements for disturbance generators are: they should have a small effect on the mean flow, they should generate disturbances of a given spectrum and they should provide a possibility to control the spectrum. Examples of

various disturbance sources, arranged after the desired disturbance type, are presented in the following.

Vibrating ribbon

One of the most well-known devices for generation of two-dimensional wave disturbances is the vibrating ribbon. This technique was first used by Schubauer & Skramstad (1947) in their classical investigation of transition in a flat plate boundary layer. A metal ribbon mounted near a wall is exposed to a stationary magnetic field and the motion of the ribbon is achieved by connecting the ribbon to an alternating current. There are some limitations with the vibrating ribbon technique such as a non-uniform amplitude distribution along the ribbon span, the need for a relaxation distance close to the ribbon and the possibility that the ribbon effects the mean flow (see Mack 1984 and Saric 1990). If the ribbon is oriented in an oblique angle to the direction of the mean flow it is also possible to generate oblique waves (as shown by e.g. Elofsson & Alfredsson 1995).

Acoustic forcing

It is known that acoustic disturbances in the free stream can generate disturbances inside the boundary layer through a receptivity process. Saric, Hoos & Radeztsky (1991) made experiments on the boundary layer receptivity of sound with two-dimensional roughness elements. They put a roughness element on their flat plate model and used acoustic forcing from the free stream to excite TS-waves, which were found to be in close agreement with results from linear stability theory. Later Breuer et al. (1996) studied the interaction between broad-band acoustic waves (the background noise in their wind tunnel) and two-dimensional roughness elements. Their results demonstrated that a similar receptivity mechanism is active in broad-band acoustic forcing as for forcing at a single frequency.

One can also note that oblique waves and pair of oblique waves can be generated with acoustic forcing and a roughness step at an oblique angle to the flow direction.

Point source

For studies of localized disturbances, loudspeakers have commonly been utilized. Gaster & Grant (1975) used a short duration acoustic pulse, injected through a small hole in their flat plate model, to generate a wave packet which later becomes modulated. Variations on the theme are harmonically excited point sources or, as in the investigation by Shaikh & Gaster (1994), excitation by deterministic white noise. Hole diameters in these studies are in the range 0.5 to 0.8 mm.

Wave packets can be decomposed into individual modes with Fourier techniques. Gaster & Grant used power spectra and were therefore limited to information about amplitudes. However, if experimental data allows a complex spanwise Fourier transform to be made, one can obtain complete information

on both amplitude growth and dispersion characteristics for various wave angles (see Kachanov & Michalke 1994).

In the experiments by Breuer & Haritonidis (1990) a localized disturbance was generated by the motion of a 9 mm by 17 mm latex membrane mounted in the flat plate model. The membrane surface was activated by connecting the cavity below it to either a high- or a low-pressure source.

Another method for generating localized disturbances is the use of a spark discharge. This technique generates strong disturbances and it has been used in stability experiments in supersonic flows and also in the study of turbulent spots by Wygnanski, Sokolov & Friedman (1976). Strong disturbances can also be generated by the injection of fluid through the flat plate surface or channel walls (see e.g. Henningson & Alfredsson 1987).

$Stationary\ disturbance\ generator$

Another category of forcing may be denoted continuous. Klebanoff, Tidstrom & Sargent (1962) used strips of tape positioned below their vibrating ribbon to control the three-dimensionality in the flow. Other examples of this type are roughness elements or obstacles, as in the investigation of subcritical transition by Nishioka & Asai (1985). A similar type of forcing can also be achieved with continuous suction or injection through slits in a wall.

Complex wave generators

Perhaps beeing the most interesting, and also the most difficult to design, are systems which allow control of the complete spectrum of a disturbance. With this we mean devices which can generate disturbances with a desired (complex) frequency-wavenumber spectrum.

Liepmann, Brown & Nosenchuck (1982) used periodic heating of a nichrome strip to generate two-dimensional disturbances on a flat plate in a water tunnel. Later Robey (1987) developed a flush-mounted heater array for the generation of phase-controlled three-dimensional disturbances. Corke & Mangano (1989) developed a spanwise array of wire segments which could be heated individually. Their disturbance generator was operated in a wind tunnel at forcing frequencies up to about 40 Hz. An additional long wire mounted just upstream of the array was used to force two-dimensional waves, and this arrangement made it possible to simultaneously generate phase-controlled two- and three-dimensional disturbances. Both types of wave generators described above use local heating near a wall to cause a change in the viscosity and the effect of the heating can be compared to a small wall-normal surface oscillation (see Liepmann et al.).

Another interesting method to generate disturbances with a given spectrum was developed by Gaponenko & Kachanov (1994). Their source consists of a spanwise array of pipes which connects to the surface of the flat plate model through a narrow slit. Each pipe is connected to a loudspeaker and the spanwise wavenumber of the disturbance can be controlled by changing the phase of the loudspeaker signals and the pattern by which the speakers are connected to the

pipes. A similar version of the disturbance source was used by Bake, Kachanov & Fernholz (1996) in their investigation of the nonlinear stages of transition in a Blasius-like flow developing on the wall of an axisymmetric wind tunnel.

Corke, Krull & Ghassemi (1992) used a 52 μ m thick piezoelectrical film to excite three-dimensional modes in their study of the far wake behind an airfoil. The film had a total area of $300 \times 150 \ \mathrm{mm^2}$ and was wrapped around the surface of the airfoil. A total of 60 forcing elements and their electrodes were created by vapor depositing an alloy onto the film. The airfoil had cavities located below the portions of the film which contained the active forcing elements. Periodic disturbances were generated by the motion obtained when applying a periodic voltage to the elements. Measurements are reported at forcing frequencies up to 100 Hz but the technique should have a potential to reach a frequency response of about 500 Hz.

3.1.2 Modelling of controlled experiments in numerical simulations.

Much success has been achieved in obtaining detailed information from the transition process by direct numerical simulations (DNS). Some numerical simulations have aimed at a direct comparison with existing experiments that have used controlled disturbances. In order to obtain a close agreement between simulations and experiments, experience has shown that it is important to model the forcing in a careful way.

Perhaps the most common and easiest way to simulate controlled disturbances is to directly include disturbance modes in the initial conditions or in the inflow boundary conditions. In a simulation with a TS-wave for instance, the disturbance mode would be the least damped Orr-Sommerfeld mode at the given conditions. Several examples of direct numerical simulations using this technique can be found in the review by Kleiser & Zang (1991).

The aim of the numerical simulation by Elofsson & Lundbladh (1994) was to find the reason for the difference in symmetry which was found when comparing experimental results of oblique transition in a plane channel flow (Elofsson & Alfredsson 1995) with a DNS by Schmid & Henningson (1992). In the experiment a pair of oblique waves were generated by vibrating ribbons mounted at 45° angle to the flow direction (one at each channel wall). To closely model the experiment Elofsson & Lundbladh used time-dependent body-forces in the regions occupied by the ribbons. By adjusting the amplitude of the body-forces to match u_{rms} from the experiment in one position, close agreement between experiments and DNS was found throughout the whole region (see figure 3.1).

In the work by Berlin, Wiegel & Henningson (1998) comparisons were made between experiments on oblique transition in a boundary layer flow and DNS. The experiments used periodic blowing and suction through a spanwise array consisting of 40 slits, each 10 mm wide. Several methods to model the experimental forcing were investigated in the simulations. The closest agreement was obtained when the wall-normal velocity was specified in a region at the wall. In this region the velocity was applied in a step-wise fashion to simulate the

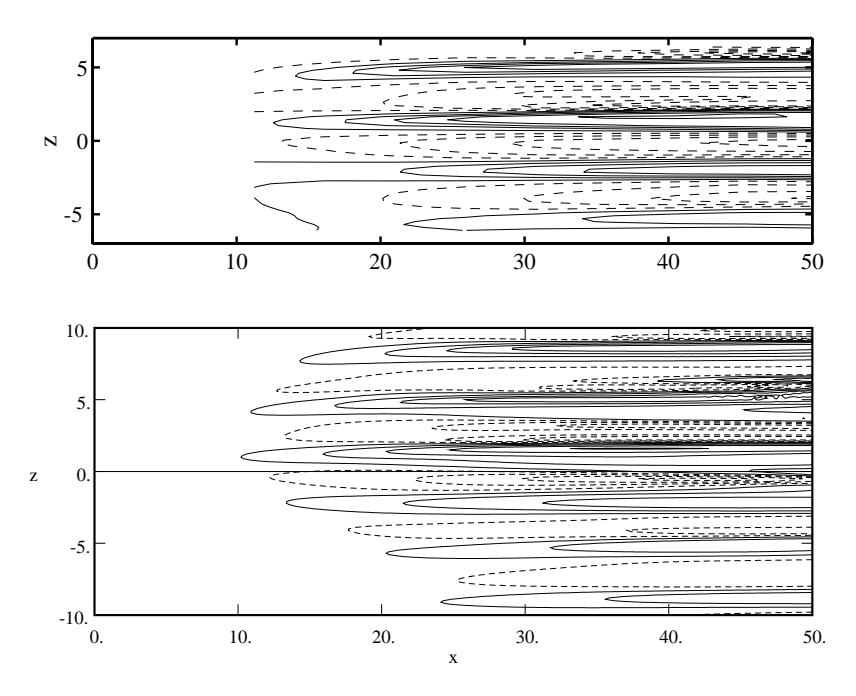


FIGURE 3.1. Stationary disturbance field caused by a pair of oblique waves in plane Poiseuille flow for Re=2000. Experimental results are shown in the top figure and simulation results in the bottom (from Elofsson & Lundbladh 1994).

individual slits, and to account for the lower response from suction than for blowing the amplitude during the suction phase was reduced.

3.2 Transition studies in plane Poiseuille flow

3.2.1 Linear and nonlinear two-dimensional disturbances. From the solution of the Orr–Sommerfeld equation it is known that plane Poiseuille flow is unstable to small-amplitude two-dimensional disturbances for Reynolds numbers above $Re_{cr}=5772$ (Orszag 1971). Experimental observations of the stability of controlled wave disturbances were first made by Kao & Park (1970), who obtained a transitional Reynolds number (Re_{tr}) of about 2200 in a water channel with an aspect ratio of 8. However, the first satisfactory experimental verification of the linear stability theory was reported by Nishioka, Iida & Ichikawa (1975). With the use of a carefully designed air-flow channel they managed to obtain a background disturbance level less than 0.05 %, which allowed the flow to stay laminar up to Re=8000, although at this Re the

flow was not fully developed¹. Disturbances generated by a vibrating ribbon were studied both at subcritical and supercritical Re and the experimental observations were found to be in accordance with linear stability theory.

In other experiments transition has been observed to occur at Reynolds numbers as low as 1000. Davies & White (1928) observed transition at Re about 1100 in a channel with a highly disturbed inlet flow and Patel & Head (1969) detected turbulent bursts at Re=1035. Since infinitesimal two-dimensional disturbances are stable at these Reynolds numbers, theories including the effect of finite amplitude disturbances were also considered. The two-dimensional mean-field theory by Meksyn & Stuart (1951) suggests a Re_{cr} of about 2900 with a threshold amplitude of 8 %. Later extensions to this theory results in similar Reynolds numbers (Stuart 1960, Watson 1960) and therefore it seems that analysis of this type is of limited interest for the understanding of subcritical transition.

3.2.2 Two- and three-dimensional disturbances. Since theories concerning finite amplitude effects of two-dimensional waves were unable to explain the values of Re_{tr} observed in experiments, interest was later focused on the influence of three-dimensional disturbances on the transition process. Orszag & Kells (1980) made direct numerical simulations and found three-dimensional disturbances to have a strongly destabilizing effect. Their simulations also showed that transition can occur at Reynolds numbers of order 1000 for finite amplitude disturbances. Similar Re_{tr} was found by Carlson, Widnall & Peeters (1982) in their flow visualization study of triggered and naturally occurring transition. Nishioka & Asai (1985) found a minimum transition Re in the same range and determined the threshold amplitude to be close to the disturbance amplitudes found in fully developed turbulent channel flows.

The secondary instability theory (see chapter 2) considers the development of three-dimensional disturbances on a base flow consisting of the mean parabolic flow and a Tollmien-Schlichting wave. Two different vortical patterns are found in numerical simulations, one in which aligned Λ -vortices appear (K-type) and one where the vortices are arranged in a staggered pattern (N-type). In experiments, however, only the K-type pattern is observed, unless disturbances with a subharmonic frequency are forced simultaneously with the fundamental wave (see Ramazanov 1985).

A general explanation for the discrepancy between experimental observations and theoretical predictions was given by Kim & Moser (1989), who demonstrated that staggered vortical structures are unlikely in transition at unforced conditions. By doing numerical simulations at Re = 10000 they found that

¹The flow had not reached a fully parabolic velocity profile at the downstream end of the channel.

subharmonic transition was only achieved if their 'minus' modes² were continuously suppressed. The minus modes are forced by background disturbances in the form of roundoff errors present in the simulations. When the product of the amplitude of the minus modes and the fundamental mode (which is exponentially growing at this Re) exceeds the amplitude of the background noise, the fundamental modes begin to grow and K-type transition will be observed.

A different explanation was offered by Singer, Reed & Ferziger (1989). They made numerical simulations and found the presence of low amplitude vortices in the base flow to cause K-type transition. They argued that streamwise vortices of these amplitudes are inherent in all experimental facilities.

Asai & Nishioka (1989) investigated the origin of the three-dimensional wave which had been observed in their experiments. They had earlier observed subcritical transition to occur when the amplitude of an artifically generated TS-wave exceeded about 1 %. Transition was initiated by a distortion of the wavefront which later developed into a peak-valley structure. It was found that the interaction between the generated TS-wave and the disturbed mean flow resulted in the three-dimensional wave. For low amplitudes of the TS-wave this was the result of a second-order coupling between the wave and the mean flow, and the three-dimensional wave decayed. At TS-amplitudes above 1 % the wavefront distortion was in the form of a secondary instability leading to a growing peak-valley structure.

In addition to the numerical simulations mentioned in the above text, there are several other numerical works which have contributed to the understanding of transition in plane Poiseuille flow. Zang & Krist made numerical simulations at Reynolds numbers of 1500, 5000 and 8000 for different initial conditions. They looked at many different aspects and gave a detailed picture of the flow field for a K-type transition at Re=1500.

Saiki et al. (1993) compared their spatial simulations, using both K- and N-type inflow conditions, with results from experiments, theory and temporal simulations. Many things were in common but some differences were found when comparing their low-amplitude case with previous temporal simulations. As opposed to findings from temporal simulations on forced secondary instability, they found a higher growth for N-type transition than for K-type. This result is though in accordance both with the secondary instability theory of Herbert and with results from temporal simulations which allow the most competitive modes to evolve (by prescribing random three-dimensional disturbances and two-dimensional modes as initial conditions).

An investigation of the late stages of transition was reported by Sandham & Kleiser (1992). They processed data from a numerical simulation of K-type transition at Re = 5000 and presented a detailed view of the transition

²Their minus mode is the sum of the Squire mode and, what essentially is, the spanwise component of the Orr–Sommerfeld mode.

process from the stage where Λ -structures are observed up to fully developed turbulence.

3.2.3 Three-dimensional disturbances. With a modern view on transition, three-dimensional disturbances are not only found to be more important than two-dimensional ones but they can also dominate the flow field during the whole transition process.

As described in section 2.2, the importance of three-dimensional disturbances in the inviscid case were demonstrated by Ellingsen & Palm (1975) and Landahl (1980). The viscous case was considered by Gustavsson (1991), who investigated the evolution of a small three-dimensional disturbance through the complete solution to the linear initial-value problem. He found an initial growth in the disturbance energy even though all the individual modes decayed. Klingmann (1991) made experiments on a localized disturbance at subritical Reynolds numbers. The disturbance, generated by the injection of a short-duration jet through one of the channel walls, developed into growing elongated streaky structures. Depending on the initial amplitude the disturbance eventually decayed or a turbulent spot was formed. Her results indicated that the important mechanism behind the growth of the structures is linear, which also supports the work by Gustavsson.

The direct numerical simulations and eigenfunction expansions by Henningson, Lundbladh & Johansson (1993) gave further support for the transient growth of disturbances through a linear mechanism. They investigated the evolution of different localized disturbances in plane Poiseuille and boundary layer flow, and their results indicated that the formation of streaky structures from localized disturbances is a general feature of transition in wall bounded shear flows.

3.3 Transition studies in Blasius flow

3.3.1 Linear stability. Boundary layer flow developing along a flat plate at zero pressure-gradient differs from plane Poiseuille flow in that the flow is not strictly parallel and that the relevant Reynolds number increases in the streamwise direction. Early experimental investigations indicated amplified disturbances at higher frequencies and lower Re than what was predicted by stability theory. The discrepancy was by many attributed to the assumption of a parallel flow in the stability calculations, although Gaster (1974) found the destabilizing effect of a non-parallel flow assumption to be small. Fasel & Konzelmann (1990) made numerical simulations where the growth of the boundary layer was taken into account and confirmed Gaster's theoretical result. Experimental evidence in the line with the results of Gaster and Fasel & Konzelmann was reported by Klingmann et al. (1993). They also suggested that a failure to achieve a Blasius like flow in the leading edge region might

be an explanation for the discrepancy between previous experiments and linear stability theory.

Although not beeing too important for predictions of Tollmien–Schlichting waves, non-parallel effects must be taken into account when three-dimensional instability waves are considered. Using PSE calculations, Bertolotti (1991) demonstrated the increasing effect of non-parallelism with growing wave angle. Kachanov & Michalke (1994) compared experimental results with parallel-flow theory and obtained larger growth rates from the experiments than from theory. They concluded that this observation most probably could be explained by non-parallel effects. However, they also demonstrated that the effect of non-parallelism on dispersion characteristics of oblique waves is small.

A comparison between experiments and stability theory for oblique waves was made by Gaster (1975) when he compared his wave packet model to the initial growth stages from the measurements by Gaster & Grant (1975). Cohen, Breuer & Haritonidis (1991) made a detailed investigation on the evolution of a wave packet, measuring distributions of all three velocity components. After the transient part of their generated disturbance had decayed the remaining wave packet could be described as a superposition of individual modes, which were in close accordance with linear stability theory. Subsequently the wave packet also entered a weakly nonlinear stage and developed into a turbulent spot.

3.3.2 Three-dimensional disturbances. Since the investigation by Klebanoff, Tidstrom & Sargent (1962), three-dimensional disturbances are known to be of great importance for the transition process in boundary layer flows. Indications of, what is now known as, N-type transition were not found in experiments until the hot-wire measurements by Kachanov, Kozlov & Levchenko (1977) and the flow visualizations of Thomas & Saric (1981). In contrast to plane Poiseuille flow, there exist many detailed data from boundary layer experiments, which is mainly because it is simpler to do experiments in a Blasius flow. As for plane channel flow most of the interest has been in studying the nonlinear breakdown originating from the combination of a finite amplitude Tollmien-Schlichting wave and oblique waves. Experimental studies have mainly concerned controlled two-dimensional waves and their interaction with three-dimensional disturbances either in the form of background noise or forced through roughness elements. However, starting with the work by Corke & Mangano (1989) experiments have also been made on two- and threedimensional waves with controlled amplitude and phase. Further information on the breakdown process in Blasius flows involving Tollmien-Schlichting waves and the concept of secondary instability can be found in the reviews by Herbert (1988), Kleiser & Zang (1991) and Kachanov (1994).

In descriptions of the secondary instability scenarios, K-type is commonly associated with an aligned pattern of Λ -structures and the appearance of 'spikes'

in velocity signals, whereas subharmonic transition results in a staggered pattern and spikes are considered to be absent. However, the study by Bake, Kachanov & Fernholz (1996) showed that spikes can also be present at conditions where subharmonic resonance occurs and a staggered pattern is observed.

Free stream turbulence

It is well known that an increased level of free stream turbulence reduces the transitional Reynolds number. The free stream vortices result in two different types of disturbances inside the boundary layer and an additional disturbance type propagating with the free stream velocity at the edge of the boundary layer. At lower levels of free stream turbulence, TS-waves can be observed coexisting with slowly fluctuating elongated structures³. As the level of free stream turbulence increases the elongated structures will dominate the flow. This latter situation occurs in e.g. turbomachinery applications and the transition process is known as bypass since it by-passes the stage with exponentially growing TS-waves.

Several interesting experiments on boundary layer receptivity at low levels of free stream turbulence has been undertaken by Kendall (1985, 1990, 1991). These studies have described the appearance and growth of wave packets and have also revealed the presence of low-frequency fluctuations growing as $x^{1/2}$. The same scaling was also seen in the study by Westin *et al.* (1994) who also showed the near similarity in profiles of the streamwise perturbation velocity. A summary of experiments on boundary layer receptivity at relatively low levels of free stream turbulence was recently presented by Kendall (1998).

The importance of the normal component of the free stream fluctuations was demonstrated by Voke & Yang (1995) in a large-eddy simulation at a high level of free stream turbulence. They did not detect transition when the free stream fluctuations only contained the streamwise component, while pure wall-normal disturbances resulted in nearly the same result as for fully isotropic free stream turbulence.

In a situation with coexisting TS-waves and low-frequency oscillations, interactions between the individual disturbances can give rise to new structures. To gain more insight into this fairly complex situation, Bakchinov et al. (1998) studied the interaction between a TS-wave and elongated streamwise streaks of high- and low-speed fluid. The latter disturbance is similar to structures observed when free stream turbulence is present. A strong interaction between the disturbances was observed and oblique structures were found to be of importance in the later transition stages.

$Localized\ disturbances$

Observations of localized disturbances in the form of wave packets are described above (see 3.3.1). Here we present some results on localized disturbances which

³Denoted Klebanoff-mode oscillations (since they were first observed by P.S. Klebanoff).

cannot simply be described as a superposition of exponentially growing eigenmodes.

Breuer & Haritonidis (1990) investigated the development of localized disturbances generated by the motion of a membrane mounted flush with the surface of a flat plate (see also 3.1.1). In addition to a wave packet of Gastertype, the up-down motion of the membrane caused a transient disturbance to form. The growth of the latter disturbance was due to a linear mechanism and it resulted in an inclined shear layer in the streamwise velocity.

In the study by Cohen, Breuer & Haritonidis (1991) the disturbance source had been modified to reduce the effect of the transient disturbance. This was achieved by the use of an air-pulse introduced through a perforated disk (with a diameter of 5 mm) located at a streamwise position corresponding to Branch I for a TS-wave at the generated frequency. They extended the work by Gaster & Grant (1975) by making detailed measurements of all three velocity components both inside and outside the boundary layer. The measurements revealed the large differences in the disturbance structure inside and outside the boundary layer during the late transition stages. These observations were ascribed to the normal vorticity, in its strong influence on the three-dimensional modes when the vorticity is forced by the large mean shear inside the boundary layer.

Another interesting study on localized disturbances is the work by Grek, Kozlov & Ramazanov (1985). At intermediate forcing amplitudes, they observed a decaying localized structure with a small, almost constant, spanwise extent. This disturbance is different from wave packets and turbulent spots, but seems to be similar to the transient disturbances observed by Breuer & Haritonidis (1990).

The streaky structures observed in studies of localized disturbances are similar to those found at elevated levels of free stream turbulence. High- and low-speed streaks are also observed in oblique transition (see chapter 4) and their general role in laminar-turbulent transition was discussed by Alfredsson & Matsubara (1996).

CHAPTER 4

Oblique transition

Oblique transition originates from the nonlinear interaction between a pair of oblique waves with wave angles of equal magnitude but opposite sign. Nonlinear interaction distributes disturbance energy among various wave numbers, and in particular to low streamwise wave numbers (i.e. streamwise streaks) which can experience a strong algebraic growth. If the amplitude of the streamwise streaks reaches above a threshold the streaks may become unstable with respect to low amplitude time-dependent disturbances and the flow will break down. Since the transition scenario utilizes the transient growth mechanism, which is operative also at low Reynolds number, transition can occur at subcritical Re.

Figure 4.1 shows a flow visualisation of oblique transition in a flat plate boundary layer (photo by Elofsson & Matsubara). The flow direction is from left to right and a homogeneous smoke layer was introduced through a spanwise oriented slit in the flat plate, located 60 mm upstream of the left edge of the picture. The picture was taken with a camera in the wind tunnel ceiling and the light was provided with a flashlight from downstream. Oblique waves are first seen to evolve into a staggered pattern of Λ -shaped structures and later the flow breaks down.

4.1 Studies on oblique transition

Schmid & Henningson (1992) used a pair of finite amplitude oblique waves as initial conditions in a direct numerical simulation of transition in plane Poiseuille flow at Reynolds numbers of 1500 and 2000. The use of oblique waves resulted in a rapid growth of disturbance energy followed by breakdown. This growth was identified to result from a linear mechanism and the dominating mode was found to be the (0,2)-component (see 2.3.1 for definitions). When compared with the traditional secondary instability scenario starting with similar initial disturbance energy, oblique transition was found to be considerably faster.

Spatial simulations of oblique transition was reported by Lundbladh et al. (1994). For plane Poiseuille flow they investigated different initial amplitudes at Re=2000 and found the spatial simulations to be in qualitative agreement with the temporal ones by Schmid & Henningson (1992).

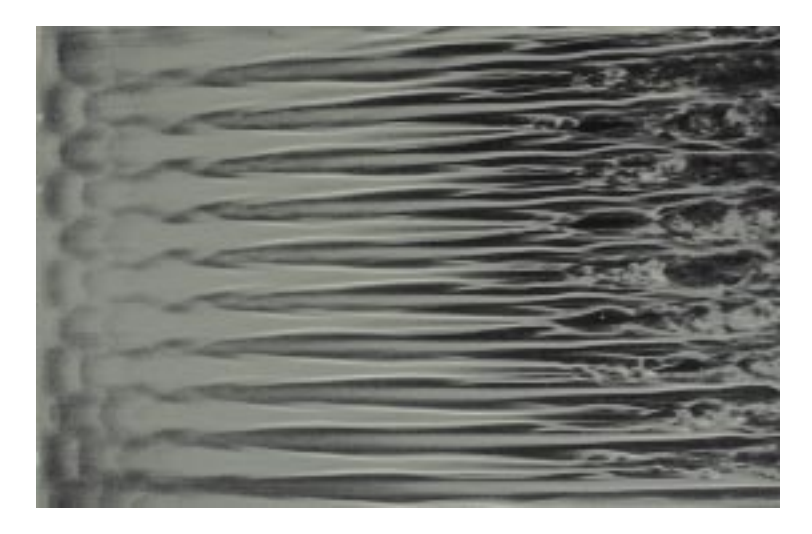


FIGURE 4.1. Flow visualisation of oblique transition in a Blasius flow ($U_0=7$ m/s and F=97). The photo covers 400 mm in the streamwise direction downstream of x=270 mm. The spanwise distance is 260 mm at the left and 235 mm at the right side of the picture.

The first experimental investigation of oblique transition in plane Poseuille flow was made by Elofsson & Alfredsson (1995). Oblique wave disturbances were generated by two vibrating ribbons, which were mounted at opposite channel walls. It was clear from the measurements that a pair of oblique waves resulted in stationary large amplitude structures. Depending on the amplitude, the structures either slowly decayed after an initial growth or wave disturbances with a fundamental or superharmonic frequency to the initial waves increased in amplitude and breakdown eventually occurred. For the investigated wave angles and a Reynolds number of 2000, streak amplitudes below $\approx 12~\%$ did not result in growing harmonics and breakdown, whereas larger streak amplitudes did. The experimental findings confirmed the results from the previous numerical simulations. However, when viewed in a cross-stream plane, the measured streamwise velocity field was not identical in symmetry with the corresponding field from the DNS.

An explanation for the observed difference in symmetries was later provided by Elofsson & Lundbladh (1994). The action of the vibrating ribbons used in the experiments of Elofsson & Alfredsson (1995) was closely modelled in spatial numerical simulations (see also section 3.1.2). This resulted in the same symmetry in the spatial DNS as observed in the experiments, and the explanation for this symmetry was a non-uniform strength of the nonlinear forcing in cross-stream planes. The strength of the nonlinear forcing at a given point is proportional to the product of the individual wave amplitudes at that

point, which in turn depends on the distance travelled from the vibrating ribbon and on the wall-normal position. However, despite the difference in symmetry compared with the simulations by Schmid & Henningson, the general features are found to be the same (i.e. the same modes are active during the transition).

Berlin, Lundbladh & Henningson (1994) studied oblique transition in a zero pressure gradient boundary layer flow with the use of direct numerical simulations. They observed a similar scenario as for the channel flow and conjectured that oblique transition in shear flows involves three stages. Firstly, a nonlinear generation of streamwise vortices by the oblique waves; secondly, generation of streaks through the lift-up effect; and thirdly, breakdown due to a secondary instability operating on the streaks. Berlin $et\ al.$ also compared their simulations with results by Joslin, Streett & Chang (1993), who did not observe fully developed turbulence despite a longer computational box and a higher Re at the inflow. It was suggested that the reason for this was a difference in inflow conditions. Berlin $et\ al.$ used Orr–Sommerfeld modes where the normal vorticity was excluded whereas Joslin $et\ al.$ made use of complete eigenmodes.

The first experimental investigation of oblique transition in a flat plate boundary layer was carried out at DLR in Göttingen by Wiegel (1996). He used particle image velocimetry (PIV) and hot-wire anemometry to document the flow field obtained by controlled forcing with a wave generator using blowing and suction. These measurements showed the flow structure and provided information about the growth in streak amplitude and u_{rms} in various frequency bands. However, the investigation did not evaluate the results by decomposing it in various spanwise wave numbers.

A comparison between Wiegels experiment and direct numerical simulations which carefully modelled the experiment was presented by Berlin, Wiegel & Henningson (1998). From the simulation results Berlin *et al.* identified similar features as had earlier been observed in investigations of K- and N-type transition. The similarities were explained by the presence of oblique waves and streamwise vortices in all three transition scenarios, although of different strength. For further details about the modelling of the wave generator see also section 3.1.2.

The results found in the experiments by Elofsson (1998) differed from the ones presented by Wiegel in that transition occurred farther downstream. It was found that even if the streak amplitudes caused by transient growth were too low to directly trigger streak instability, breakdown was initiated at a later stage after the initially damped oblique waves had amplified through the unstable region. The difference between the two experiments is mainly explained by the use of different parameters, but may also be explained by the methods used to generate the disturbances and the difference in wind tunnel flow quality. Whereas Wiegel (1996) generated disturbances which entered the boundary layer through individual slits, Elofsson allowed disturbances from individual pipes to mix in a slit before entering the flow.

4.1.1 The generality of oblique transition. The importance of a pair of oblique waves has also been recognized in other flow situations, thus indicating the generality of the transition scenario. For a flat plate boundary layer at low supersonic Mach numbers, the most unstable wave modes are oblique. This fact makes the oblique transition concept interesting also in compressible flows. Fasel, Thumm & Bestek (1993) investigated two different transition scenarios in a compressible boundary layer at a Mach number (M) of 1.6 with the aid of direct numerical simulations. Despite a lower initial amplitude, the simulation with a pair of oblique waves as boundary conditions resulted in much faster breakdown than for their simulation of a fundamental transition. Similar results were obtained from nonlinear PSE-calculations by Chang & Malik (1994) at M=1.6. They compared oblique transition results with subharmonic transition and found the subharmonic type to require larger initial amplitudes. Chang & Malik also pointed out (as earlier hypothesized by Schmid & Henningson 1992 in an incompressible flow) that oblique transition constitutes the second stage in the secondary instability with subharmonic waves.

Other studies of oblique transition are those of Gathmann, Si-Ameur & Mathey (1993) in a supersonic shear layer between streams with M=4.5 and M=1.6, and Sandham, Adams & Kleiser (1994) in a compressible flat plate boundary layer at a Mach number of 2.

4.2 The different stages in oblique transition

This section contains a brief description of the characteristic stages observed in oblique transition, accompanied by experimental results which exemplify some of its features.

Forcing of streamwise vortices through nonlinear interactions

The first stage in the oblique transition scenario is the generation of streamwise vortices through nonlinear interactions between the oblique waves. It was shown in section 2.3.1 that the first generation of nonlinear interactions between the pair of waves $(1,\pm 1)$ will result in an energy transfer to the $(0,\pm 2)$ -modes (or the streamwise vortex modes). The generation of vortices from the oblique waves can also be understood by considering the streamwise component of the vorticity equation (see Elofsson & Alfredsson 1998). If the nonlinear forcing terms in the equation are averaged over one period in time, the net contribution is seen to form a pattern which would give rise to streamwise vortices.

Transient growth of streaks

Streamwise vortices, forced by the oblique waves, will generate streaks through an interaction with the mean shear (a process also known as lift-up). The streaks will grow in amplitude and come to dominate the structure of the flow. In addition to the streaks, a Λ -structure is also observed as the flow evolves. These vortices appear in a staggered pattern and they are clearly seen in figure 4.1. The appearance of Λ -vortices can also be seen in hot-wire

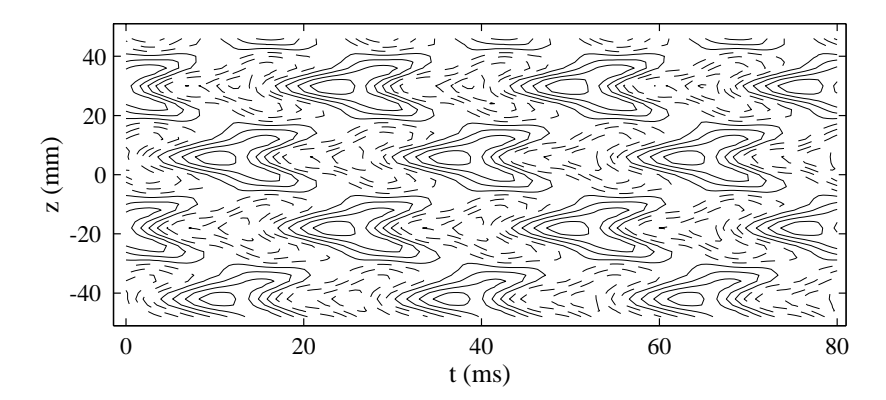


FIGURE 4.2. Contours of u obtained from measurements at x = 300 mm and $y/\delta^* = 0.9$ in a Blasius flow.

measurements (figure 4.2). This figure shows the evolution in time of the total velocity with the time-averaged field subtracted for the boundary layer on a flat plate.

4.2.1 Breakdown caused by streak instability. The last stage in the oblique transition scenario can be described as streak breakdown due to a secondary instability operating on the streaks (not to be confused with the secondary instability theory for TS-waves).

It was found by Reddy et al. (1998) that the threshold energy for transition in channel flows through streak breakdown is at least two orders of magnitude lower than for transition initiated by TS-waves at subcritical Reynolds numbers. The streaks were either initiated by streamwise vortices directly or by vortices generated from a pair of oblique waves. The experimental study by Elofsson, Kawakami & Alfredsson (1997) on streak instability in plane Poiseuille flow showed that growth rates for the secondary instability increased linearly with the streak amplitude and that the most unstable mode was sinuous. The streaks were generated by continuous suction through slits and the secondary instability was studied by using controlled forcing from an earphone or a pair of earphones. Figure 4.3 shows some results from this investigation of the instability of streaks. The top figure (a) shows the N-factor $(\ln(u/u_0))$ plotted against the streamwise coordinate for initial amplitudes ranging from $u_{rms}=0.12\%$ to 0.6%. From the figure it is clear that the initial growth rate is independent of the forcing amplitude over a fairly wide amplitude range. Figure 4.3(b) displays the dependence of the growth-rate, $\gamma = N/(x_1 - x_0)$, on the streak amplitude for Reynolds numbers ranging between 2000 and 2900, whereas the dependence on the angular frequency ω (=2 $\pi fh/U_{CL}$) is shown in (c). It can be noticed that since the range of amplified frequencies is rather wide, the frequencies

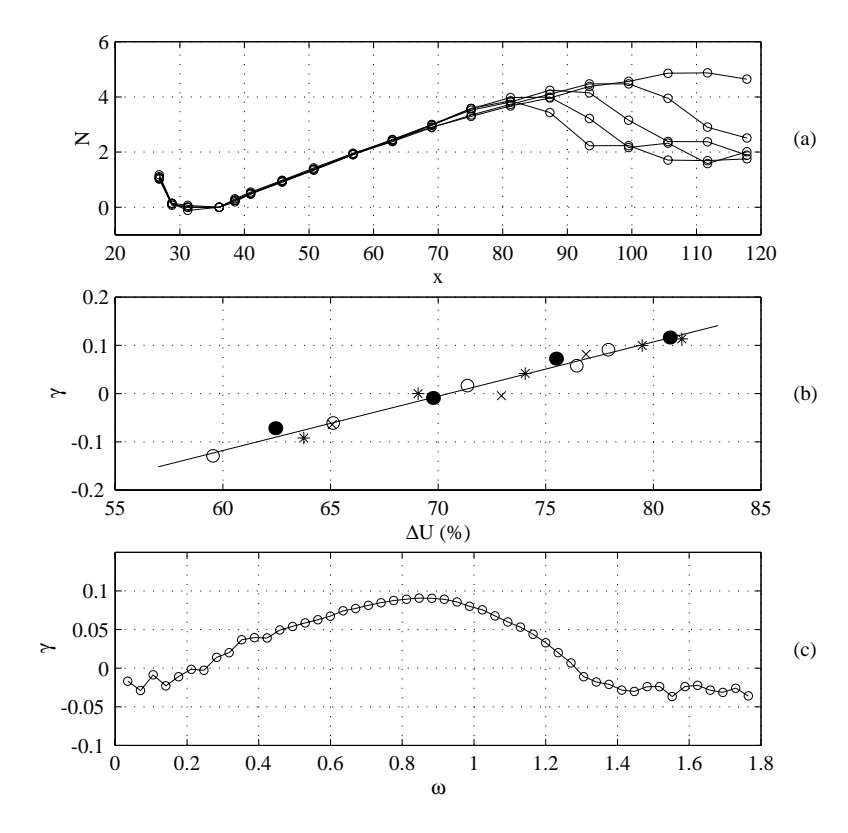


FIGURE 4.3. (a) Amplitude growth for different forcing amplitudes. (b) The dependence of γ on ΔU_{max} for three different $Re: \circ, 2000; \bullet, 2500; *, 2900.$ (c) The dependence of γ on forcing frequency ω .

seen in the breakdown stage of oblique transition will probably be the harmonics to the initial waves which are in the amplified range, which is in contrast to the situation where streak breakdown is initiated by random background disturbances.

In the work by Waleffe (1995, 1997), breakdown of streaks was identified as one element in a self-sustaining process for shear flow instability. The process described by Waleffe also occurs in the near-wall region of turbulent shear flows at high Re.

Experimental observations of the breakdown give a similar view in plane Poiseuille and Blasius flow. Spectra indicates that harmonics to the fundamental frequency grow in the downstream direction and later, the spectra are also filled between the harmonics. At some positions velocity signals show large fluctuations occurring locally within the fundamental period.

4.3 Oblique transition in relation to other scenarios

What are the similarities between oblique transition and other studies of transition? A staggered pattern of Λ -vortices is usually connected to subharmonic transition but is also observed in transition starting from a pair of oblique waves (see figure 4.2). This is not that surprising since once the oblique waves in the subharmonic scenario have reached a sufficient amplitude, the same nonlinear interactions as seen in oblique transition should be activated. Similarities between oblique transition and K- and N-type transition are further described in Berlin $et\ al.\ (1998).$

Elongated regions of high and low-speed fluid are observed in investigations of localized disturbances and the growth of these disturbances has been shown to be due to a linear mechanism. Yet another example of a flow situation which show similarities with oblique transition is transition influenced by free stream turbulence. The wall-normal distribution of the streamwise disturbance velocity and a disturbance growth proportional to $x^{1/2}$ are similar in both cases.

CHAPTER 5

Summary of papers

Paper 1

This paper describes results from hot-wire measurements of oblique transition in an air channel. The aim of the study was to experimentally investigate transition originating from a pair of oblique waves, which at the time the study was initiated, had recently been shown from direct numerical simulations (Schmid & Henningson 1992) to cause rapid transition at subcritical Reynolds numbers. A pair of oblique waves were generated with vibrating ribbons mounted at oblique angles to the flow direction, with one ribbon at each channel wall.

The oblique waves resulted in a growth of elongated structures of alternating high- and low-speed fluid in the spanwise direction (denoted streamwise streaks). For the investigated wave angles, transition was seen to occur through the growth of higher harmonics to the generated waves if the amplitude of the streamwise streaks become large. For amplitudes below the threshold, the streaks decayed slowly downstream after the initial growth. Fourier transforms were used for decomposing the data from the measurements into frequency-wavenumber modes, and the streamwise evolution of the energy in the modes were found to be in good qualitative agreement with earlier results from direct numerical simulations. The regions with the highest amplitude of time-dependent disturbances were found to be associated with large spanwise gradients in the mean flow. In addition, the stability characteristics of single disturbance waves at low amplitudes were determined and the results were found to be in agreement with linear stability calculations. These results extended the rather limited amount of experimental results on wave disturbances in plane Poiseuille flow previously reported in the literature.

Paper 2

The second paper considers oblique transition in a Blasius boundary layer and the investigation involved hot-wire measurements and flow visualizations in the MTL wind tunnel at the Department of Mechanics, KTH. Wave disturbances were generated through periodic blowing and suction through a transverse slit in the flat plate model and the quality of the disturbance source was verified against results from stability calculations. A dominant feature of the flow was the appearance of streamwise streaks with spanwise positions and wave length governed by the initial waves. However, the spanwise wave length of the streaks

changed during the breakdown stage and this observation was more distinct for measurements with a narrower spanwise length, which was suggested to be connected to the wave length of optimal disturbances. In addition to the streaks, Λ shaped structures were seen in contour plots of the streamwise disturbance velocity in zt-planes at upstream positions.

Fourier transforms were applied to decompose the disturbance velocity in frequency-wavenumber modes, which allowed the downstream development of the amplitude in various modes to be followed, and also wall-normal profiles of individual modes to be plotted. The flow visualizations displayed the whole transition process, from the upstream pattern of the oblique waves to the appearance of a short-wavelength motion on the side of the low-speed regions followed by a turbulent state.

Paper 3

Spatial direct numerical simulations were used to clarify the cause of a spanwise non-symmetry with respect to the channel centreline, which was observed in paper 1. The vibrating ribbons in the experiment were modeled by adding volume forces to the Navier-Stokes equations in the regions occupied by the ribbons. Both the stationary blockage effect and the time-dependent forcing from the ribbons were investigated by the use of different numerical models. The stationary blockage effect could be observed to change the flow direction close to the ribbons but was found to be of negligible influence some distance downstream. It was also found that the spanwise non-symmetry seen in the experiments resulted from the placement of the ribbons at opposite channel walls, causing the onset of nonlinear interactions to occur at different downstream positions for different cross stream coordinates.

The investigation further indicated that close agreement between simulation results and experimental data can be obtained by using a numerical model that closely reflects the actual geometry in an experimental situation.

Paper 4

In Paper 4 the last stage of the oblique transition scenario was investigated in a model experiment through hot-wire measurements and flow visualizations. The instability and breakdown of streamwise streaks was studied in a plane Poiseuille channel, both at unforced conditions and when phase-controlled forcing was applied with earphones at one of the channel walls. Local suction through slits in the wall was used for generating the streaks, which showed a linear growth with the streamwise distance in the region located closest to the slits. For an unforced secondary disturbance, exponentially growing time-dependent disturbances appeared if the amplitude of the streaks increased above a threshold amplitude. These secondary disturbances were out-of-phase across low-speed streaks which is the result of a sinuous (or anti-symmetric)

disturbance mode. The same kind of mode also appeared at forced conditions, even a symmetrically forced disturbance mode eventually developed into a sinuous mode.

Secondary disturbances at forced conditions showed an exponential growth and for streak amplitudes above the threshold, the growth rates were found to increase linearly with the streamwise co-ordinate. These observations together with a phase velocity determined to $0.69\ U_{CL}$ were similar to theoretical observations. However, the experiments differed from theory in that the threshold in streak amplitude for growth of secondary disturbances did not change with the Reynolds numbers studied in the experiments.

Acknowledgments

I wish to thank my supervisor Prof. Henrik Alfredsson for all advise and suggestions during the work and for reading and giving critique on numerous manuscripts. His great enthusiasm has also helped a lot in inspiring the work.

I would also like to direct thanks to co-authors Dr. Anders Lundbladh and Mitsuyoshi Kawakami, as well as other persons that have directly contributed to the work. Dr. Ardeshir Hanifi helped with PSE calculations and Dr. Masaharu Matsubara assisted during the flow visualisations and has given valuable advice concerning the experiments.

Thanks are also due to Prof. Dan Henningson for explanations, advice and discussions on oblique transition and related topics. Stellan Berlin, Prof. Satish Reddy and Prof. Peter Schmid have also participated in these discussions and Stellan helped during the work with the simulations.

My colleagues at the Department of Mechanics are thanked for providing a nice atmosphere. During my years in the lab I shared office with Johan Westin and Daniel Söderberg. Johan has assisted with many things during all years and Daniel has helped to solve many computer related problems. I have also enjoyed the company in the lab and on other activities together with: Andrey Bakchinov, Carl Häggmark, Bo Johansson, Viktor Kozlov, Renaud Lavalley, Björn Lindgren, Rune 'Texas' Lindgren, John Matsson, Barbro Muhammad-Klingmann, Mikael Sima, Alessandro Talamelli, Nils Tillmark and Jens Österlund.

I would like to thank Prof. H.H. Fernholz and the people at the Hermann Föttinger Institut in Berlin for making my stay in Berlin fruitful and enjoyable. A special thanks to Sebastian and Sabine Bake for their hospitality, and the course in applied fluid mechanics at the glider club.

Markus Gällstedt and Ulf Landén are thanked for many advices and skilful help with manufacturing equipment used in the experiments.

Financial support from the Swedish Research Council for Engineering Sciences (TFR) is gratefully acknowledged.

Finally I wish to thank my mother Christina and my brothers Anders and Jonas for all their support.

Bibliography

- ALFREDSSON, P. H. & MATSUBARA, M. 1996 Streaky structures in transition. In Proc. Transitional Boundary Layers in Aeronautics (Henkes, R. A. W. M. & VAN INGEN, J. L., editors), pp. 373–386, Royal Netherlands Academy of Arts and Sciences, Elsevier.
- Asai, M. & Nishioka, M. 1989 Origin of the peak-valley wave structure leading to wall turbulence. J. Fluid Mech. 208, 1–23.
- Bakchinov, A. A., Westin, K. J. A., Kozlov, V. V. & Alfredsson, P. H. 1998 Experiments on localized disturbances in a flat plate boundary layer. Part 2. Interaction between localized disturbances and TS-waves. *Eur. J. Mech., B/Fluids* (accepted).
- BAKE, S., KACHANOV, Y. S. & FERNHOLZ, H. H. 1996 Subharmonic K-regime of boundary-layer breakdown. In *Proc. Transitional Boundary Layers in Aeronautics* (Henkes, R. A. W. M. & VAN INGEN, J. L., editors), pp. 81–88, Royal Netherlands Academy of Arts and Sciences. Elsevier.
- Berlin, S., Lundbladh, A. & Henningson, D. S. 1994 Spatial simulations of oblique transition in a boundary layer. *Phys. Fluids* 6, 1949–1951.
- Berlin, S., Wiegel, M. & Henningson, D. S. 1998 Numerical and experimental investigations of oblique boundary layer transition. *J. Fluid Mech.* (submitted).
- Bertolotti, F. P. 1991 *Linear and Nonlinear Stability of Boundary Layers with Streamwise Varying Properties.* PhD thesis, The Ohio State University, Department of Mechanical Engineering, Columbus, Ohio.
- Breuer, K. S., Dzenitis, E. G., Gunnarsson, J. & Ullmar, M. 1996 Linear and nonlinear evolutions of boundary layer instabilities generated by acoustic-receptivity mechanisms. *Phys. Fluids* 8, 1415–1423.
- Breuer, K. S. & Haritonidis, J. H. 1990 The evolution of a localized disturbance in a laminar boundary layer. Part I: Weak disturbances. J. Fluid Mech. 220, 569–594.
- Carlson, D. R., Widnall, S. E. & Peeters, M. F. 1982 A flow visualization study of transition in plane Poiseuille flow. *J. Fluid Mech.* **121**, 487–505.
- CHANG, C.-L. & MALIK, M. R. 1994 Oblique-mode breakdown and secondary instability in supersonic boundary layers. J. Fluid Mech. 273, 323–360.
- COHEN, J., BREUER, K. S. & HARITONIDS, J. H. 1991 On the evolution of a wave packet in a laminar boundary layer. *J. Fluid Mech.* **225**, 575–606.
- CORKE, T. C., KRULL, J. D. & GHASSEMI, M. 1992 Three-dimensional-mode resonance in far wakes. J. Fluid Mech. 239, 99–132.
- CORKE, T. C. & MANGANO, R. A. 1989 Resonant growth of three-dimensional modes in transitional Blasius boundary layers. J. Fluid Mech. 209, 93–150.
- CRAIK, A. D. D. 1971 Nonlinear resonant instability in boundary layers. J. Fluid Mech. 50, 393–413.
- Davies, S. J. & White, C. M. 1928 An experimental study of the flow of water in pipes of rectangular section. *Proc. Roy. Soc. Lond. Ser. A* 119, 92–107.
- Ellingsen, T. & Palm, E. 1975 Stability of linear flow. Phys. Fluids ${\bf 18},\,487-488.$
- ELOFSSON, P. A. 1998 An experimental study of oblique transition in a Blasius boundary layer flow. TRITA-MEK, Technical Report 1998:4, Dept. of Mechanics, KTH, Stockholm.
- ELOFSSON, P. A. & Alfredsson, P. H. 1995 Experiments on nonlinear interaction between oblique Tollmien-Schlichting waves. In *Laminar-Turbulent Transition* (Kobayashi, R., editor), pp. 465–472, IUTAM Symposium, Sendai 1994, Springer.

- ELOFSSON, P. A. & ALFREDSSON, P. H. 1998 An experimental study of oblique transition in plane Poiseuille flow. *J. Fluid Mech.* 358, 177–202.
- ELOFSSON, P. A., KAWAKAMI, M. & ALFREDSSON, P. H. 1997 Experiments on the stability of streamwise streaks in plane Poiseuille flow. *Phys. Fluids* (submitted).
- ELOFSSON, P. A. & LUNDBLADH, A. 1994 Ribbon induced oblique transition in plane Poiseuille flow. In *Bypass Transition Proceedings from a Mini Workshop* (HENNINGSON, D. S., editor), pp. 29–41, TRITA-MEK, Technical Report 1994:14, Dept. of Mechanics, KTH, Stockholm.
- FASEL, H. & KONZELMANN, U. 1990 Non-parallel stability of a flat-plate boundary layer using the complete Navier-Stokes equations. J. Fluid Mech. 221, 311–347.
- FASEL, H., THUMM, A. & BESTEK, H. 1993 Direct numerical simulation of transition in supersonic boundary layers: Oblique breakdown. In *Transitional and turbulent com*pressible flows, ASME FED-Vol. 151 (KRAL, L. D. & ZANG, T. A., editors), pp. 77–92.
- Gaponenko, V. R. & Kachanov, Y. S. 1994 New methods of generation of controlled spectrum instability waves in the boundary layers. In *International Conference on Methods of Aerophysical Research*. Part 1, pp. 90–97, Novosibirsk, ITAM.
- Gaster, M. 1974 On the effects of boundary-layer growth on flow stability. *J. Fluid Mech.* **66.** 465–480.
- Gaster, M. 1975 A theoretical model for the development of a wave packet in a laminar boundary layer. *Proc. Roy. Soc. Lond. Ser. A* **347**, 271–289.
- GASTER, M. & GRANT, I. 1975 An experimental investigation of the formation and development of a wave packet in a laminar boundary layer. Proc. Roy. Soc. Lond. Ser. A 347, 253–269
- Gathmann, R. J., Si-Ameur, M. & Mathey, F. 1993 Numerical simulations of three-dimensional natural transition in the compressible confined shear layer. *Phys. Fluids A* 5, 2946–2968.
- GREK, H. R., KOZLOV, V. V. & RAMAZANOV, M. P. 1985 Three types of disturbances from the point source in the boundary layer. In *Laminar-Turbulent Transition* (KOZLOV, V. V., editor), pp. 267–272, IUTAM Symposium, Novosibirsk 1984, Springer.
- Gustavsson, L. H. 1991 Energy growth of three-dimensional disturbances in plane Poiseuille flow. J. Fluid Mech. 224, 241–260.
- HALLBÄCK, M., HENNINGSON, D. S., JOHANSSON, A. V. & ALFREDSSON, P. H. 1996 Turbulence and transition modelling. Kluwer.
- Henningson, D. S. 1995 Bypass transition and linear growth mechanisms. In $Advances\ in\ Turbulence\ V$ (Benzi, R., editor), pp. 190–204, Kluwer.
- Henningson, D. S. & Alfredsson, P. H. 1987 The wave structure of turbulent spots in plane Poiseuille flow. J. Fluid Mech. 178, 405–421.
- Henningson, D. S., Johansson, A. V. & Alfredsson, P. H. 1994 Turbulent spots in channel flows. *J. Eng. Math.* **28**, 21–42.
- Henningson, D. S., Lundbladh, A. & Johansson, A. V. 1993 A mechanism for bypass transition from localized disturbances in wall bounded shear flows. *J. Fluid Mech.* **250**, 169–207.
- Herbert, T. 1983 Secondary instability of plane channel flow to subharmonic three-dimensional disturbances. *Phys. Fluids* **26**, 871–874.
- HERBERT, T. 1988 Secondary instability of boundary layers. Ann. Rev. Fluid Mech. 20, 487–526.
- HULTGREN, L. S. & GUSTAVSSON, L. H. 1981 Algebraic growth of disturbances in a laminar boundary layer. *Phys. Fluids* **24**, 1000–1004.

- JOSLIN, R. D., STREETT, C. L. & CHANG, C. L. 1993 Spatial direct numerical simulations of boundary-layer transition mechanisms: Validation of PSE theory. Theor. Comp. Fluid Dyn. 4, 271–288.
- KACHANOV, Y. S. 1987 On the resonant nature of the breakdown of a laminar boundary layer. J. Fluid Mech. 184, 43–74.
- KACHANOV, Y. S. 1994 Physical mechanisms of laminar-boundary-layer transition. Ann. Rev. Fluid Mech. 26, 411–482.
- KACHANOV, Y. S., KOZLOV, V. V. & LEVCHENKO, V. Y. 1977 Nonlinear development of a wave in a boundary layer. *Izv. Akad. Nauk SSSR, Mekh. Zhid. Gaza.* **3**, 49–53. (in Russian, English transl. 1978 in *Fluid Dyn.* **12**, 383–390).
- KACHANOV, Y. S., KOZLOV, V. V., LEVCHENKO, V. Y. & RAMAZANOV, M. P. 1985 On nature of K-breakdown of a laminar boundary layer. New experimental data. In *Laminar-Turbulent Transition* (KOZLOV, V. V., editor), pp. 61–73, IUTAM Symposium, Novosibirsk 1984, Springer.
- KACHANOV, Y. S. & MICHALKE, A. 1994 Three-dimensional instability of flat-plate boundary-layers: Theory and experiment. *Eur. J. Mech.*, *B/Fluids* 13, 401–422.
- KAO, T. W. & PARK, C. 1970 Experimental investigations of the stability of channel flows. Part 1. Flow of a single liquid in a rectangular channel. J. Fluid Mech. 43, 145–164.
- Kendall, J. M. 1985 Experimental study of disturbances produced in a pre-transitional laminar boundary layer by weak freestream turbulence. AIAA Paper 85-1695.
- KENDALL, J. M. 1990 Boundary layer receptivity to freestream turbulence. AIAA Paper 90-1504.
- Kendall, J. M. 1991 Studies on laminar boundary-layer receptivity to freestream turbulence near a leading edge. In *Boundary Layer Stability and Transition to Turbulence* (Reda, D. C., Reed, H. L. & Kobayashi, R., editors), volume 114, pp. 23–30.
- Kendall, J. M. 1998 Experiments on boundary-layer receptivity to freestream turbulence. AIAA Paper 98-0530.
- Kim, J. & Moser, R. 1989 On the secondary instability in plane Poiseuille flow. Phys. Fluids A 1, 775–777.
- Klebanoff, P. S., Tidstrom, K. D. & Sargent, L. M. 1962 The three-dimensional nature of boundary layer instability. *J. Fluid Mech.* 12, 1–34.
- KLEISER, L. & ZANG, T. A. 1991 Numerical simulation of transition in wall-bounded shear flows. Ann. Rev. Fluid Mech. 23, 495–537.
- KLINGMANN, B. G. B. 1991 Laminar-turbulent transition in plane Poiseuille flow. PhD thesis, KTH, Stockholm, Sweden.
- KLINGMANN, B. G. B., BOIKO, A. V., WESTIN, K. J. A., KOZLOV, V. V. & ALFREDSSON, P. H. 1993 Experiments on the stability of Tollmien-Schlichting waves. Eur. J. Mech., B/Fluids 12, 493-514.
- Landahl, M. T. 1977 Dynamics of boundary layer turbulence and the mechanism of drag reduction. *Phys. Fluids* **20** (10, Part II), 55–63.
- Landahl, M. T. 1980 A note on an algebraic instability of inviscid parallel shear flows. *J. Fluid Mech.* **98**, 243–251.
- LIEPMANN, H. W., BROWN, G. L. & NOSENCHUCK, D. M. 1982 Control of laminar-instability waves using a new technique. J. Fluid Mech. 118, 187–200.
- LUCHINI, P. 1996 Reynolds-number-independent instability of the boundary layer over a flat surface. J. Fluid Mech. 327, 101–115.
- Lundbladh, A., Schmid, P. J., Berlin, S. & Henningson, D. S. 1994 Simulations of bypass transition for spatially evolving disturbances. AGARD-CP-551.
- MACK, L. M. 1984 Line sources of instability waves in a Blasius boundary layer. AIAA Paper 84-0168.

- MEKSYN, D. & STUART, J. T. 1951 Stability of viscous motion between parallel planes for finite disturbances. *Proc. Roy. Soc. Lond. Ser. A* 208, 517–526.
- NIKURADSE, J., 1933 Experimentelle Untersuchungen zur Turbulenzentstehung. Z. angew. Math. Mech., Bd.13, 174–176.
- NISHIOKA, M. & ASAI, M. 1985 Some observations of the subcritical transition in plane Poiseuille flow. J. Fluid Mech. 150, 441–450.
- NISHIOKA, M., IIDA, S. & ICHIKAWA, Y. 1975 An experimental investigation of the stability of plane Poiseuille flow. J. Fluid Mech. 72, 731–751.
- Orszag, S. A. 1971 Accurate solution of the Orr-Sommerfeld stability equation. *J. Fluid Mech.* **50**, 689–703.
- Orszag, S. A. & Kells, L. C. 1980 Transition to turbulence in plane Poiseuille and plane Couette flow. J. Fluid Mech. 96, 159–205.
- Orszag, S. A. & Patera, A. T. 1983 Secondary instability of wall-bounded shear flows. *J. Fluid Mech.* 128, 347–385.
- Patel, V. C. & Head, M. R. 1969 Some observations in skin friction and velocity profiles in fully developed pipe and channel flows. *J. Fluid Mech.* 38, 181–201.
- RAMAZANOV, M. P. 1985 Development of finite amplitude disturbances in Poiseuille flow. In *Laminar-Turbulent Transition* (KOZLOV, V. V., editor), pp. 183–190, IUTAM Symposium, Novosibirsk 1984, Springer.
- Reddy, S. C., Schmid, P. J., Baggett, J. S. & Henningson, D. S. 1998 On stability of streamwise streaks and transition thresholds in plane channel flows. *J. Fluid Mech.* (in press).
- RILEY, J. J. & GAD-EL HAK, M. 1985 The dynamics of turbulent spots. In *Frontiers of Fluid Mechanics* (DAVIS, S. H. & LUMLEY, J. L., editors), pp. 123–155, Springer.
- ROBEY, H. F. 1987 On the use of a phased heater array for the controlled excitation of arbitrary three-dimensional perturbations in a laminar boundary layer. *Exp. Fluids* 5, 33–35
- Saiki, E. M., Biringen, S., Danabasoglu, G. & Streett, C. L. 1993 Spatial simulation of secondary instability in plane channel flow: comparison of K- and H-type disturbances. *J. Fluid Mech.* **253**, 485–507.
- Sandham, N. D., Adams, N. A. & Kleiser, L. 1994 Direct simulation of breakdown to turbulence following oblique instability waves in a supersonic boundary layer. In *Direct and Large-Eddy Simulation I* (Voke, P. R., Kleiser, L. & Chollet, J. P., editors), pp. 213–223, Kluwer.
- Sandham, N. D. & Kleiser, L. 1992 The late stages of transition to turbulence in channel flow. J. Fluid Mech. 245, 319–348.
- SARIC, W. S. 1990 Low-speed experiments: requirements for stability measurements. In *Instability and Transition I* (Hussaini, M. Y. & Voigt, R. G., editors), pp. 162–174, Springer.
- SARIC, W. S., HOOS, J. A. & RADEZTSKY, R. H. 1991 Boundary-layer receptivity of sound with roughness. In *Boundary Layer Stability and Transition*, ASME FED-Vol. 114 (REDA, D. C., REED, H. L. & KOBAYASHI, R., editors), pp. 17–22.
- Schmid, P. J. & Henningson, D. S. 1992 A new mechanism for rapid transition involving a pair of oblique waves. *Phys. Fluids A* 4, 1986–1989.
- Schubauer, G. B. & Skramstad, H. K. 1947 Laminar boundary layer oscillations and the stability of laminar flow. *J. Aero. Sci.* 14, 69–78.
- Shaikh, F. N. & Gaster, M. 1994 The nonlinear evolution of modulated waves in a boundary layer. J. Eng. Math. 28, 55–71.
- SINGER, B. A., REED, H. L. & FERZIGER, J. H. 1989 The effects of streamwise vortices on transition in the plane channel. *Phys. Fluids A* 1, 1960–1971.

- Squire, H. B. 1933 On the stability for three-dimensional disturbances of viscous fluid flow between parallel walls. *Proc. Roy. Soc. Lond. Ser. A* 142, 621–8.
- STUART, J. T. 1960 On the nonlinear mechanics of wave disturbances in stable and unstable parallel flows. Part 1. The basic behaviour in plane Poiseuille flow. *J. Fluid Mech.* 9, 353–370.
- Thomas, A. S. W. & Saric, W. S. 1981 Harmonic and subharmonic waves during boundary-layer transition. *Bull. Am. Phys. Soc.* 26, 1252.
- Trefethen, L. N., Trefethen, A. E., Reddy, S. C. & Driscoll, T. A. 1993 Hydrodynamic stability without eigenvalues. *Science* **261**, 578–584.
- Voke, P. R. & Yang, Z. 1995 Numerical study of bypass transition. *Phys. Fluids* 7, 2256–2264.
- WALEFFE, F. 1995 Hydrodynamic stability and turbulence: Beyond transients to a self-sustaining process. *Stud. Appl. Math.* **95**, 319–343.
- Waleffe, F. 1997 On a self-sustaining process in shear flows. Phys. Fluids 9, 883–900.
- Watson, J. 1960 On the nonlinear mechanics of wave disturbances in stable and unstable parallel flows. Part 2. The development of a solution for plane Poiseuille and for plane Couette flow. J. Fluid Mech. 9, 371–389.
- Westin, K. J. A., Boiko, A. V., Klingmann, B. G. B., Kozlov, V. V. & Alfredsson, P. H. 1994 Experiments in a boundary layer subjected to free-stream turbulence. Part I. Boundary layer structure and receptivity. *J. Fluid Mech.* **281**, 193–218.
- WIEGEL, M. 1996 Experimentelle Untersuchung von kontrolliert angeregten dreidimensionalen Wellen in einer Blasius-Grenzschicht. PhD thesis, TH Hannover.
- Wygnanski, I., Sokolov, M. & Friedman, D. 1976 On the turbulent spot in a laminar boundary layer. J. Fluid Mech. 78, 785–819.

An experimental study of oblique transition in a Blasius boundary layer flow

PER A. ELOFSSON

Department of Mechanics, KTH, S-100 44 Stockholm, Sweden

Abstract

Transition initiated by a pair of oblique waves was investigated experimentally in a Blasius boundary layer flow by using hot-wire measurements and flow visualisation. The oblique waves were generated by periodic blowing and suction through an array of pipes connecting to the flow through a transverse slit in the flat plate model. The structure of the flow field is described and the amplitude of individual frequency-spanwise wave number modes was determined from Fourier transforms of the disturbance velocity. In contrast to results from investigations of oblique transition at subcritical flow conditions, the transition process at the present conditions suggests the combined effect of transient growth of streaks and a second stage with exponential growth of oblique waves to initiate the final breakdown stage.

1 Introduction

The importance of three-dimensional disturbances in the transition process has been recognized since the boundary layer measurements by Klebanoff, Tidstrom & Sargent (1962), who found it necessary to control the three-dimensionality in their experiments by placing strips of tape below the vibrating ribbon used for generating wave disturbances. The secondary instability scenario considers initially two-dimensional (Tollmien–Schlichting or TS) waves which grow in amplitude and develop into a three-dimensional stage. Two different three-dimensional stages have been identified, one in which Λ -shaped structures appear in an aligned pattern and another stage where Λ -shaped structures are seen in a staggered pattern. Transition involving the former is usually denoted K-type (after the first investigation by Klebanoff et al. 1962) or fundamental transition, whereas the staggered structures are part of the transition scenario denoted H-type, N-type or subharmonic. The first experimental observation of subharmonic transition was made by Kachanov, Kozlov & Levchenko (1977) and the transition scenario

has later been carefully investigated by Corke & Mangano (1989) with the use of controlled two- and three-dimensional waves.

The secondary instability theory was put forward by Orszag & Patera (1983) and Herbert (1983). Further information on the concept of secondary instability can be found in the review by Herbert (1988). Experimental studies on the breakdown mechanisms of boundary layer flows are described by Kachanov (1994) and information on numerical investigations is presented in the review by Kleiser & Zang (1991).

Results both from experiments with forced TS-waves and direct numerical simulations (DNS) have indeed been in close agreement with the secondary instability theory, but this scenario needs a two-dimensional wave to be present. An alternative route to transition in contrast to the secondary instability mechanism may be the so-called oblique transition scenario, which operates without the need for a two-dimensional wave.

1.1 Oblique transition. Oblique transition originates from the nonlinear interaction between a pair of oblique waves with wave angles of equal magnitude but opposite sign. Nonlinear interaction distributes disturbance energy among various wave numbers, and in particular to low streamwise wave numbers which can experience a strong growth due to a linear mechanism. This so-called transient growth of the streamwise independent structures is essentially due to the combined effect of an inviscid growth and a viscous decay. However, if the amplitude of the streamwise streaks reaches above a threshold the streaks may become unstable with respect to low amplitude time-dependent disturbances and the flow may break down. Since the transition scenario utilizes the transient growth mechanism, which is operative also at low Reynolds number, transition can occur at subcritical Re.

The first study of oblique transition in an incompressible flow was the direct numerical simulations by Schmid & Henningson (1992). They used a pair of finite amplitude oblique waves as initial conditions in temporal simulations of transition in plane Poiseuille flow at subcritical Reynolds numbers. The use of oblique waves resulted in a rapid growth of disturbance energy followed by breakdown. This growth was identified to result from a linear mechanism and the dominating structure was a streamwise independent structure with twice the spanwise wavenumber of the original oblique waves. When compared with the traditional secondary instability scenario starting with similar initial disturbance energy, oblique transition was found to be considerably faster.

Other investigations of oblique transition are the calculations using PSE theory and spatial DNS by Joslin, Streett & Chang (1993) and the spatial DNS by Berlin, Lundbladh & Henningson (1994). Both of these studies governed oblique

transition in a boundary layer flow at zero pressure gradient. Joslin et al. did not reach a fully developed turbulent stage despite a longer computational box and a higher Re at the inflow. It was suggested that the reason for this was a difference in inflow conditions. Berlin et al. used Orr–Sommerfeld modes where the normal vorticity was excluded whereas Joslin et al. made use of complete eigenmodes. Berlin et al. also conjectured that oblique transition in shear flows involves three stages. Firstly, a nonlinear generation of streamwise vortices by the oblique waves; secondly, generation of streaks through the lift-up effect; and thirdly, breakdown due to a secondary instability operating on the streaks.

Elofsson & Alfredsson (1995, 1998) made experiments on oblique transition in plane Poiseuille, where the pair of waves were generated by two vibrating ribbons mounted at opposite channel walls. For initial wave amplitudes in a lower range, elongated streamwise structures slowly decayed after an initial growth. For higher wave amplitudes, disturbances with a fundamental or superharmonic frequency to the initial waves increased in amplitude and breakdown eventually occurred. The experimental findings confirmed the results from the previous numerical simulations.

An experimental investigation of oblique transition in a flat plate boundary layer was carried out at DLR in Göttingen by Wiegel (1996). He used particle image velocimetry (PIV) and hot-wire anemometry to document the flow field obtained by controlled forcing with a wave generator using blowing and suction. These measurements showed the flow structure and provided information about the growth in streak amplitude and u_{rms} in various frequency bands.

Berlin, Wiegel & Henningson (1998) presented a comparison between the measurements of Wiegel and direct numerical simulations. The closest agreement was obtained when the experimental wave generator was modelled in detail by prescribing the boundary conditions for the wall-normal disturbance velocity at the wall in a step-wise fashion, and by using different amplitudes for positive and negative disturbance velocity. By imposing a pressure gradient in the simulations, the initial agreement with the experimental data was further improved. Berlin et al. also described the similarities between oblique transition and the two transition scenarios that are described with the secondary instability theory (K- and N-type transition).

The importance of a pair of oblique waves has also been recognized in other flow situations, thus indicating a generality of the transition scenario. For a flat plate boundary layer at low supersonic Mach numbers, the most unstable modes are oblique. This fact makes the oblique transition concept perhaps even more interesting in compressible flows. Fasel, Thumm & Bestek (1993) investigated two

different transition scenarios in a compressible boundary layer at a Mach number of 1.6 with the aid of direct numerical simulations. Despite a lower initial amplitude, the simulation with a pair of oblique waves as boundary conditions resulted in much faster breakdown than for their simulation of fundamental transition (i.e. transition initiated by a two-dimensional wave and a pair of oblique waves with a fundamental frequency). Similar results were obtained by Chang & Malik (1994) who used nonlinear PSE calculations to compare oblique and subharmonic transition at a Mach number of 1.6. They found that transition originating from a pair of oblique waves required lower initial amplitudes than for the secondary instability of subharmonic type. It is important to recognize that once the amplitude of the oblique waves in the subharmonic transition scenario becomes large, similar conditions exist as for the initial stage in oblique transition and a similar downstream development can therefore be expected.

Other studies of oblique transition are those of Gathmann, Si-Ameur & Mathey (1993) in a supersonic shear layer and Sandham, Adams & Kleiser (1994) in a compressible flat plate boundary layer at a Mach number of 2.

1.2 Transient growth. The second stage in the oblique transition scenario is the generation and transient growth of streaks. Transient growth results from an inviscid algebraic instability (see Ellingsen & Palm 1975 and Landahl 1980) which is limited by viscous damping.

One of the first studies which showed the existence of transient growth in a viscous flow was the work by Hultgren & Gustavsson (1981). They investigated the temporal development of three-dimensional disturbances in a parallel boundary layer flow and found an initial linear growth followed by a viscous decay. Later investigations of transient growth have been able to quantify the growth in different flow situations and also to determine the optimal disturbance type. Some examples of studies of transient growth are Boberg & Brosa (1988), Gustavsson (1991), Butler & Farrell (1992), Klingmann (1992) and Trefethen et al. (1993). For further references see the review by Henningson (1995).

Recent work on the spatial instability in Blasius flows have shown that the largest spatial energy growth occurs for streamwise vortices near the leading edge which evolves into streamwise streaks further downstream. Luchini (1997) used a Reynolds number independent formulation and found that the maximum spatial growth occurred for vortices with a spanwise wavenumber of $\beta\delta=0.45$, ($\beta=2\pi/\lambda_z$ where λ_z is the spanwise wavelength and $\delta=\sqrt{\nu x/U_0}$). The same value of the optimal spanwise wavenumber was also found by Andersson, Berggren & Henningson (1998) for $Re_x=10^6$ and larger. In addition to these results they also proposed a simple model for prediction of the transition location. The model

involved a single constant which was found to correlate well with experimental data on transition at free stream turbulence levels ranging from 1% to 5%.

1.3 Breakdown of streaks. The last stage in the oblique transition scenario can be described as streak breakdown due to a secondary instability operating on the streaks (not to be confused with the secondary instability theory for TS-waves). For streaks initiated either by streamwise vortices directly or by vortices generated from a pair of oblique waves, Reddy et al. (1998) found that the threshold energy for transition in channel flows through streak breakdown is at least two orders of magnitude lower than for transition initiated by TS-waves at subcritical Reynolds numbers.

An experimental work by Elofsson, Kawakami & Alfredsson (1997) on streak instability in plane Poiseuille flow showed that growth rates for the secondary instability increased linearly with the streak amplitude and that the most unstable mode was sinuous (or anti-symmetric). The streaks were generated by continuous suction and the secondary instability was studied by using controlled forcing from an earphone or a pair of earphones.

It can be noticed that since the range of amplified frequencies is rather wide, the frequencies seen in the breakdown stage of oblique transition will rather be the harmonics of the initial waves which are in the amplified range and not the specific frequency which experiences the largest growth. This is in contrast to the situation where streak breakdown is initiated by random background disturbances.

In the work by Waleffe (1995, 1997), streak breakdown was identified as one element in a self-sustaining process for shear flow instability. Waleffe also hypothesized that this process occurs in the near-wall region of turbulent shear flows.

Bakchinov et al. (1995) observed streak breakdown in an experimental work in a Blasius boundary layer flow. Streamwise vortices were generated by elongated roughness elements and the breakdown of the streaks were investigated both at unforced conditions and for the case with controlled excitation of wave disturbances by a vibrating ribbon. The instability of the spanwise modulated mean flow was found to be similar to the sinuous mode observed in Görtler flows.

The experimental setup is described in \S 2 with special emphasis on the method used for generating the wave disturbances. In \S 3 the flow quality is adressed, both by describing the characteristics of the mean flow and by comparing experimental results for single waves with stability theory. Experimental results on oblique transition are presented in \S 4, and \S 5 contains some further discussion and concluding remarks.

2 Experimental arrangement

The measurements were made in the MTL wind tunnel at the Department of Mechanics, KTH. This is a closed return tunnel with a streamwise turbulence intensity in the empty test-section of less than 0.02~% in the velocity range 10-60~m/s. A flat plate model was installed horizontally in the 7 m long test section (cross section $0.8~\text{by}~1.2~\text{m}^2$). The model is equipped with a trailing edge flap and has an asymmetric leading edge which results in a short pressure gradient region at the leading edge. A fine-meshed screen was installed 50 mm upstream of the hinge for the trailing edge flap. The combination of the screen and the flap was used to adjust the flow at the leading edge to compensate for the extra blockage below the plate due to the pipes and tubes for the disturbance generation, (without the screen a flap angle of about 11° would have been required). The experimental setup is shown in figure 1~(a).

A co-ordinate system is used with the x-axis in the streamwise direction, the y-axis is normal to the flat plate and the z-axis is in the spanwise direction. The origin is located on the centreline at the leading edge and the y-position is the distance from the surface of the plate. The velocities associated with the (x, y, z) co-ordinate system are (u, v, w).

The streamwise velocity component was measured with 2.5 μ m platinum single wire probes using an AN-1003 constant temperature anemometer. A calibration function of the following type was used

$$U = k_1 (E^2 - E_0^2)^{1/n} + k_2 (E - E_0)^{1/2},$$
(1)

where E is the anemometer voltage at the velocity U, E_0 the voltage at zero velocity and the coefficients k_1, k_2 and n are determined from a best fit of the data to the calibration function. The variation in the wind tunnel air temperature during measurements was within $\pm 0.1^{\circ}$ and no temperature corrections of the anemometer signal was therefore deemed necessary. The hot-wire probe was positioned with a 5-axis traversing system controlled by a Macintosh Q950. This computer also controlled the National Instruments cards that were used for data acquisition and waveform generation. In order to avoid aliasing problems, the hot-wire signal was low-pass filtered before it was acquired with a 16-bit A–D converter. Two different methods were used during the measurement sessions, either the filter built into the anemometer or an external programmable filter with a linear phase (Kemo VBF10).

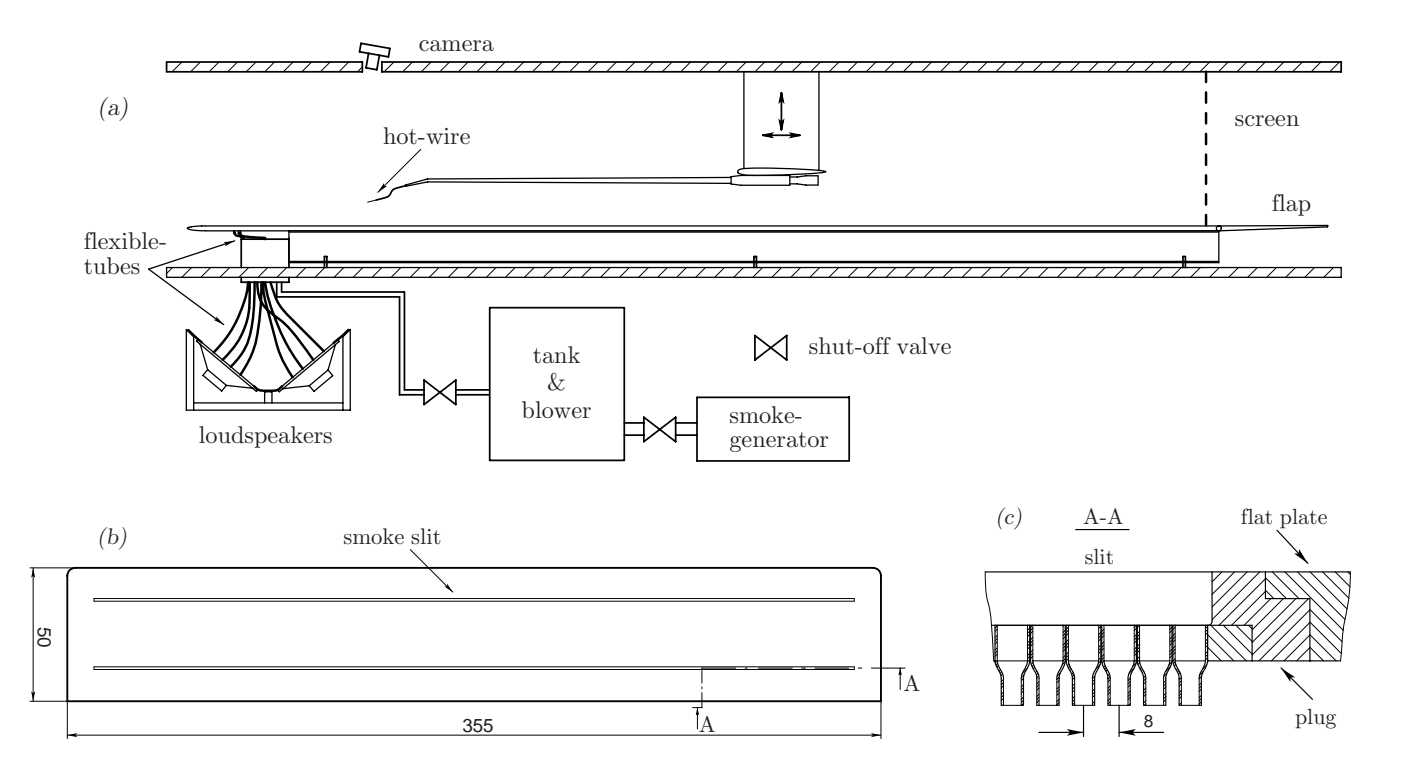


FIGURE 1. Experimental arrangement; (a) side-view of part of the test section with external equipment; (b) plug containing smoke slit and disturbance source; (c) cut-view.

For the flow visualisation studies, a thin sheet metal was placed on top of the flat plate model in the region downstream of the disturbance source. The sheet metal (with a thickness of 0.5 mm) was painted black and its upstream end was chamfered to give a smooth junction to the surface of the flat plate model. A homogeneous smoke layer was introduced inside the boundary layer through a transverse slit located 166 mm downstream of the leading edge. The smoke produced by a fog-generator entered a tank which was connected to the smoke slit in the flat plate. To control the thickness of the smoke layer, the tank was equipped with a variable pressure blower and a valve at the outlet. Pictures were taken through a hole in the upper wall with a camera mounted on the roof of the wind tunnel and light provided by a flashlight mounted downstream the camera but inside the test section.

2.1 Generation of wave disturbances. Controlled wave disturbances are generated through a transverse slit located 189 mm downstream the leading edge. The slit has a spanwise length 330 mm, a streamwise width of 0.8 mm and is 10 mm deep. An insert, consisting of 40 pipes equidistantly spaced in the spanwise direction, is mounted below the slit. The pipe outlets that face the bottom of the slit have been flattened to give a rectangular cross section and the other end of the pipes are connected to loudspeakers (diameter=254 mm, 100 W) with flexible tubes. Details of the disturbance source are shown in figure 1 together with an overview of the experimental setup. Inserts with different cross sections and spanwise spacing were manufactured, however the reported measurements were made with a pipe cross section of 0.8 mm by 6.0 mm and a spanwise spacing of 8.0 mm, unless otherwise stated. By changing the loudspeaker signals and the connection pattern of the tubes, it was possible to generate two-dimensional and/or oblique waves and also to control the spanwise wavelength (in discrete steps) of the oblique waves. The method used for disturbance generation is similar to the one reported by Bake, Kachanov & Fernholz (1996) and originally described by Gaponenko & Kachanov (1994).

At maximum six loudspeakers were used in the present measurements. The signals for the loudspeakers were generated with a 6 channel D–A board and audio amplifiers were used for driving the loudspeakers. A connector box equipped with precision potentiometers allowed fine adjustment of the amplitude of separate loudspeakers. Each loudspeaker was fitted with a cover plate from which flexible tubes connected to the pipes of the disturbance source.

The experiments were focused on measurements of transition initiated by a pair of oblique waves with equal streamwise wavenumbers and spanwise wavenumbers of equal magnitude but opposite sign. In addition to the studies of oblique transition initial measurements were also made on single oblique waves.

pipe no.	0	1	2	3	4	5
pair of waves	$2\sin(\omega t)$	$\sin(\omega t)$	$-\sin(\omega t)$	$-2\sin(\omega t)$	$-\sin(\omega t)$	$\sin(\omega t)$
single wave	$\sin(\omega t + \frac{n\pi}{3})$					

Table 1. Forcing signals for one wavelength at $\Delta \varphi = 60^{\circ}$.

A single oblique wave is obtained if the following signal is used for the loudspeaker driving the pipe with index n

$$A_n = A\sin(\omega t + n\Delta\varphi)$$

where A is the amplitude, ω is the angular frequency and $\Delta \varphi$ is the phase shift between consecutive pipes. Using the same notation, the loudspeaker signal required when generating a pair of oblique waves can be written as

$$A_n = A\sin(\omega t + n\Delta\varphi) + A\sin(\omega t - n\Delta\varphi)$$
$$= 2A\sin(\omega t)\cos(n\Delta\varphi)$$

As an example table 1 compares the signals required for a single wave and for a pair of waves when the phase shift between individual pipes is 60°. This case corresponds to the conditions used for most of the measurements and it results in a spanwise wavelength of 48 mm. From the table it can be seen that for the generation of a single oblique wave six different signals are needed for each spanwise wavelength, whereas only four different signals are required when a pair of oblique waves are being forced. Therefore, the generation of a single oblique wave requires more amplifiers, loudspeakers etc. than the generation of a pair of oblique waves at the same conditions.

Adjustment of the loudspeaker signals

The procedure for adjusting the loudspeaker signals was facilitated by the loudspeakers linear amplitude response through the whole operating range. This linearity was verified for all loudspeakers at three different frequencies; at the highest and lowest expected operating frequencies and at the mid-frequency. Although the measured value of the wave amplitude (at the generated frequency) showed an almost linear response to the loudspeaker voltage over a wide range, the amplitude of the harmonics limited the operating voltage. The maximum operating voltage was chosen to be the voltage for which the wave amplitude of the first harmonic was one decade below the amplitude at the fundamental when measuring 10 mm downstream of the disturbance source. Typically this resulted in a loudspeaker voltage of about $5.5\ V_{rms}$ at an impedance of $8\ \Omega$.

The first step in the adjustment procedure was to obtain base-settings for the speaker voltages, which was done by connecting each loudspeaker to the same set of pipes and then adjust the voltages until the measured wave amplitude was the same. This set of base voltages was found to be the same at different frequencies, although the absolute wave amplitude of course changed with the frequency. During different measurement sessions extending over a period of 18 months, the changes made in the base settings were less than 0.5 %.

The method used in the final stage of the adjustment procedure depended on which case was going to be measured. For measurements with a single oblique wave or with a pair of oblique waves using a phase shift of 90°, the procedure was quite straightforward. All loudspeakers were then connected to the corresponding pipes and the spanwise distribution of the wave amplitude was measured while the speakers were operated at their base voltages (or at the base settings multiplied with a constant). From the measured distribution the settings were adjusted and the distribution was remeasured. After the final iteration the new base settings were registered.

For the most common operating conditions with a pair of oblique waves and a phase shift of 60° between the individual pipes, the procedure was slightly different. An initial matching of speaker voltages was now first made within two groups. One group consisted of the pipes operated at a lower amplitude (pipes with numbers 1,2,4 and 5 in table 1) and the other of the pipes driven by speakers operated at a higher voltage (pipes with number 0 and 3 in table 1). The speaker voltages were matched so that the higher wave amplitudes were twice the lower ones. After this matching all loudspeakers were operated at the same time and the spanwise distribution was measured, and in some cases the loudspeaker voltages were readjusted.

After finishing the adjustment of the speakers at one wave amplitude, the voltages at a higher wave amplitude were easily obtained by multiplying all base voltages by the same constant. The spanwise uniformity in wave amplitude was always better than 1 %, whereas the variation in phase across the span was less than 0.4°. Note that for the case with a pair of oblique waves, the uniformity in amplitude applies to the amplitude at peaks and the uniformity in phase is within the regions between the 180° phase shifts.

2.2 Experimental conditions and procedure. Most of the measurements were made with free stream velocities of $U_0 = 8.2 \text{ m/s}$ or 9.1 m/s. Initial measurements with a single oblique wave were also made at lower velocities and the flow visualisations were made for velocities ranging from about 4 m/s up to 10 m/s. Wave frequencies range from f = 38 Hz to f = 80 Hz and they are usually expressed as the non-dimensional frequency parameter $(F = 2\pi f \nu \cdot 10^6/U_0^2)$.

Measurements of length are expressed in millimeters in horizontal planes whereas wall-normal distances are either given in mm or as the non-dimensional Blasius co-ordinate $(\eta = y\sqrt{U_0/\nu x})$.

As a measure of the strength of the stationary disturbance field we use U_d defined as

$$U_d(x, y, z) = \overline{U(x, y, z)} - \frac{1}{z_1 - z_0} \int_{z_0}^{z_1} \overline{U(x, y, z)} \, dz, \tag{2}$$

where z_0 and z_1 are the spanwise limits of the measurement region. For the fluctuating disturbance field we either use the amplitude (half the peak-to-peak value) or the root mean square of the streamwise disturbance velocity. These measures are denoted u' and u_{rms} , respectively. The notation u' is connected to a single frequency component (usually the generated frequency), whereas u_{rms} is the sum over all frequencies unless a specific frequency is stated, $u_{rms,f}$.

The structure of the flow was mapped out by traversing the hot-wire probe and measuring sets of data triggered by a reference signal from the waveform generation. Data was obtained in the following ways; by measuring wall-normal profiles at a fixed spanwise location for various streamwise positions (xy-plane), by traversing the probe in the spanwise direction at a fixed η for various streamwise positions (xz-plane) and by measurements of wall-normal profiles at a fixed streamwise location for various spanwise positions (yz-plane). In addition to these measurements in complete planes, numerous profiles were measured at single locations. Besides the measurements of the perturbed flow, wall-normal profiles were also measured at fully laminar (unperturbed) conditions. These profiles were used for obtaining the wall-normal position.

Each measurement position typically involved 20 triggered sets of 4096 points acquired with a sampling frequency in the range between 3.5 kHz and 5 kHz. The frequency was adjusted so that each set contained an integer number of periods of the generated wave. The laminar measurements involved fewer (untriggered) samples acquired with a lower frequency.

3 Flow quality

Information about the flow quality in the setup is presented by showing the pressure distribution along the flat plate model and also by comparing measurements for a single oblique wave with results from stability calculations.

Figure 2 shows the pressure distributions above the plate, obtained from hot-wire measurements outside the boundary layer edge and then calculated as $c_p = 1 - (u/u_{ref})^2$. Local peaks are observed in the streamwise distribution of c_p near x = 120 and x = 160 mm. The former is probably caused by a sealed

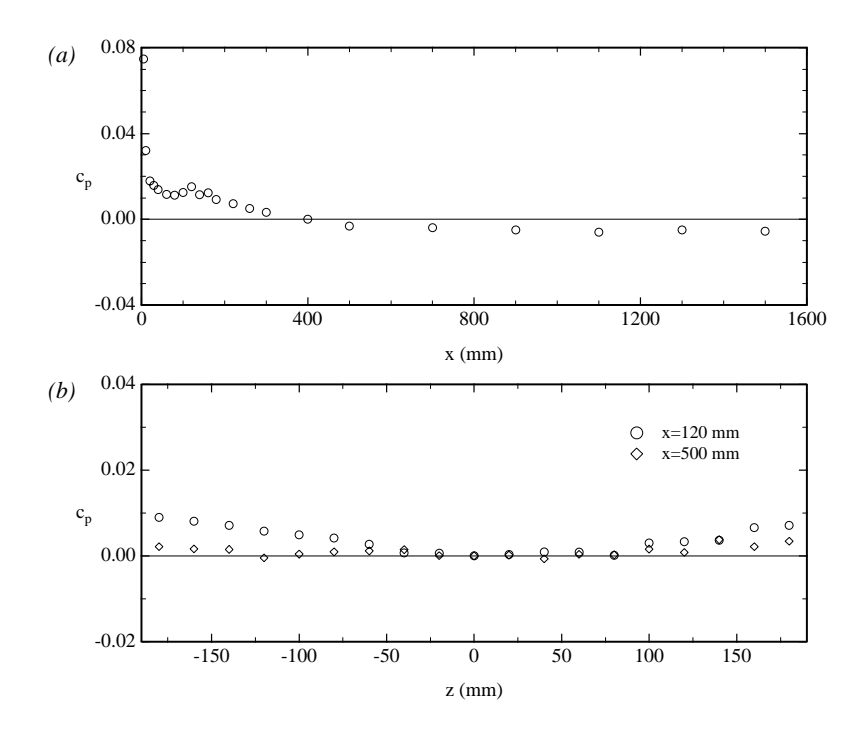


FIGURE 2. Pressure distribution obtained from hot-wire measurements for $U_0 = 7.0 \text{ m/s}$. (a) Streamwise distribution, reference position is at x = 400 mm; (b) spanwise distributions at x = 120 & 500 mm.

slit at x=95 mm, which was used in a previous experiment, whereas the latter peak is at the leading edge junction. The spanwise distribution at x=120 mm shows a minimum at z=0 and an increasing value of c_p to the sides. This is probably a result of the blockage from the tubes of the disturbance source, which extend ≈ 20 mm below the plate at a position of 190 mm from the leading edge. However, this effect is not observed in the measurements at x=500 mm.

The variation in the shape factor (H_{12}) was found to be within ≈ 0.5 % from measurements, on several occasions, at five spanwise positions over a region of $z=\pm 150$ mm for every 100 mm in the streamwise direction. However, the mean value was $H_{12}=2.63$ which is slightly above the theoretical value for a Blasius boundary layer. The reason for this deviation is not clear, but the results may suffer from not measuring close enough to the flat plate surface, to measure the y=0 position accurately.

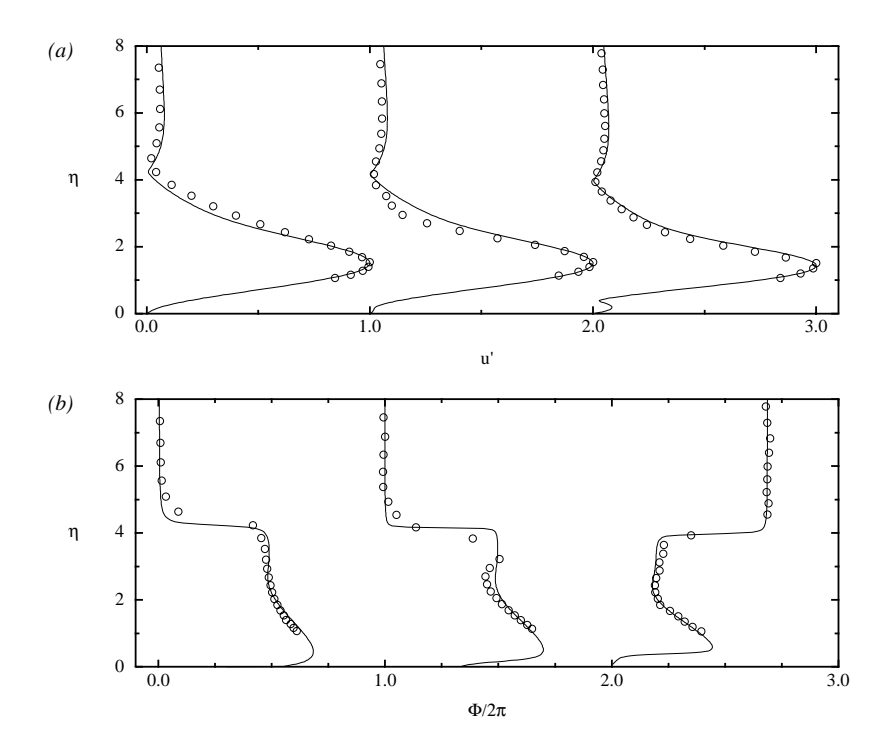


FIGURE 3. Comparison between: \circ , measurements; ——, PSE calculations by A. Hanifi. (a) Amplitude profiles at x=210, 270 and 510 mm; (b) corresponding phase profiles. F=106, $U_0=8.2\,\mathrm{m/s}$ and $\beta=131\,\mathrm{m}^{-1}$.

3.1 Comparison with stability theory. In order to verify the quality of the disturbance source, measurements were also made when a single oblique wave was generated and the results were compared with PSE calculations.

Figure 3 shows wall-normal profiles of amplitude and phase at the frequency of the generated oblique wave. Results from measurements with $U_0=8.2\,\mathrm{m/s}$ and F=106 at three different streamwise positions are compared with stability theory. The amplitudes have been normalised with their maximum (the largest amplitude from the measurements was u'=1.0~% at $x=210~\mathrm{mm}$) and the phase profiles were uniformly shifted to match in the outer part of the boundary layer. Both the amplitude and the phase profiles are in agreement with theoretical distributions at $x=510~\mathrm{mm}$, but the deviation between measurements and PSE calculations is larger closer to the disturbance source. One can note that the first amplitude and phase profiles were measured at a position located only 20 mm downstream

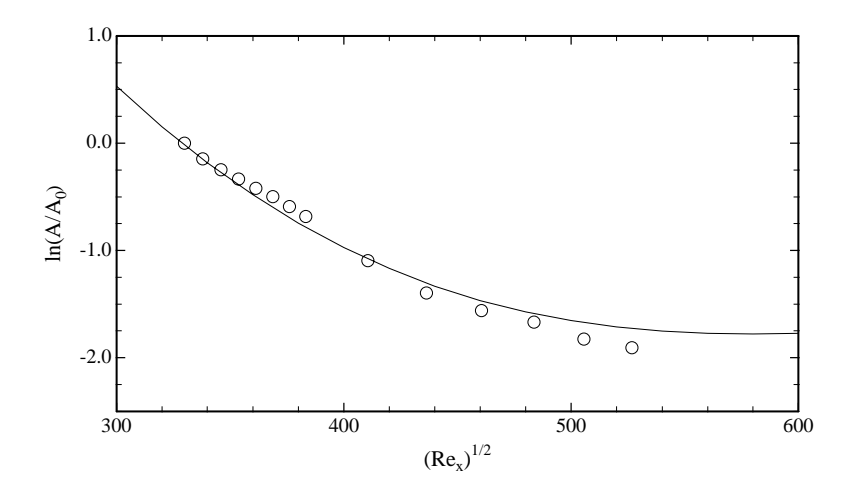


FIGURE 4. Amplitude evolution: \circ , measurements; —, PSE calculation by A. Hanifi. F = 59, $U_0 = 8.2 \,\mathrm{m/s}$ and $\beta = 131 \,\mathrm{m^{-1}}$.

of the slit. This distance should be related to the streamwise wavelength at these conditions which is ≈ 41 mm.

The streamwise evolution of the maximum of a measured amplitude is compared with PSE results in figure 4. These experimental data were obtained by traversing the hot-wire probe through the amplitude maximum at conditions for which $U_0 = 8.2$ m/s and F = 59. Streamwise coordinates are expressed as $\sqrt{Re_x}$ and the amplitude from measurements and calculations have been normalised with their respective values at the first measurement position ($\sqrt{Re_x} = 330$). The measured amplitude maximum initially decays less than the calculated, but downstream of $\sqrt{Re_x} = 400$ the measurements indicate a lower amplitude. One explanation for the deviation between measurements and theory may be the relatively high initial amplitude, which is required if one should be able to measure the amplitude downstream at these damped conditions. The maximum amplitude at the first streamwise position was $u' \approx 1.6$ %.

Another aspect which is important to consider when evaluating the quality of a disturbance generator is the spanwise uniformity of the generated waves. With the technique used in the present experiment, the spanwise uniformity is mainly governed by the similarity of the individual pipes and how the loudspeaker amplitudes have been adjusted. For the test measurements with a single oblique wave, one iteration with adjustments of the loudspeaker amplitudes was usually considered sufficient. The uniformity obtained after such a coarse adjustment is shown in figure 5. This figure shows the spanwise distribution of wave amplitude

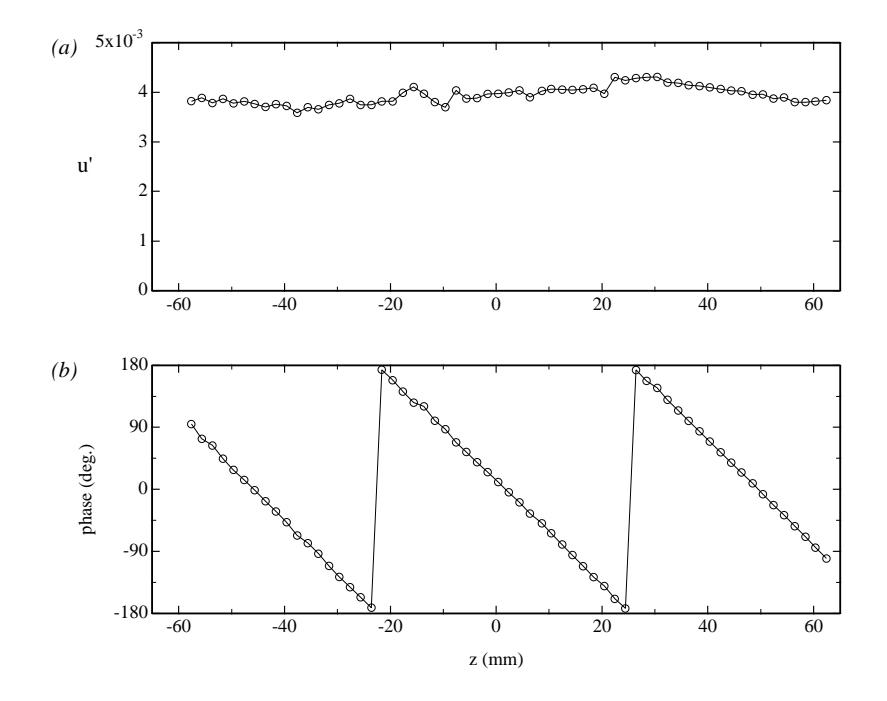


FIGURE 5. Oblique wave at F = 200 and $\beta = 131 \,\mathrm{m}^{-1}$. (a) Spanwise profile of amplitude; (b) corresponding phase profile. Measurements at $x = 210 \,\mathrm{mm}$ near $\eta = 1.5$.

and phase obtained by traversing the hot-wire probe at a constant height 20 mm downstream of the wave generator. The deviation from the average wave amplitude is within 9 % at this streamwise position, however, further away from the disturbance source the uniformity is improved.

4 Oblique transition results

4.1 Flow structure. A dominating feature of the oblique transition scenario is the formation of large amplitude longitudinal structures. Figure 6 shows contours of U_d and u' in a streamwise-spanwise plane at $\eta=1.55$ for a high-amplitude forcing. The notation high-amplitude forcing corresponds to a maximum initial amplitude of ≈ 7.5 % in the fundamental frequency when measured at x=210 mm, whereas forcing at 30 % lower speaker voltages is denoted low-amplitude. The spanwise extent of the figure represents $2\lambda_{z,0}{}^1$ and the streamwise region covers the distance from the position where the forcing is applied to x=1520 mm. U_d

¹The spanwise wave length of the oblique waves is denoted $\lambda_{z,0}$.

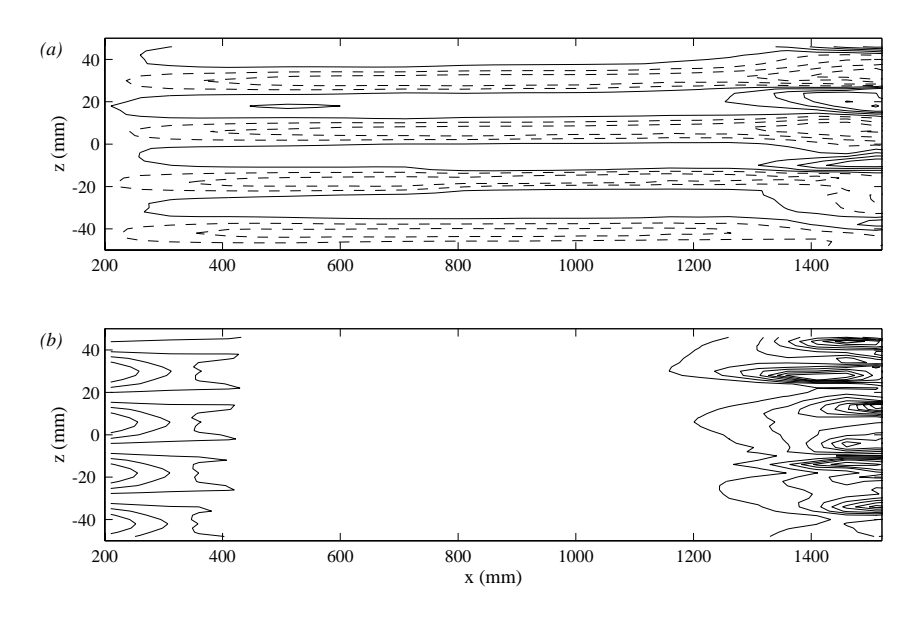


FIGURE 6. Contour plots in a streamwise-spanwise plane at $\eta = 1.55$ with a high-amplitude forcing for $U_0 = 9.1$ m/s and F = 43. (a) U_d , contours: $\pm 2\%$, $\pm 6\%$,...; (b) u', contours: 2%, 4%, ...

is characterized by narrow elongated regions of positive and negative values with a spanwise wavelength of $\lambda_{z,0}/2$ (see figure 6 a, note that the z-axis is stretched relative to the x-axis by a factor of two). After an initial growth in amplitude, U_d stays almost constant between x=400 mm and x=1200 mm. Starting at $x\approx 1200$ mm both the amplitude and the dominating spanwise wavelength is seen to increase downstream. The wave amplitude u' (see figure 6 b) decays downstream of the disturbance source, and at the same time the spanwise positions of the maxima change from the centre of low-speed streaks to regions between low-and high-speed streaks at x=400 mm. Near x=1200 mm the amplitude starts to grow and downstream of $x\approx 1300$ mm maxima of u' are located at spanwise positions between low- and high-speed regions.

The formation of the streaks and how their spanwise positions relate to the forcing is illustrated by figure 7, which shows spanwise profiles of amplitude and phase at the fundamental frequency and also U_d . At x=210 mm, which is about 20 mm downstream of the wave generator, the maximum amplitude of the wave disturbance is approximately 7.5 % and the phase changes by 180° at each position where the amplitude goes to zero. The streaks are not fully developed at this position but a cosine shaped distribution can be observed with minima in U_d at spanwise positions where the wave amplitude attains maxima. However, at

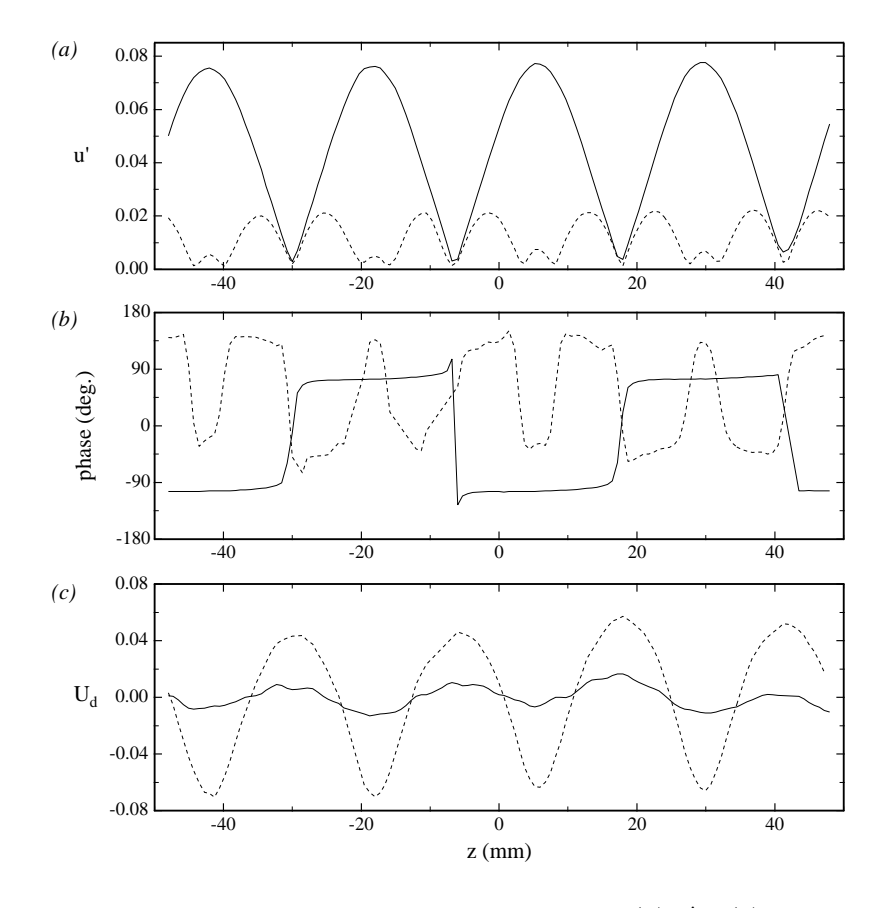


FIGURE 7. Spanwise profiles at $\eta=1.55$ of: (a) u'; (b) phase; (c) U_d . ——, Measurements at x=210 mm; ——, x=410 mm. Same conditions as in figure 6.

the second streamwise position U_d has increased to a value of about ± 6 % while the wave amplitude has decayed ($u' \approx 2$ %) and changed its structure. Maxima in u' are now connected to spanwise positions located at the zero-crossings of U_d , which is the result of a higher amplitude in the spanwise wavenumber $3\beta_0$ than in the original wavenumber β_0 .

Figure 8 shows contours of U_d in cross-stream planes. In order to illustrate the increase of disturbance size with the streamwise direction, the wall-normal coordinate is here presented in dimensional units. For reference, the boundary layer edge $(\eta = 5)$ and $\eta = 2$ are indicated by horizontal dotted lines at each streamwise position. A wall normal position of $\eta = 2$ is approximately where the maximum streak amplitude is located and also where so-called Klebanoff

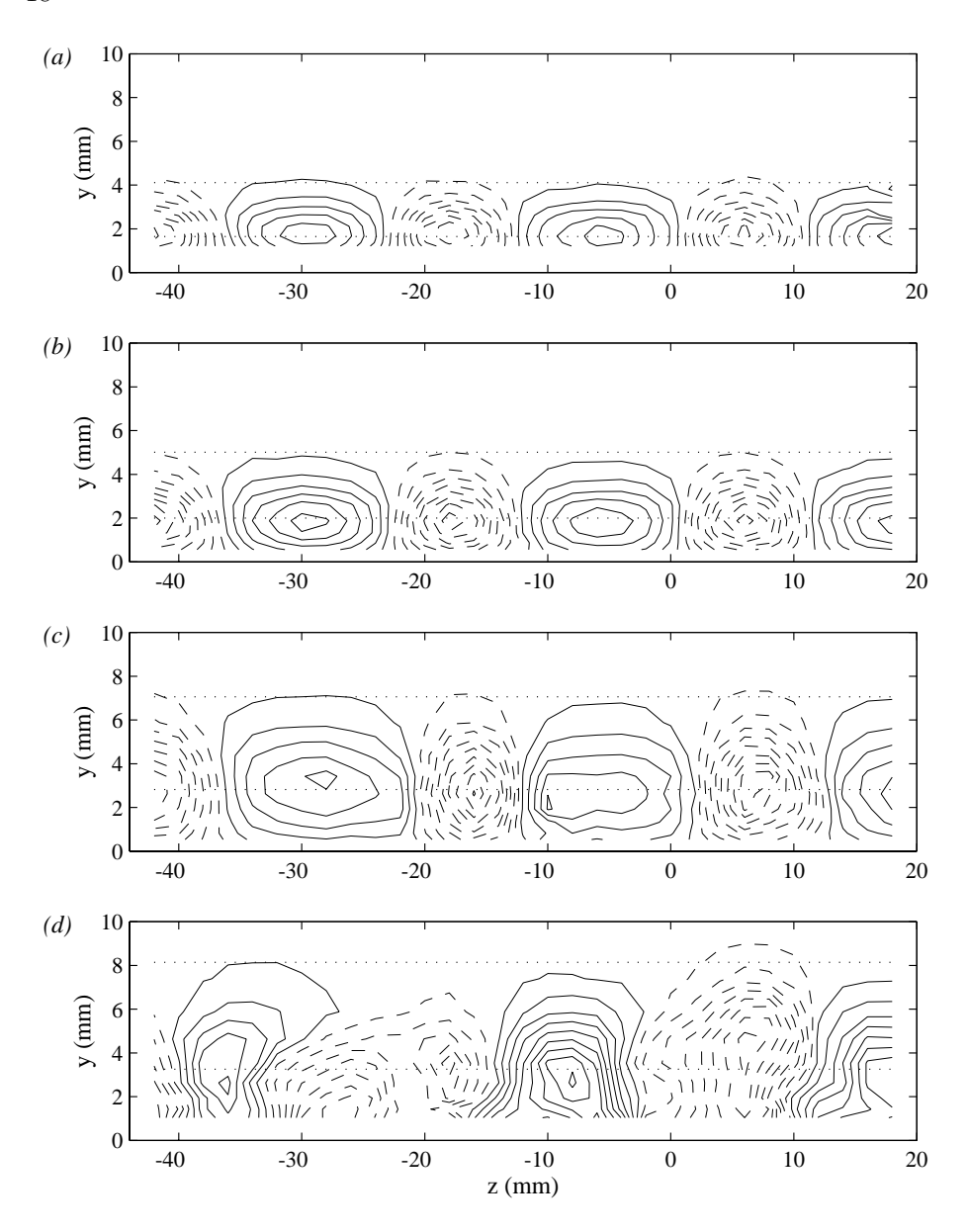


FIGURE 8. Contour plots of U_d in cross-stream planes for a high-amplitude forcing with $F{=}43$ at $U_0{=}9.1$ m/s. (a) Measurements at $x{=}410$ mm; (b) $x{=}610$ mm; (c) $x{=}1210$ mm; (d) $x{=}1610$ mm. Contours in $(a{-}c)$: $\pm 0.5\%$, $\pm 1.5\%$,..; in (d): $\pm 1\%$, $\pm 3\%$, ...

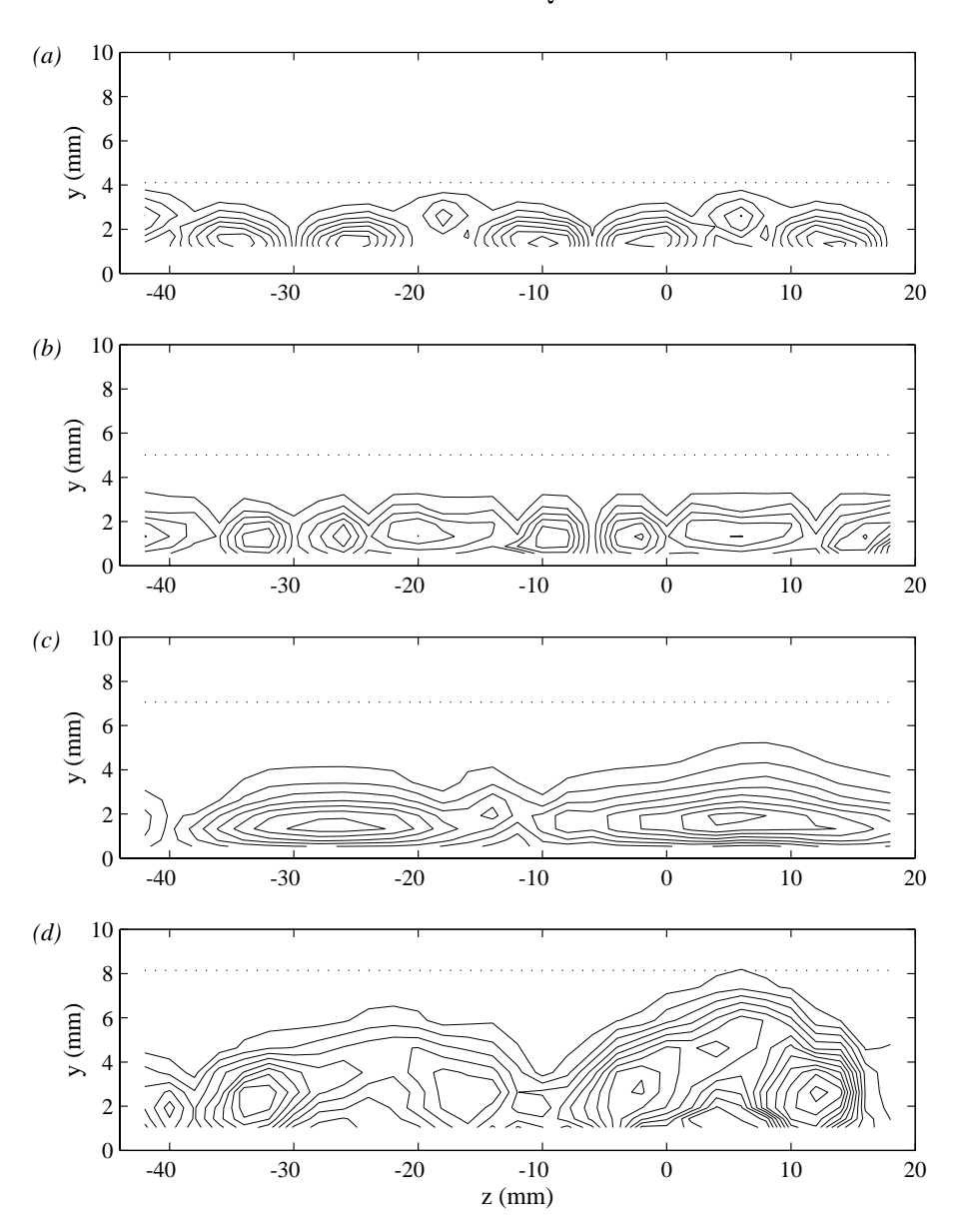


FIGURE 9. Contour plots of u' in cross-stream planes for a high-amplitude forcing with $F{=}43$ at $U_0{=}9.1\,\mathrm{m/s.}$ (a) Measurements at $x{=}410\,\mathrm{mm}$; (b) $x{=}610\,\mathrm{mm}$; (c) $x{=}1210\,\mathrm{mm}$; (d) $x{=}1610\,\mathrm{mm}$. Contours in $(a{-}c)$: 0.2%, 0.4%,...; in (d): 1%, 2%, ...

modes² have their maximum amplitude. When comparing the figures at x=410, x=610 and x=1210 mm (figure $8\,a$ –c) the maximum amplitude is observed to be similar, and also the spanwise position of the streaks is constant. It can be observed that the streaks grow in the wall-normal direction with increasing x and extend at all x across the full boundary layer. However, the disturbance is small outside the boundary layer in contrast to e.g. the vortex dominated Görtler flow. This indicates that the vortical motion is weak in the present case. At x=1610 mm (figure $8\,d$) the picture is quite different. Both the streak positions and the spanwise wavelength have now changed and the amplitude has increased from its value at x=1210 mm.

The corresponding contours of u' are shown in figure 9. At x=410 mm the structure is dominated by amplitude maxima located at $y\approx 1.5$ mm and at spanwise positions between the streaks. Maxima with a slightly lower amplitude are also observed further out from the wall at spanwise positions where U_d is negative. These maxima grow in amplitude and move closer to the wall at the next measurement station (x=610 mm), whereas the amplitude maxima associated with spanwise gradients in U_d have decayed at this position. Figure 9(c) displays contours at x=1210 mm where a larger spanwise wavelength is observed together with an increased peak amplitude. Yet a larger amplitude appears at x=1610 mm where the structure bears some resemblance with the one at the first streamwise position, though extended in the wall-normal direction and slightly shifted along the z-axis. When forcing with a 20 % lower amplitude the structure will look in a similar way except for x=610 mm, where only the maxima associated with low-speed regions are visible.

4.2 Spectral representation. Information about the behaviour of individual frequency-wavenumber modes was obtained by applying Fourier transforms to the measured data. Data sets were multiplied with a Kaiser-Bessel type window before time sequences were Fourier transformed and the resulting amplitudes were corrected for the window functions. The amplitudes were recalculated to correspond to amplitudes in frequency bands of 1 Hz before being plotted. No windowing was used for the spanwise Fourier transform.

Figure 10 shows the streamwise evolution of the amplitude of (ω, β) -modes for two different forcing amplitudes. A frequency-wavenumber decomposition was made at 10 heights through the boundary layer, and for each mode the maximum amplitude was plotted. The data was measured over a distance of one spanwise wavelength of the original wave with a separation of 2 mm between the points. From the two figures it can be seen that, the difference in forcing amplitude does

 $^{^2}$ Klebanoff modes are e.g. observed in Blasius flows subjected to elevated levels of free stream turbulence (described in Kendall 1985).

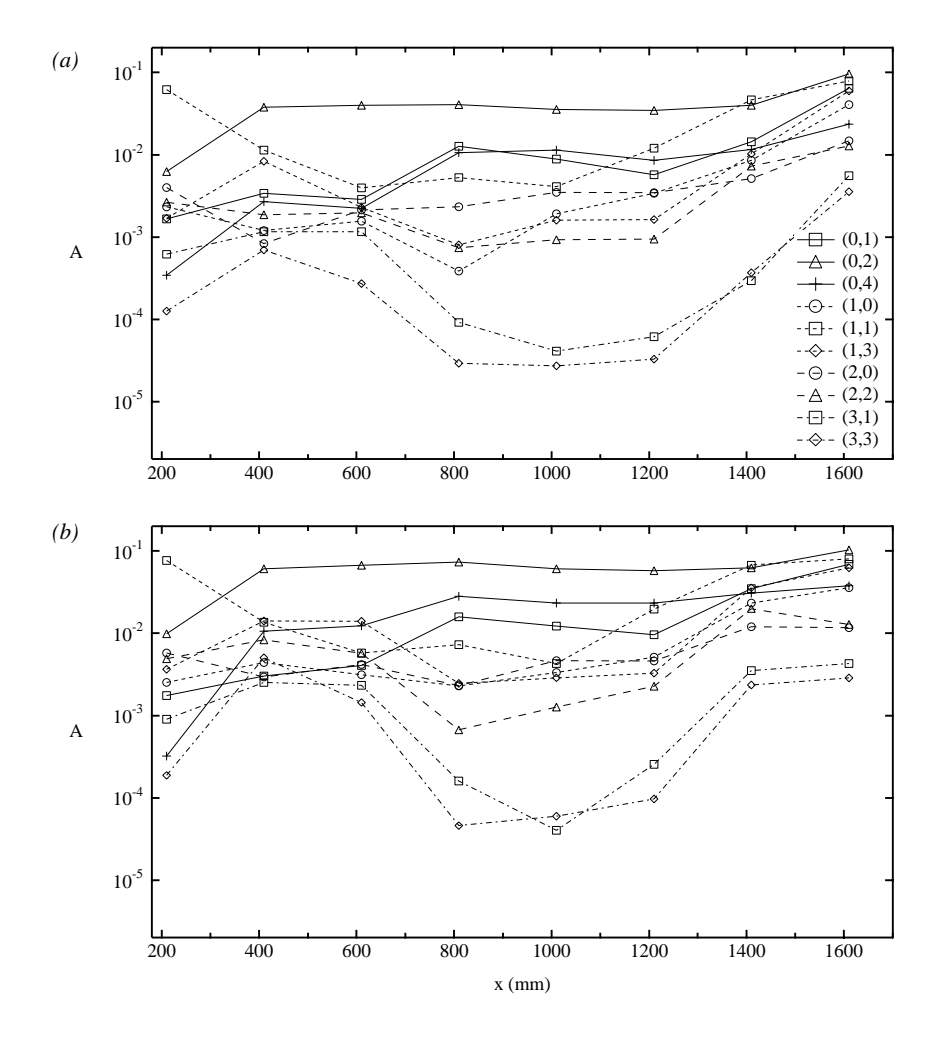


FIGURE 10. Amplitude of (ω, β) -modes normalized by $U_0 = 9.1 \text{ m/s}$ for different forcing amplitudes with F = 43 and $\beta_0 = 131 \text{ m}^{-1}$. (a) Low-amplitude forcing; (b) high-amplitude forcing.

not influence the general character. For a higher initial amplitude (figure $10\,b$), the mode amplitudes are generally higher and the growth of modes with higher frequencies sets in at an earlier streamwise position than for the lower initial amplitude (figure $10\,a$). Initially the modes of highest amplitude are the (1,1) and the (0,2), where the former initially decays and the amplitude of the latter is almost constant after $x=400\,\mathrm{mm}$. The initial decay of the (1,1) mode ceases near $x=600\,\mathrm{mm}$ and the mode starts to grow downstream, which can be understood

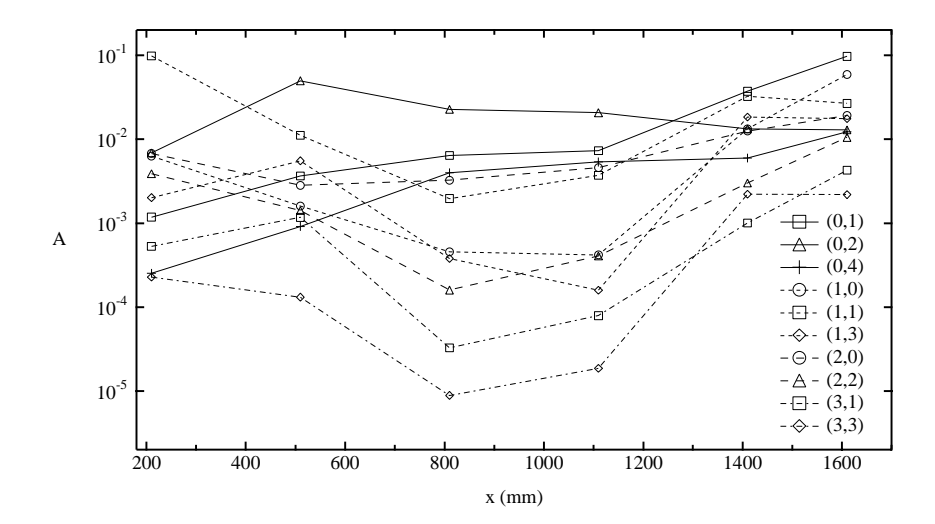


FIGURE 11. Amplitude of (ω, β) -modes normalized by $U_0 = 9.1 \text{ m/s}$ for a high-amplitude forcing with F = 43 and $\beta_0 = 163 \text{ m}^{-1}$.

by comparing with the conditions for neutral growth. For a growing boundary layer at the conditions of figure 10, branch I is located near x=680 and branch II near x=1360 mm. A strong growth of modes with non-zero frequencies sets in at $x\approx 1200$ mm for the lower initial amplitude and further upstream for the higher. One can also note that the (0,1) mode grows to a large amplitude at the last measurement positions, which was also seen as a change in the streak spacing in figure 6(a). A similar distribution of mode-amplitudes at the first streamwise positions was also obtained from an decomposition of measurements extending over two spanwise wavelengths at a constant boundary layer height of $\eta=1.55$.

From studies on optimal transient growth it is known that the largest growth occurs for a specific value of the spanwise wavenumber β . We investigated two different spanwise wavelengths and figure 11 shows the amplitude growth for a smaller wavelength (a higher value of β) than in figure 10. The major difference compared with the smaller β is that starting from $x \approx 1200$ mm the dominating stationary disturbance is now the (0,1)-mode instead of the (0,2). This can probably be explained by comparing with the β that gives the largest transient growth. Butler & Farrell (1992) found the optimal spanwise wavelength to be $\beta\delta^* = 0.65$ at $Re_{\delta^*} = 1000$ for a parallel Blasius flow, where $\delta^* = 1.72(\nu x/U_0)^{1/2}$. This can be compared with the experimental values of the fundamental spanwise wavenumber which are $\beta\delta^* = 0.37$ for the standard spacing and $\beta\delta^* = 0.46$ for

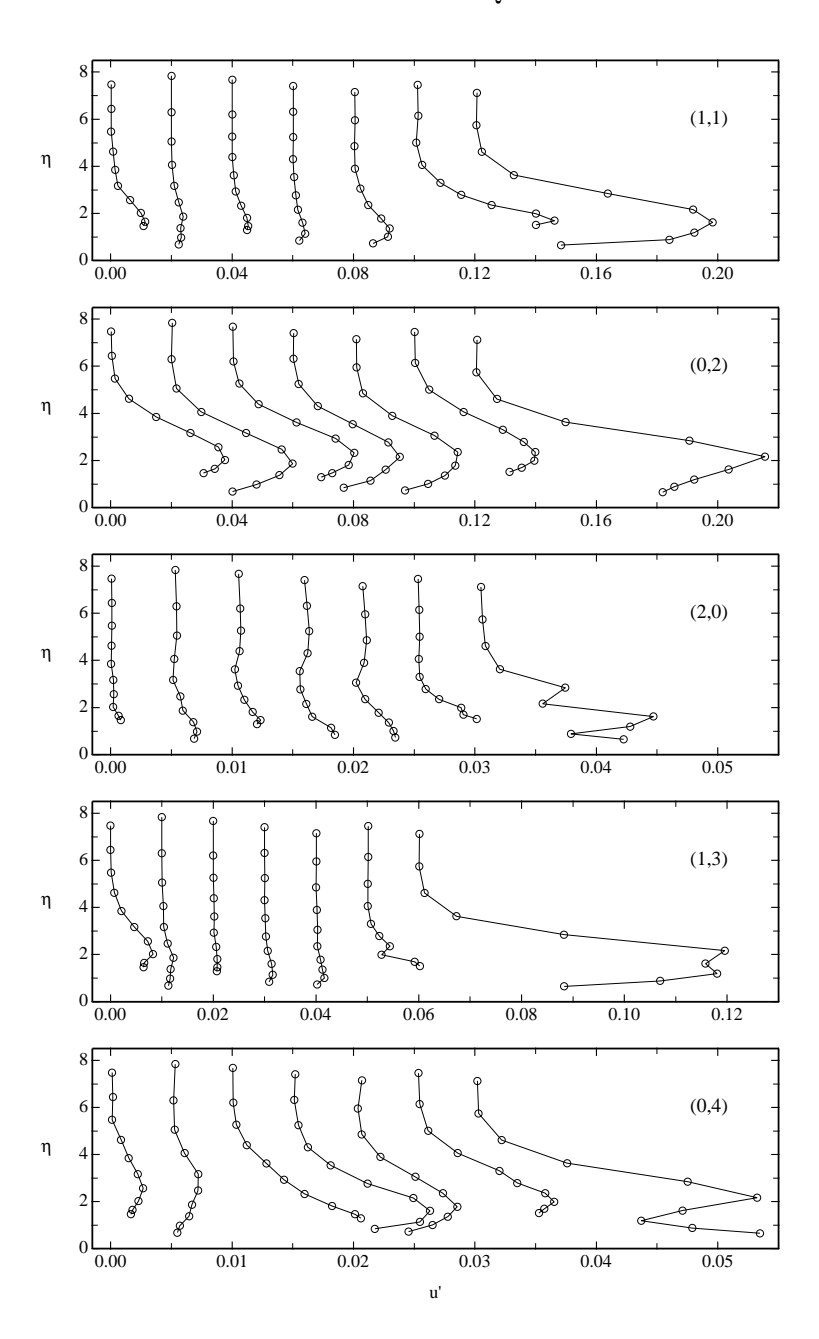


FIGURE 12. Wall-normal profiles of amplitude in (ω,β) -modes from measurements at $x=410,\ 610,\ 810,\ 1010,\ 1210,\ 1410$ & 1610 mm. Same conditions as in figure 10 (a).

the narrow spacing at x=1610. The corresponding values for the (0,2) mode are twice as large and at the last streamwise position for the narrow case, β for (0,1) is closer to the optimal spanwise wavenumber than (0,2). However, according to the investigation by Andersson, Berggren & Henningson (1998) on spatial optimal disturbances in a growing boundary layer, the optimal β would rather be $\beta\delta=0.45$ or $\beta\delta^*=0.77$. Their calculations determined the disturbance at the leading edge which experienced the largest spatial energy growth when observed at a downstream position x.

Wall-normal profiles of some of the most important modes are presented in figure 12 for various streamwise positions. The figures are based on the same data as was used in figure 10. During the measurements the main interest was in capturing the streak amplitude and therefore information is lacking in the region closest to the wall. Profiles of the (0,2)-mode have similar shape at all streamwise positions with the maximum located near $\eta=2.2$, while the amplitude maximum of the other stationary mode appears at an increasing height with increasing x (if the two first streamwise positions are excluded).

Figure 13 shows amplitude spectra measured at different streamwise positions for a fixed η and spanwise position. A reference level is indicated to the right of each spectrum. Besides the generated frequency and its harmonics, additional peaks are observed at the first streamwise positions. These elevations above the background level are believed to originate from probe vibrations caused by vortex shedding from the midsection of the boundary layer probe. When proceeding downstream transition is first observed as an increase in the amplitude of harmonics, later followed by a distributed elevation of the amplitude at all frequencies. One can note the rapid increase in the amplitude of higher frequencies occurring between x=1360 and x=1510 mm, a distance of approximately two streamwise wavelengths of the initial oblique waves. Spectra measured at z=24.7 mm (not shown) had a narrower range of frequencies that were elevated above the background level. For this case the rapid growth started a bit further downstream than for the spanwise position shown in figure 13, however, spectra measured at the two most downstream positions were similar for both cases.

4.3 Time representation. Phase-averaged velocity data from streamwise positions near the disturbance generator are shown in figure 14. Each figure shows contours of u over three periods in time from a region covering two spanwise wavelengths of the oblique waves. The data is the average of 25 sets of triggered velocity traces measured at 129 equidistant spanwise positions. Since the horizontal axes displays the time, a spatial representation of the fields is obtained by assuming that the flow is from right to left. The first figure shows the field at x = 210 mm where a regular wave pattern is seen. Further downstream Λ -shaped

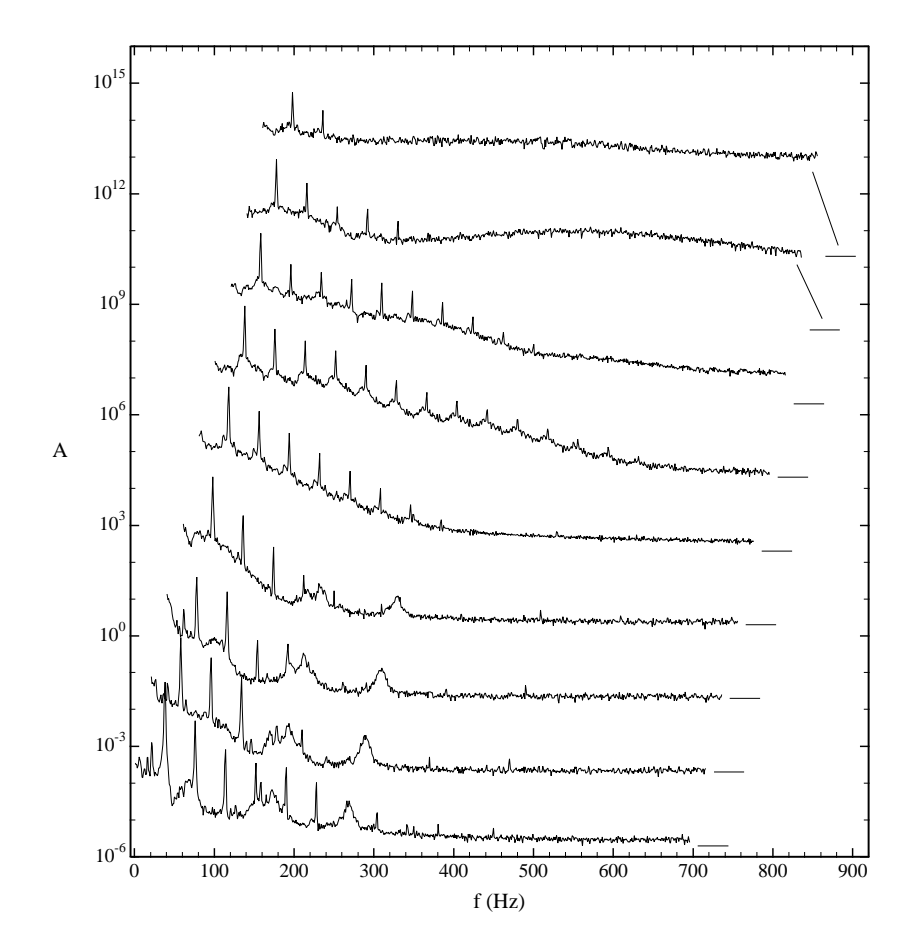


FIGURE 13. Amplitude spectra for a low-amplitude forcing at $U_0 = 9.1$ m/s and F = 43. Measurements at $\eta = 1.5$, z = 29.2 and x = 210, 610, 1010, 1210, 1310, 1360, 1410, 1460 & 1510 mm. Consecutive spectra are shifted 20 Hz and multiplied by 10^{2n} .

regions of positive or negative deviations from the time average are observed in a staggered pattern. At the streamwise positions shown in this figure, the amplitude of the time dependent disturbances decays (as the stationary streaks increase in amplitude).

Characteristic velocity traces from three streamwise positions are shown in figure 15 for 6 periods of the initial waves. The traces are grouped after which height in the boundary layer they were measured at, and the traces within each group represents from bottom to top $x=1410,\,1510$ & 1610 mm. All traces were

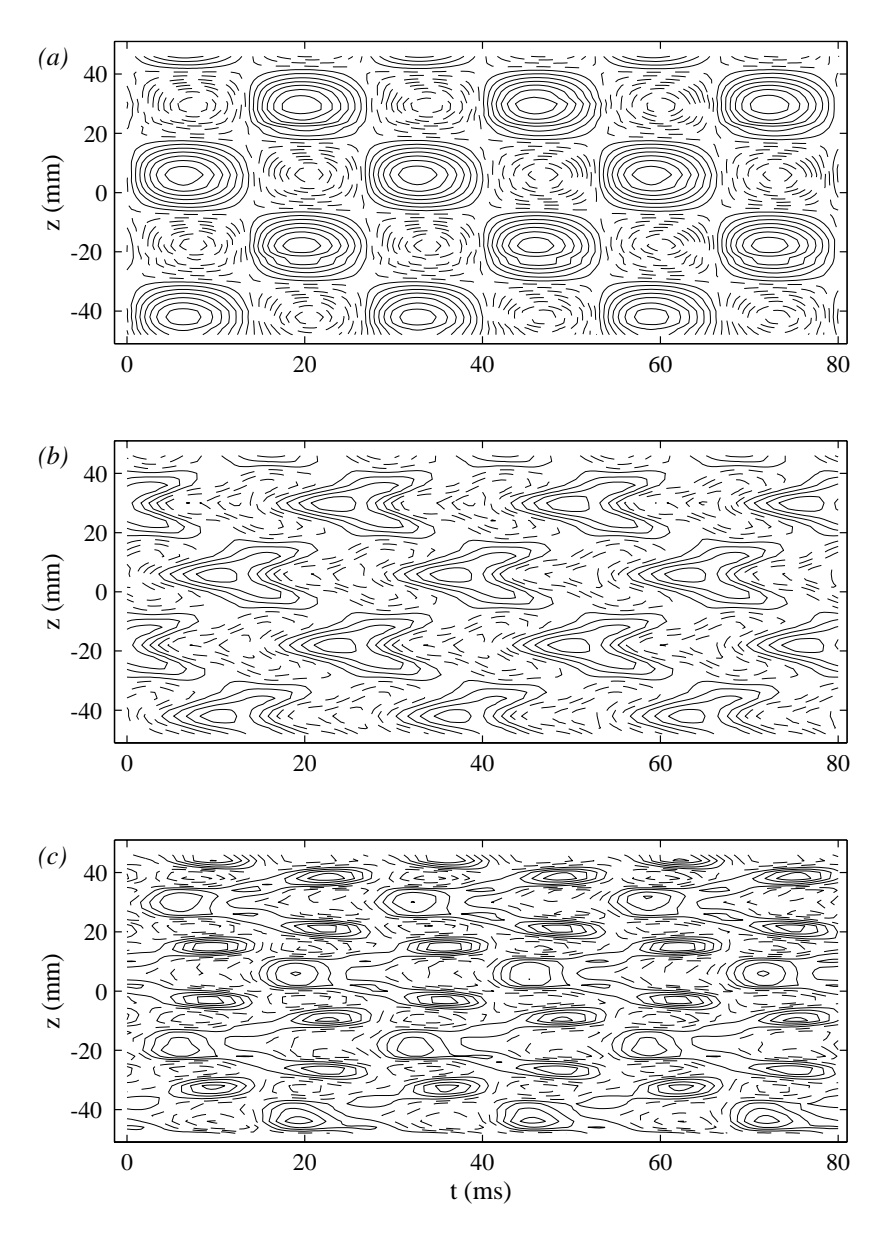


FIGURE 14. Contours of u at $\eta=1.5$ for a high-amplitude forcing with F=43 and $\beta_0=131~\mathrm{m}^{-1}$ at $U_0=9.1~\mathrm{m/s}$. (a) Measurements at x=210; (b) x=310; (c) x=610. Contour spacing is 1% in (a,b) and 0.5 % in (c).

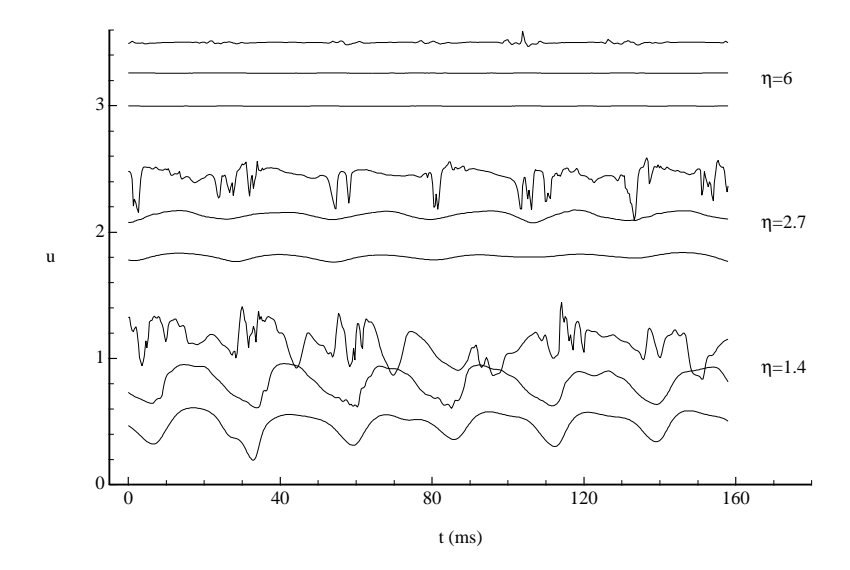


FIGURE 15. Velocity traces at z = -12 and x = 1410, 1510 and 1610 mm are shown at three heights through the boundary layer. Traces at each height are separated by 0.3 U_0 and represents, from bottom to top, x = 1410, 1510 & 1610 mm.

measured for a high-amplitude forcing at z=-12, which corresponds to a position between a low- and high-speed streak. At $\eta=1.4$ and x=1510 a high-frequency motion of low amplitude is seen over a few periods and at the last streamwise position the amplitude of higher frequencies have increased substantially and can now be seen at all three wall-normal positions.

4.4 Flow visualisation. Flow visualisations were made to obtain a clearer picture of the spatial development of the oblique transition. The photos in figure 16 show top views of the flow at two different conditions. In both cases a dimensional forcing frequency of f=51 Hz was used, however, figure $16\,(a)$ is at a free stream velocity of about 8.4 m/s and the velocity used in figure $16\,(b)$ is $U_0=7.0$ m/s. The corresponding dimensionless frequency parameters are then F=69 and F=97, respectively. Both photos displays a streamwise length of 422 mm starting 40 mm downstream of the slit from which the disturbances are generated. The spanwise distance is 229 mm at the upstream side of the photos (the flow is from left to right in the figures) and 206 mm at the downstream end. For constant free stream and forcing conditions, the breakdown position can be altered by changing the amount of smoke seeped into the boundary layer. This was utilized in the figures to allow the whole transition scenario to be observed



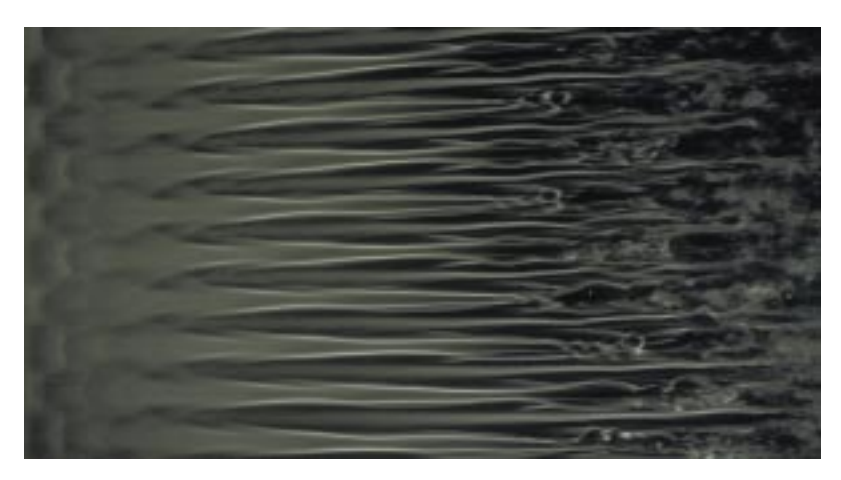


FIGURE 16. Flow visualisation showing a streamwise-spanwise plane where the flow is from left to right. (a) At $U_0 = 8.4$ m/s and F = 69; (b) $U_0 = 7.0$ m/s and F = 97.

at one camera position. A wave field is observed in the left part of the photos and further downstream Λ -shaped structures appear in a staggered pattern. Breakdown is seen in the downstream end of both photos, but the pictures differ slightly in the way and also at which streamwise location breakdown occurs. The forcing amplitude for F=69 (figure 16~a) was lower than for the higher F. One should note that the streamwise position at which the flow breaks down in the visualisations is farther upstream than for the hot-wire measurements.

Details of the breakdown for F=69 is shown in figure 17, which covers 162 mm in the streamwise direction and a spanwise distance of 90 mm in the



FIGURE 17. Detail of the breakdown stage in figure 16(a).

upstream end. The photo indicates a vortical motion having a streamwise wavelength shorter than that of the initial waves.

5 Concluding remarks

Results from an experimental investigation of oblique transition in a Blasius boundary layer have been reported, where wave disturbances were generated with periodic blowing and suction through a spanwise array of pipes. The disturbance generating system was found to give waves which developed in agreement with linear theory.

The forcing of two oblique waves resulted in an interaction and the formation of streamwise streaks. The streaks were found to grow initially until they saturate and then their amplitude stays nearly constant over a streamwise distance of about 800 mm. When viewed in cross-stream planes, the streaks were seen to be located inside the boundary layer with their maximum amplitude at a wall-normal position near $\eta=2$.

The breakdown of the streaks occurs through the growth of higher harmonics of the initial waves and from a decomposition of the disturbance amplitude into individual frequency-wavenumber modes, the streamwise evolution of the amplitude in (ω, β) modes could be followed. The decomposition also allowed wall-normal profiles to be plotted. Other features seen in the transition process was the appearance at upstream positions of Λ -shaped structures in a staggered pattern.

Results from flow visualizations where a smoke-layer was introduced near the flat plate surface showed oblique waves followed by the Λ -structures and finally

U_0	F	β	u_0'	$\Delta U(x=1000 \text{ mm})$
9.1 m/s	43	$131 \; \mathrm{m}^{-1}$	8.5 %	±5 %
$9.1~\mathrm{m/s}$	43	131 m^{-1}	6.3~%	$\pm 3.5~\%$
$9.1 \mathrm{m/s}$	43	163 m ⁻¹ 131 m ⁻¹	9.5~%	$\pm 2.5~\%$
$8.2 \mathrm{m/s}$	59	$131 \; \mathrm{m}^{-1}$	9.0 %	$\pm 13~\%$

TABLE 2. Experimental conditions and results for some of the investigated cases. u'_0 is the maximum amplitude of the two oblique waves at x=210 mm.

breakdown. Structures with a short streamwise wavelength were observed on the sides of the low-speed regions prior to breakdown.

In the present investigation of oblique transition, a general picture of the transition scenario can be described as: a rapid growth of streamwise streaks together with a decay in the amplitude of the initial oblique waves, a second stage where the streak amplitude is constant and a growth of the oblique waves which might be governed by linear stability, followed by the final stage where both stationary and time-dependent modes grow, eventually evolving into a turbulent state.

The amplitude of the streaks in the first stage depends on the wave amplitude, the decay rate of the oblique waves, the spanwise wavenumber and the Reynolds number at the disturbance source. The strength of the transient growth is governed by the latter two, whereas the first two determines the input to the streamwise vortices through a nonlinear interaction. For the conditions presented in this report a streak amplitude of $\approx \pm 5$ % was reached near x=800 mm. From measurements at a higher F, where the initial decay of the oblique waves is smaller, a streak amplitude of about ± 13 % was reached (see also table 2). Despite the larger streak amplitude in this case, the location for the transition onset did move upstream with less than 100 mm. The growth of the waves in the second stage is motivated by the observations made in connection with figure 10, where it was found that the growth of the (1,1) mode started at the location of branch I for the present conditions. In the final stage, the mode which has the highest amplitude will depend on the specific conditions. In particular, the effect of the initial amplitude and the spanwise wavenumber was shown in section 4.2.

Berlin, Wiegel & Henningson (1998) reported on measurements and direct numerical simulations at U=12 m/s and F=59. The measurements indicated the appearance of high-frequency fluctuations approximately 350 mm downstream of

the disturbance source. A similar development could be obtained in the direct numerical simulations by a detailed modelling of the disturbance source. The growth observed in the DNS was quite sensitive to the method used for modelling the disturbances and the method which was finally chosen resulted in the most rapid development. It can be hypothesized that the forcing method used in the present experiments, where disturbances from individual pipes are mixed in a common slit before entering the boundary layer, results in a different transition location than for the wave generator used in the measurements reported by Berlin et al. They used separate slits for each spanwise position and the edge effects of these slits may result in disturbance energy also in smaller spanwise scales. However, the main reason for the difference with the present investigation is probably the conditions that determines the strength of the transient growth of the streaks, and thereby the conditions for streak instability.

In an experimental investigation of oblique transition in plane Poiseuille flow at a subcritical Reynolds number (Elofsson & Alfredsson 1998), transition only occurred if the streak amplitude reached above a threshold level. For the present study in a Blasius flow, there is a second chance for transition to occur even if the streak amplitude at the initial stage is not sufficiently high to directly trigger a streak instability. Initially the generated oblique waves are damped, but as the wave travels downstream it reaches the unstable region and starts to grow, whereafter the final stage shows a strong growth of both stationary and time-dependent modes.

Acknowledgments

This work was supported by the Swedish Research Council for Engineering Sciences (TFR). I wish to thank Prof. Henrik Alfredsson for numerous discussions and comments on the manuscript. The original design of the disturbance source greatly benefited from discussions with Sebastian Bake and Prof. Y.S. Kachanov during a research visit to the Hermann Föttinger Institut at TU-Berlin arranged by Prof. H.H. Fernholz and supported by the Swedish Institute. The flow visualisations were made in co-operation with Dr. Masaharu Matsubara. Dr. Ardeshir Hanifi kindly provided results from his PSE-calculations. Thanks are also due to Markus Gällstedt for help with manufacturing parts for the experimental setup.

References

- Andersson, P., Berggren, M. & Henningson, D. S. 1998 Optimal disturbances and bypass transition in boundary layers. *Phys. Fluids* (submitted).
- Bakchinov, A. A., Grek, G. R., Klingmann, B. G. B. & Kozlov, V. V. 1995 Transition experiments in a boundary layer with embedded streamwise vortices. *Phys. Fluids* 7, 820–832.
- BAKE, S., KACHANOV, Y. S. & FERNHOLZ, H. H. 1996 Subharmonic K-regime of boundary-layer breakdown. In *Proc. Transitional Boundary Layers in Aeronautics* (Henkes, R. A. W. M. & VAN INGEN, J. L., editors), pp. 81–88, Royal Netherlands Academy of Arts and Sciences, Elsevier.
- Berlin, S., Lundbladh, A. & Henningson, D. S. 1994 Spatial simulations of oblique transition in a boundary layer. *Phys. Fluids* 6, 1949–1951.
- Berlin, S., Wiegel, M. & Henningson, D. S. 1998 Numerical and experimental investigations of oblique boundary layer transition. *J. Fluid Mech.* (submitted).
- Boberg, L. & Brosa, U. 1988 Onset of turbulence in a pipe. Z. Naturforsch. 43 a, 697–726.
- Butler, K. M. & Farrell, B. F. 1992 Three-dimensional optimal perturbations in viscous shear flow. *Phys. Fluids A* 4, 1637–1650.
- CHANG, C.-L. & MALIK, M. R. 1994 Oblique-mode breakdown and secondary instability in supersonic boundary layers. J. Fluid Mech. 273, 323–360.
- CORKE, T. C. & MANGANO, R. A. 1989 Resonant growth of three-dimensional modes in transitional Blasius boundary layers. *J. Fluid Mech.* **209**, 93–150.
- Ellingsen, T. & Palm, E. 1975 Stability of linear flow. Phys. Fluids 18, 487-488.
- ELOFSSON, P. A. & ALFREDSSON, P. H. 1995 Experiments on nonlinear interaction between oblique Tollmien-Schlichting waves. In *Laminar-Turbulent Transition* (KOBAYASHI, R., editor), pp. 465–472, IUTAM Symposium, Sendai 1994, Springer.
- Elofsson, P. A. & Alfredsson, P. H. 1998 An experimental study of oblique transition in plane Poiseuille flow. *J. Fluid Mech.* **358**, 177–202.
- ELOFSSON, P. A., KAWAKAMI, M. & ALFREDSSON, P. H. 1997 Experiments on the stability of streamwise streaks in plane Poiseuille flow. *Phys. Fluids* (submitted).
- Fasel, H., Thumm, A. & Bestek, H. 1993 Direct numerical simulation of transition in supersonic boundary layers: Oblique breakdown. In *Transitional and turbulent compressible flows*, ASME FED-Vol. 151 (Kral, L. D. & Zang, T. A., editors), pp. 77–92.
- GAPONENKO, V. R. & KACHANOV, Y. S. 1994 New methods of generation of controlled spectrum instability waves in the boundary layers. In *International Conference on Methods of Aerophysical Research*. Part 1, pp. 90–97, Novosibirsk, ITAM.

- Gathmann, R. J., Si-Ameur, M. & Mathey, F. 1993 Numerical simulations of threedimensional natural transition in the compressible confined shear layer. *Phys. Fluids A* 5, 2946–2968.
- GUSTAVSSON, L. H. 1991 Energy growth of three-dimensional disturbances in plane Poiseuille flow. J. Fluid Mech. 224, 241–260.
- Henningson, D. S. 1995. Bypass transition and linear growth mechanisms. In *Advances in Turbulence V* (Benzi, R., editor), pp. 190–204, Dordrecht. Kluwer.
- HERBERT, T. 1983 Secondary instability of plane channel flow to subharmonic three-dimensional disturbances. *Phys. Fluids* **26**, 871–874.
- HERBERT, T. 1988 Secondary instability of boundary layers. Ann. Rev. Fluid Mech. 20, 487–526.
- HULTGREN, L. S. & GUSTAVSSON, L. H. 1981 Algebraic growth of disturbances in a laminar boundary layer. Phys. Fluids 24, 1000–1004.
- JOSLIN, R. D., STREETT, C. L. & CHANG, C. L. 1993 Spatial direct numerical simulations of boundary-layer transition mechanisms: Validation of PSE theory. Theor. Comp. Fluid Dyn. 4, 271–288.
- KACHANOV, Y. S. 1994 Physical mechanisms of laminar-boundary-layer transition. Ann. Rev. Fluid Mech. 26, 411–482.
- KACHANOV, Y. S., KOZLOV, V. V. & LEVCHENKO, V. Y. 1977 Nonlinear development of a wave in a boundary layer. *Izv. Akad. Nauk SSSR, Mekh. Zhidk. Gaza.* 3, 49–53. (in Russian, English transl. 1978 in *Fluid Dyn.* 12, 383–390).
- Kendall, J. M., 1985 Experimental study of disturbances produced in a pre-transitional laminar boundary layer by weak freestream turbulence. AIAA Paper 85-1695.
- KLEBANOFF, P. S., TIDSTROM, K. D. & SARGENT, L. M. 1962 The three-dimensional nature of boundary layer instability. J. Fluid Mech. 12, 1–34.
- KLEISER, L. & ZANG, T. A. 1991 Numerical simulation of transition in wall-bounded shear flows. Ann. Rev. Fluid Mech. 23, 495–537.
- KLINGMANN, B. G. B. 1992 On transition due to three-dimensional disturbances in plane Poiseuille flow. J. Fluid Mech. 240, 167–195.
- LANDAHL, M. T. 1980 A note on an algebraic instability of inviscid parallel shear flows. J. Fluid Mech. 98, 243–251.
- Luchini, P. 1997 Reynolds-number-independent instability of the boundary layer over a flat surface. Part 2: Optimal perturbations. (submitted for publication).
- Orszag, S. A. & Patera, A. T. 1983 Secondary instability of wall-bounded shear flows. J. Fluid Mech. 128, 347–385.
- Reddy, S. C., Schmid, P. J., Baggett, J. S. & Henningson, D. S. 1998 On stability of streamwise streaks and transition thresholds in plane channel flows. *J. Fluid Mech.* (in press).
- Sandham, N. D., Adams, N. A. & Kleiser, L. 1994 Direct simulation of breakdown to turbulence following oblique instability waves in a supersonic boundary layer. In *Direct and Large-Eddy Simulation I* (Voke, P. R., Kleiser, L. & Chollet, J. P., editors), pp. 213–223, Kluwer.
- Schmid, P. J. & Henningson, D. S. 1992 A new mechanism for rapid transition involving a pair of oblique waves. *Phys. Fluids A* 4, 1986–1989.
- Trefethen, L. N., Trefethen, A. E., Reddy, S. C. & Driscoll, T. A. 1993 Hydrodynamic stability without eigenvalues. *Science* **261**, 578–584.

34 REFERENCES

Waleffe, F. 1995 Hydrodynamic stability and turbulence: Beyond transients to a self-sustaining process. Stud. Appl. Math. 95, 319–343.

Waleffe, F. 1997 On a self-sustaining process in shear flows. Phys. Fluids. $\bf 9,~883-900.$

Wiegel, M. 1996 Experimentelle Untersuchung von kontrolliert angeregten dreidimensionalen Wellen in einer Blasius-Grenzschicht. PhD thesis, TH Hannover.

Ribbon induced oblique transition in plane Poiseuille flow

PER A. ELOFSSON

Department of Mechanics, KTH, S-100 44 Stockholm, Sweden

AND

Anders Lundbladh FFA, $Box\ 11021$, S-16111 Bromma, $Sweden^{\dagger}$

Abstract

Results from spatial numerical simulations on ribbon induced oblique wave transition in plane Poiseuille flow are presented and comparisons are made with experimental results. The vibrating ribbons were modeled by adding volume forces to the Navier-Stokes equations in the regions occupied by the ribbons. The spanwise non-symmetry seen in experiments was found to result from the placement of the ribbons at opposite channel walls, causing the onset of nonlinear interactions to occur at different downstream positions for different cross stream coordinates.

1 Introduction

Transition to turbulence takes place even if the linearized disturbance equations for the laminar flow only exhibit damped eigenmodes. Traditionally this fact has been explained by the effect of nonlinearity and a large number of nonlinear mechanisms have been proposed for the disturbance growth in various flows. More recently the necessity of energy growth for the linearized equations have been emphasized. When all eigenmodes are damped this comes in the form of a transient growth, which, although limited in time, can be quite strong in shear flows.

In plane two dimensional incompressible shear flows, the growth of eigenmodes is first observed (i.e. for the lowest Reynolds numbers) for purely two-dimensional waves, and many studies of instability, both theoretical and experimental, have concentrated on these. However, the transient growth is found to be significantly greater for three dimensional, oblique, waves and especially for the streamwise vortex - streak interaction, denoted lift-up by Landahl (1975).

[†]Present address: Volvo Aerospace Corp., S-461 81 Trollhättan, Sweden

An interesting scenario for transition is found for a disturbance starting as two oblique waves each making an angle to the mean flow of the same magnitude but with opposite sign. These may grow transiently and also nonlinearly produce streamwise vortices. The vortices in turn force a strong transient growth of streamwise streaks with high and low streamwise velocity alternating in the spanwise direction. Provided the amplitude is high enough, the streaks which have inflectional velocity profiles may become unstable to small scales and the laminar flow rapidly breaks down into turbulence.

The coupling of oblique waves – streamwise vortices and streaks was found to give a rapid transition for localized disturbances in plane channel and boundary layer flows in the investigation of Henningson, Lundbladh & Johansson (1993). The localized disturbance was then modeled by a periodic one using two oblique waves by Schmid & Henningson (1992) They performed numerical simulations of plane channel flow, where they found a similar rapid transition as observed for localized disturbances. In their study the initial disturbance was spanwise symmetric, and as this symmetry is preserved by the Navier-Stokes equations, the subsequent transition process retained the symmetry.

In the experiments of Elofsson & Alfredsson (1995) two oblique waves were generated in a plane channel flow by two vibrating ribbons which were placed at opposite channel walls. The resulting flow had strong similarities to that simulated by Schmid & Henningson, giving a transition at relatively low amplitudes in spite of the low Reynolds number, 2000 based on half channel width and laminar centreline velocity. The transition proceeded primarily through the generation of a number of harmonics to the primary frequency, only eventually giving a more smooth spectrum. This shows that although the amplitude is high and has the appearance of the turbulence the flow is almost periodic in time for some distance downstream of the ribbons.

However, the flow downstream of the ribbons was not found to be spanwise symmetric. In a view normal to the channel wall the experimental arrangement is spanwise symmetric, but due to the fact that the vibrating ribbons are placed near either wall the symmetry is not exact.

The present study aims to reconciliate previous numerical and experimental results with the use of a numerical model, which more closely reflects the geometry of the physical experiment reported by Elofsson & Alfredsson. Especially we try to find the cause of the observed non-symmetry in the experiment. A general comparison of the experimental and numerical data is also attempted.

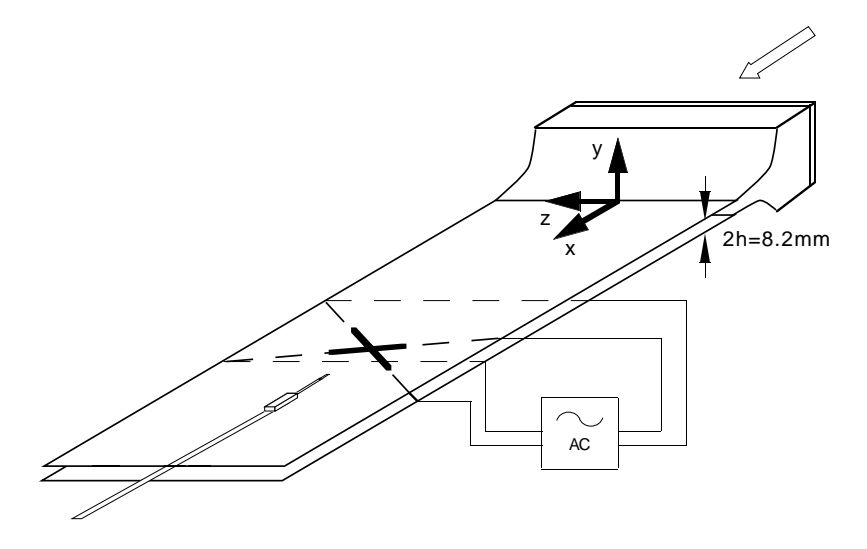


FIGURE 1. Experimental setup

2 Experimental apparatus and reference quantities

The experiments by Elofsson & Alfredsson(1995) were carried out in an air-flow channel consisting of two parallel glass plates separated by a distance 8.2 mm and having an aspect ratio of 101 (see Figure 1). Wave disturbances were generated with the two vibrating ribbons positioned approximately 1000 mm downstream of the channel entrance. The ribbons were made of a phosphor bronze alloy and they had a width, thickness and working length of 3 mm, 0.05 mm and 320 mm, respectively. The ribbons were positioned 0.5mm from the channel walls in a magnetic field from five horseshoe type permanent magnets evenly distributed along each ribbon and mounted outside the channel walls. A sinusoidal signal provided by a function generator and amplified by a stereo amplifier excited the ribbons. A 2.5 μ m diameter platinum hot-wire was used for measuring the streamwise velocity component, and the hot-wire probe could be traversed automatically in the spanwise and wall-normal directions and manually in the streamwise direction.

We will take the reference length for both the experiment and simulation to be the half channel width h=4.1 mm, and the reference velocity scale to be the the centreline velocity of the undisturbed laminar flow U_{cl} . This velocity was adjusted so that the Reynolds number was $R=hU_{cl}/\nu=2000$, which gave a centreline velocity of about $U_{cl}=7.3$ m/s. The coordinate system has the x-axis aligned in the streamwise, the y-axis in the wall normal and the z-axis in the

spanwise direction, the corresponding velocities are u, v and w. The origin is at the crossing point for the two ribbons and halfway between the lower and upper plate, so that their coordinates are y=-1 and y=1 respectively. We will also use the ribbonwise z' and chordwise x' coordinates in a system rotated 45° around the y-axis.

In the results discussed in this paper the angular frequency of oscillation was held at $\omega = 0.34$ which corresponds to a dimensional frequency of about 96 Hz.

3 Numerical method

We will use a numerical simulation program solving the full three-dimensional incompressible Navier-Stokes equations developed by Lundbladh, Henningson & Johansson (1992). The program uses Fourier-Chebyshev spectral methods, similar to those of Kim, Moin & Moser (1987). The simulation program has recently been modified to handle spatial development of disturbances in channel and boundary layer flows. In a fringe region a forcing term is added to the Navier-Stokes equations. It is implemented such that the disturbances flowing out of the box were eliminated and the flow returned to its laminar state. This technique, which allows the streamwise expansion in Fourier modes to be retained while prescribing inflow and outflow conditions, is described in Lundbladh & Henningson (1993).

3.1 Model of vibrating ribbons. The effect of the vibrating ribbons can most easily be modeled by application of a time varying volume force. The following force is applied to the streamwise momentum equation for the lower and upper ribbon:

$$F_{l} = A\cos(\omega t)exp\{-[(x-z)/c]^{2} - [(y-y_{l})/d]^{2} - (z/l)^{30}\}$$

$$F_{u} = A\cos(\omega t)exp\{-[(x+z)/c]^{2} - [(y-y_{u})/d]^{2} - (z/l)^{30}\}$$
(1)

Here A and ω are the amplitude and angular frequency of the forcing. The half chord c=1 and half thickness d=0.02 are chosen larger than the physical dimension in order to limit the demands on the numerical resolution. The physical distance from the wall of the ribbons is set by using $-y_l = y_u = 0.878$. To limit the computational domain we have chosen to set the half span of the ribbons l=12. The high power for the z dependence yields a forcing which for the central 85 % of the ribbon span is constant to within 1 %.

A partial justification for this rough modeling is that the amplitude of the ribbons is not known from the experiments. Thus it is necessary to adjust the amplitude to correspond to a measurement of the disturbance amplitude at some position downstream of the ribbons. The exact cross section of the ribbon then to a first approximation only affects the flow close to the ribbon itself.

3.2 Model of a stationary ribbon. Even when not vibrating, the ribbons act as a flow blockage and generate a non-homogeneous flow downstream, which although weak, would break the spanwise symmetry. Since the oblique ribbons are placed at either wall they may act as guiding vanes, giving the flow a small amount of streamwise vorticity. To investigate this effect the flow around a stationary ribbon needs to be solved. Unlike the non-stationary disturbance we cannot adjust the strength of the stationary ribbon to the experiments since no measurements exist for this effect (and because of its small magnitude found below it would be extremely hard to measure except close to the ribbon).

We are thus forced to use a more accurate modeling for this part. In the region occupied by the ribbon we add a damping term to the Navier-Stokes which is proportional to the velocity:

$$\mathbf{u}_t = NS(\mathbf{u}) - \lambda(x, y, z)\mathbf{u} \tag{2}$$

Where $\mathbf{u} = (u, v, w)^T$ and $NS(\mathbf{u})$ is the Navier-Stokes operator. λ is only (signficantly) nonzero inside the ribbon. This is equivalent to the action of a porous medium, and in the limit of infinite λ we obtain the solution for a solid ribbon.

For a ribbon running along the z'-direction we choose :

$$\lambda(x,y) = \lambda_0 \exp\{-[x'/c']^8 - [(y-y_l)/d]^4\}$$
(3)

Since we do not have any data to match the far field to, the parameters must now be taken as the real physical values c' = 1.5mm = 0.36h and $d = 25\mu m = 0.006h$. The magnitude of the damping was increased until no flow occurred inside the ribbon. The final value used was $\lambda_0 = 4000$.

The small size of the ribbon and the sharp gradients of the flow around it require very fine grids to resolve, thus it is in practise impossible to simulate the full 3D flow around the ribbons in this way. However, we can find the flow around one ribbon accurately if we assume that the flow is homogeneous in the z'-direction , which is usually designated the infinite sweep approximation. To this solution a simplified model of the same type as for the time dependent problem above can be matched. The simplified model can then be extended to two ribbons with finite length.

Figure 2 shows the solution for the flow around one infinite swept ribbon near the lower wall. Note that there is a wake formed behind the ribbon. At x'-positions

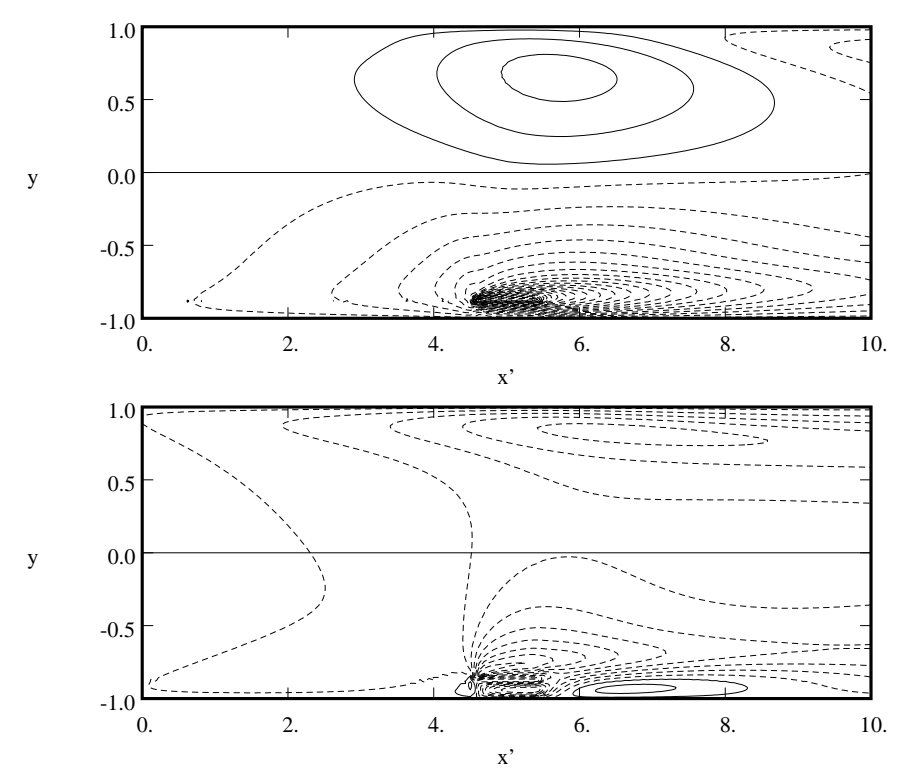


FIGURE 2. Flow around infinite stationary ribbon. (top) streamwise disturbance velocity, contour spacing 0.01; (bottom) spanwise velocity, contour spacing 0.005. Negative contours are dashed.

close to the ribbon it acts as a blockage. This moves the position of maximum streamwise velocity towards the opposite wall, leading to a surplus velocity in the upper half of the channel. Further downstream there is a velocity deficit in the whole channel due to the increased resistance.

As can be seen in the spanwise velocity component the flow deflects from the streamwise direction to become more chordwise after the ribbon.

The present effect can be understood in terms of a pressure gradient driven flow. There is a pressure drop across the ribbon which deflects the flow towards the chord direction. An analogy can be made with a porous wall (or screen) inserted in the channel perpendicular to the channel walls and parallel to the ribbon. It is well known that the flow in this case is deflected towards the normal to the screen. In the limiting case of very low porosity (high pressure drop) the flow leaves the porous wall in the direction normal to it. Under the ribbon the flow is

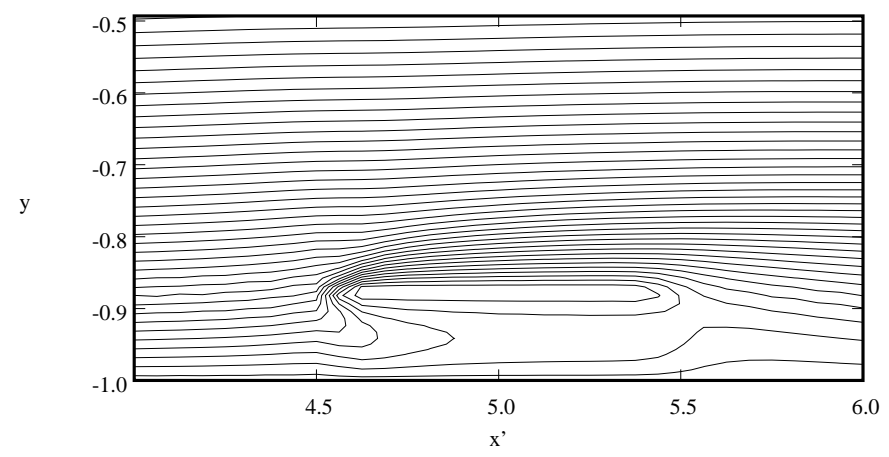


FIGURE 3. Close up of flow around ribbon. Streamwise velocity, contour spacing 0.02.

indeed deflected by about 43°, i.e the flow is almost chordwise. However, further downstream at x' = 10 the deflection is about 0.7° at the channel centreline increasing to about 2° at the lower wall and 4° at the upper wall.

A close-up of the streamwise velocity near the ribbon shown in Figure 3 reveals the sharp gradients near the ribbon. The closed contour line gives the extent of the ribbon, and shows that the no-slip condition is satisfied. There is a reduced flow under the ribbon and in the boundary layer above it which means that the ribbon acts as a partial blockage.

A simple model for the effect of the ribbon is given by the following volume force applied to the momentum equation:

$$\mathbf{F} = \begin{pmatrix} A_{u'} \\ 0 \\ A_{w'} \end{pmatrix} \exp\{-[\mathbf{x'/c'}]^2 - [(\mathbf{y} - \mathbf{y_l})/\mathbf{d}]^2\}$$
(4)

Here we use the same dimension of the ribbon as for the stationary force, i.e., $c'=1/\sqrt{2}$ and d=0.02. The resulting flow for $A_{u'}=-0.07$ and $A_{w'}=-0.04$ is given in Figure 4. Although there are significant discrepancies close to the ribbon when compared to Figure 2, the far field is remarkably similar. The extension to a finite length ribbon is now made in the same way as for the non-stationary force given by equation (1). Note that $A_{u'}$ and $A_{w'}$ are given in the ribbon oriented coordinate system, when rotated to the streamwise coordinate system they correspond to $A_u=-0.0778$ and $A_w=0.0212$ for the lower ribbon with the spanwise component negative for the upper ribbon.

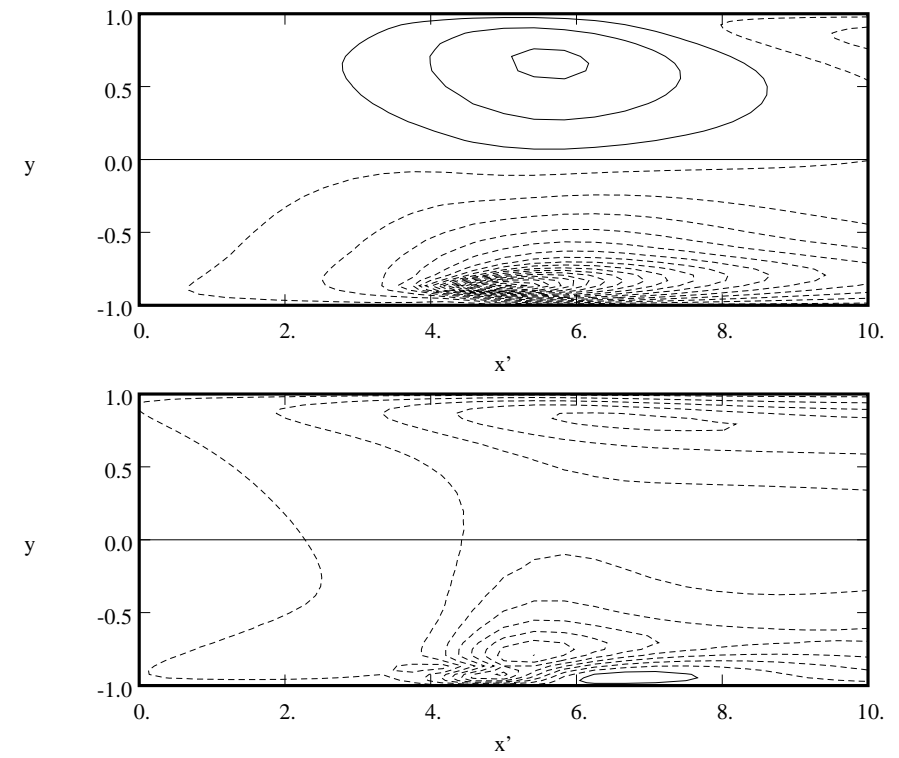


FIGURE 4. Flow around infinite stationary ribbon. Ribbon modeled by a volume force. (top) streamwise disturbance velocity, contour spacing 0.01; (bottom) spanwise velocity, contour spacing 0.005. Negative contours are dashed.

4 Numerical results

It is now possible to use the models developed above to compute the flow resulting from two oblique ribbons. We are especially interested in the time averaged velocity resulting from the oscillating ribbons which in the experiments showed a broken spanwise symmetry.

4.1 Stationary ribbons. The flow around the stationary ribbons was computed as a baseline case to be compared to simulations of time dependent flow. In Figure 5 (top) the streamwise velocity defect in the lower part of the channel can be seen. Near the ribbon at the lower wall (increasing x increasing z) the velocity defect is a few percent, near the upper ribbon there is a small velocity surplus in this half of the channel. The wake at the central part of the ribbons is quite weak except around z=0 where the ribbons cross. At the ends of the

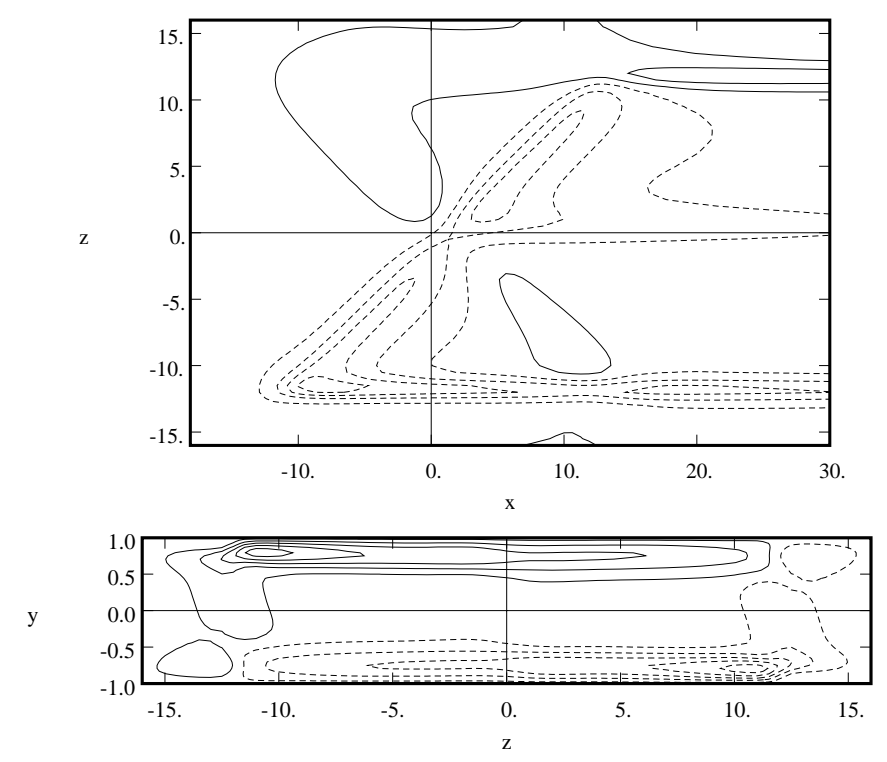


FIGURE 5. Flow around two stationary ribbons. (top) streamwise disturbance velocity at y = -0.75, contour spacing 0.02; (bottom) spanwise velocity at x = 20, contour spacing 0.001. The vertical scale has been stretched. Negative contours are dashed.

ribbons streamwise vortices are generated which leave an imprint on the streamwise velocity in the form of high and low speed streaks. The bottom part of Figure 5 gives the spanwise velocity in a cross stream plane downstream of the ribbons. There is a weak clockwise swirl which deflects the mean flow by about 0.5° near each wall at the spanwise centreline, with increasing spanwise flow near the surface and side where each ribbon is pointing downstream.

4.2 Low amplitude forcing. The stationary part of the disturbance field is a non-linear effect of the oscillation and hence quadratic in the forcing for small amplitudes. According to previous studies this part of the disturbance contains most of the disturbance energy before transition for moderate amplitude forcing. To avoid influence of higher order terms in the amplitude expansion the forcing is set to A=0.0001. In this first case we study the flow with time-dependent forcing only, i.e. no stationary forcing is applied.

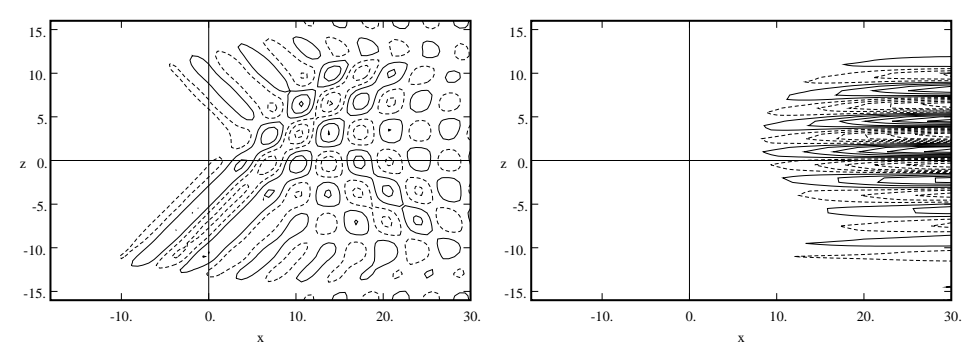


FIGURE 6. Flow around two oscillating ribbons. Streamwise disturbance velocity at y = -0.75. (left) instantaneous flow, contour spacing 0.0005; (right) time averaged flow, contour spacing 0.0001.

Figure 6 (left) shows the streamwise disturbance velocity near the lower wall. The waves coming from each ribbon cross and create a checkerboard pattern downstream. Note that the waves coming from the ribbon at the lower wall are visible earlier than the waves from the upper wall. The right part of the figure gives the time averaged streamwise disturbance velocity near the lower wall. A number of alternating high and low speed streaks are observed downstream of the ribbons, increasing in amplitude downstream.

Figure 7 shows a cross stream cut of a time averaged flow field downstream of the ribbons. Like in previous simulations and experiments we find in each channel side a series of high and low speed streaks which are associated with counterrotating streamwise vortices. The vorticity changes sign at about $y=\pm 0.8$. This is most likely an effect of the no-slip condition at the wall which requires the spanwise velocity in the vortex to go to zero more rapidly than for an irrotational motion. The sign change is observed also for wall bounded streamwise vortices in the buffer layer of a turbulent boundary layer.

The spanwise symmetry is broken in two respects. First, the high speed streaks in the lower and upper channel are not aligned with each other and the streaks are close to antisymmetric around the plane z=0; and secondly, the disturbance is stronger in the second and fourth quadrant. The latter observation together with the previous figure gives a clue to the reason for the symmetry breaking. The vortices are forced by a term which is proportional to the product of the left and right going waves' amplitudes. Since the wave does not spread immediately from a ribbon to the opposite wall the interaction between the waves occurs some distance downstream of the downstream pointing ribbon in quadrant one and three. As the

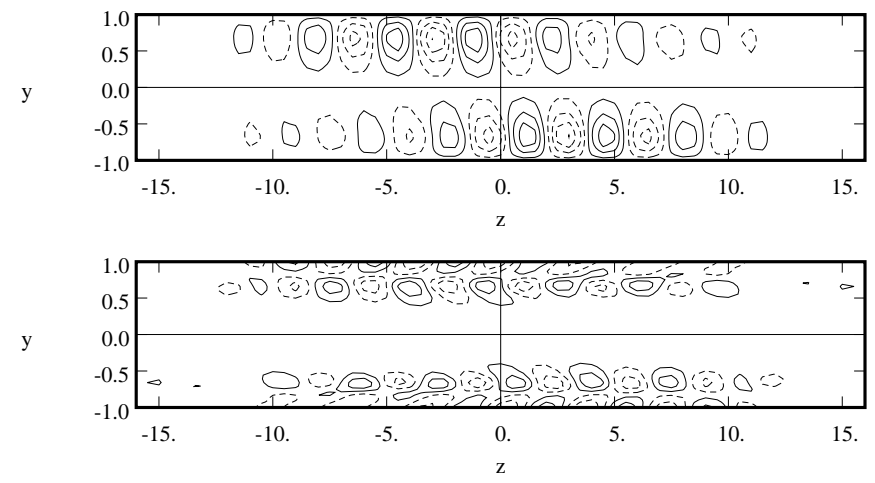


FIGURE 7. Time averaged flow from two oscillating ribbons at x=30. (top) streamwise disturbance velocity, contour spacing 0.00002; (bottom) streamwise vorticity, contour spacing 0.00001. The vertical scale has been stretched. Negative contours are dashed.

waves are damped at this Reynolds number the wave interaction is much weaker than in the quadrants where the interaction occurs closer to the ribbons.

4.3 Stationary and time dependent forcing. As found in the previous section the spanwise symmetry is broken even when no account is taken for the stationary flow blockage of the ribbon. When the stationary and low amplitude time dependent forcing is combined, the stationary forcing dominates due to its higher forcing amplitude. If, however, we are interested in the effect of the time dependent forcing on the mean flow we can subtract the mean flow calculated for stationary ribbons above. This part of the mean flow, although small at the present amplitude A=0.0001, grows quadratically with the forcing amplitude and will become important for stronger forcing.

Figure 8 shows a cross stream cut through the time averaged flow field, where the disturbance field of the stationary forcing is subtracted. Compared to Figure 7 without stationary forcing the amplitude has increased and the spanwise spacing between streaks and vortices have decreased somewhat.

However, the changes in the spanwise positions of the streaks and vortices near z=0 are small. If they followed the mean flow which is deflected $\alpha=0.5^{\circ}$ by the stationary ribbons, they would move about 0.25h to the right in the upper half and to the left in the lower part. The observed motion is in both directions in

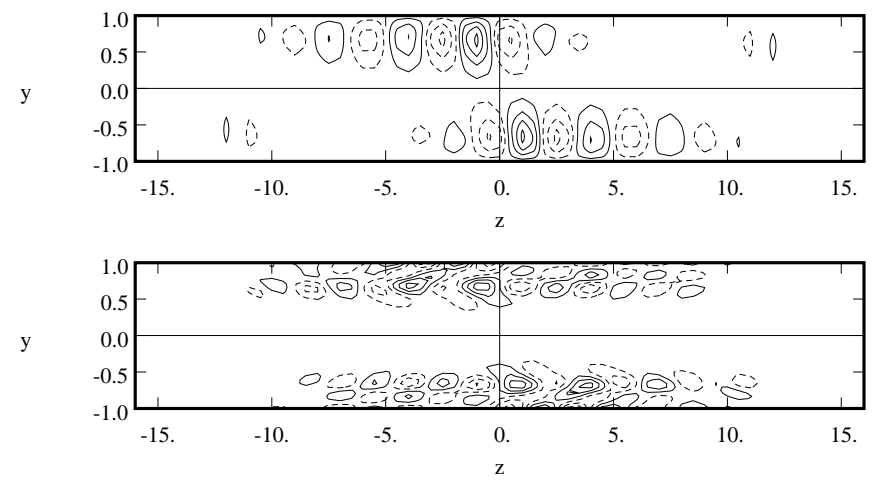


FIGURE 8. Time averaged flow from two oscillating ribbons less the flow for stationary ribbons at x=30. (top) streamwise disturbance velocity, contour spacing 0.0001; (bottom) streamwise vorticity, contour spacing 0.00005. The vertical scale has been stretched. Negative contours are dashed.

each channel half and thus does not seem to be a result of the spanwise deflection by the ribbons.

The increase in amplitude is most likely an effect of that the stationary forcing slows down the fluid at the ribbon position, thus the time dependent force becomes more effective in moving the fluid. The increased amplitude is observed also for the time dependent part of the solution (figure not shown). However, the increased amplitude of the wave is of no consequence for the model as the amplitude must be adjusted to that of the experiment a small distance downstream of the forcing. Thus it appears most straightforward to neglect the stationary force altogether in the following simulations.

4.3.1 Both ribbons at the lower wall

To demonstrate clearly that the spanwise symmetry is broken due to the placement of the ribbons at either wall a calculation with both ribbons on the lower wall was performed.

Figure 9 shows the resulting time averaged flow, the spanwise symmetry of the solution is of course trivial since the forcing as well as the equations are spanwise symmetric. Compared to Figure 7 the strength of the streaks has increased in the lower half and decreased in the upper half. This is consistent with the result above

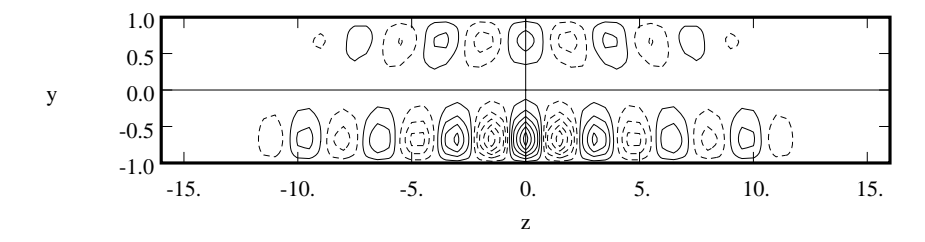


FIGURE 9. Time averaged flow from two oscillating ribbons at the lower wall. Streamwise disturbance velocity at x = 30, contour spacing 0.00002.

that the spanwise symmetry is broken due to the delay of the wave to reach full amplitude in the half-channel opposite to the ribbon.

4.4 High amplitude forcing. To be able to compare with experimental data obtained for the case with a large initial disturbance we need to increase the amplitude of the forcing. In accordance with what is said above the high amplitude simulation is performed without stationary forcing. The experimental data indicated a level of $u_{rms} = 0.04$ at (x, y, z) = (15, -0.75, 0). This level was achieved by adjustment of the A to 0.04 (the numerical agreement with u_{rms} is fortuitous).

Figure 10 shows the mean streamwise disturbance velocity in the lower part of the channel. Low and high velocity regions are formed downstream of the ribbons and in agreement with the previous section the streaks are weaker and appear further downstream for negative z. The spacing between the streaks is equal for the experiment and the simulation and also the amplitude evolution shows close correspondence.

The rms of the streamwise velocity shown in Figure 11 indicates a fair agreement between the experiment and the simulation. Regions of high rms appear at the same spanwise position but the maximum levels are different in the two cases.

Figure 12 shows contours of the time averaged streamwise disturbance velocity from a cross stream plane at x=16. As can be seen from the top part of the figure the experimental flow field is almost symmetric under rotation, except for the low velocity regions near z=0 which have a different amplitude in the lower and the upper channel half.

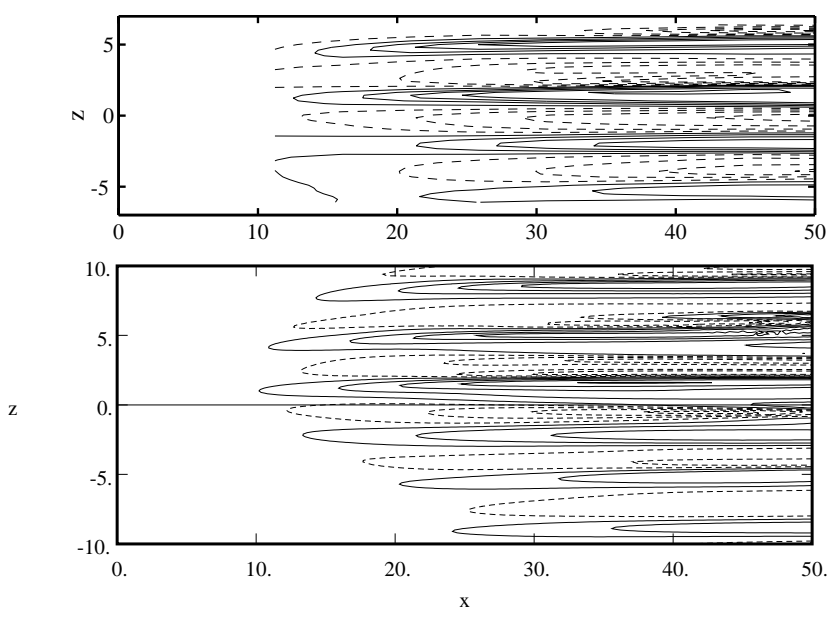


FIGURE 10. Mean streamwise disturbance velocity at y=-0.75. (top) experiment; (bottom) simulation. Contour spacing 0.05.

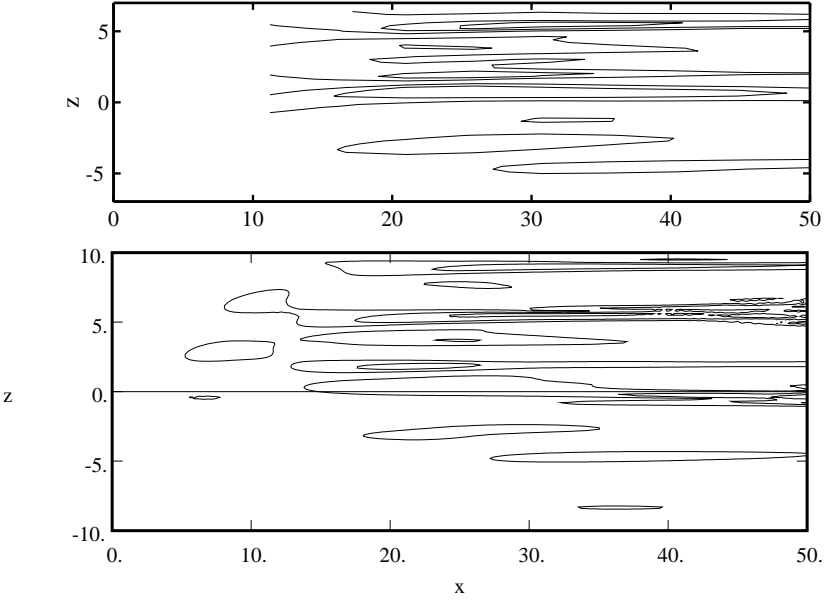


FIGURE 11. Streamwise velocity rms at y=-0.75. (top) experiment; (bottom) simulation. Contour spacing 0.04.

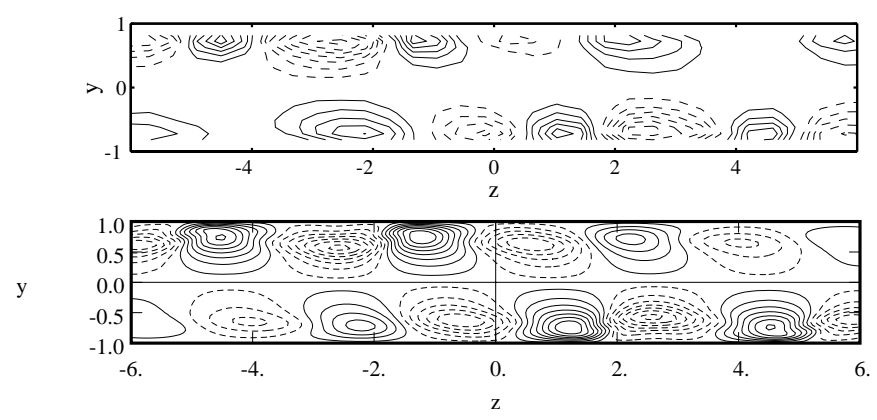


FIGURE 12. Time averaged flow from two oscillating ribbons at x = 16. (top) experiment; (bottom) simulation. Contour spacing 0.01. Negative contours are dashed.

5 Conclusions

Numerical simulations of oblique transition have been carried out using a numerical model which closely reflects the geometry of the experimental apparatus used in the experiments of Elofsson & Alfredsson (1995). The effect of the vibrating ribbons used in the experiments was simulated by adding a time dependent volume force to the Navier-Stokes equations at the position of the ribbons. Different numerical models were employed to investigate the stationary blockage effect of the ribbons and the flow field resulting from the vibrating ribbons.

The symmetry break observed in the experiments was found to result from the placement of the ribbons at opposite walls, which caused the nonlinear interaction to occur at different distances downstream of the ribbons for different cross stream positions. Also, the stationary blockage effect of the ribbons was shown to have negligible influence on the flow field some distance downstream of the ribbons.

When comparing the present simulation result and the experimentally obtained data they were found to be in close agreement with each other.

References

- ELOFSSON, P. A. & ALFREDSSON, P. H. 1995 Experiments on nonlinear interaction between oblique Tollmien-Schlichting waves. In *Laminar-Turbulent Transition* (KOBAYASHI, R., editor), pp. 465–472, Proc. IUTAM Symposium, Sendai 1994, Springer.
- Henningson, D. S., Lundbladh, A. & Johansson, A. V. 1993 A mechanism for bypass transition from localized disturbances in wall bounded shear flows. *J. Fluid Mech.* **250**, 169–207.
- KIM, J., MOIN, P. & MOSER, R. 1987 Turbulence statistics in fully developed channel flow. J. Fluid Mech. 177, 133–166.
- Landahl, M. T. 1975 Wave breakdown and turbulence. SIAM J. Appl. Math. 28, 735–756.
- Lundbladh, A. & Henningson, D. S., 1993 Numerical simulation of spatial disturbance development in rotating channel flow. FFA-TN 1993-30, Aeronautical Research Institute of Sweden, Bromma.
- Lundbladh, A., Henningson, D. S. & Johansson, A. V., 1992 An efficient spectral integration method for the solution of the Navier-Stokes equations. FFA-TN 1992-28, Aeronautical Research Institute of Sweden, Bromma.
- Schmid, P. J. & Henningson, D. S. 1992 A new mechanism for rapid transition involving a pair of oblique waves. *Phys. Fluids A* $\bf 4$, 1986–1989.

Experiments on the stability of streamwise streaks in plane Poiseuille flow

PER A. ELOFSSON¹, MITSUYOSHI KAWAKAMI² AND P. HENRIK ALFREDSSON¹

¹Department of Mechanics, KTH, S-100 44 Stockholm, Sweden ²Inst. of Fluid Science, Tohoku University, Sendai, Japan

Abstract

The development and stability of streamwise streaks are studied in an air-flow channel experiment at sub-critical Reynolds numbers. The streaks were generated by continuous suction through small slits at the wall. The streak amplitude first grows algebraically, and if the amplitude exceeds a certain threshold secondary instability in the form of travelling waves are observed. These waves give rise to high u_{rms} values in the region of large spanwise mean flow gradient. Measurements with two hot-wire probes indicate that velocity fluctuations are 180° out of phase at two neighbouring peaks at each side of a low velocity region and implies the existence of a sinuous type instability.

Measurements were also made with controlled disturbances where earphones were used to force the secondary instability. Phase averaged data clearly shows the oscillation of the low velocity region and also provides the growth rate, phase speed as well as amplitude and phase distributions of the secondary instability. Several of these features suggest that the instability is of inflectional origin. Finally the disturbance breaks down and the flow undergoes transition to turbulence. It is hypothesized that this scenario resembles certain types of bypass transition.

1 Introduction

1.1 Instabilities through transient growth. Non-modal amplification of three-dimensional disturbances has recently attracted several researchers to investigate the possibility that such disturbances may be part of subcritical transition known to occur in many wall bounded shear flows. Ellingsen & Palm 1975 and Landahl 1980 showed for the inviscid case that three-dimensional disturbances could grow linearly in time, and Gustavsson 1991 extended their analysis to viscous plane Poiseuille flow. He found that three-dimensional streamwise oriented structures

could be amplified also at subcritical Reynolds numbers, i.e. the disturbance energy would at first grow linearly in time, but that the disturbance ultimately would decay due to viscosity. The streaky structures will not lead to transition by themselves even though their growth can be substantial. A possible route to transition would be that the streaks, after growing to some threshold amplitude (which depends on for instance the Reynolds number and the spanwise wavelength of the streaks) become unstable and develop a time dependent wave instability. This type of instability will in the following be referred to as a secondary instability.

Many theoretical papers on transient growth have appeared in addition to the paper by Gustavsson 1991 (see for instance Boberg & Brosa 1988, Butler & Farrell 1992, Henningson 1995, Trefethen $et\ al.$ 1993). Most papers deals with the temporal amplification of disturbances although in a physical experiment the growth is rather spatial than temporal. One exception is the theoretical work of Luchini 1996 who was able to find a similarity solution for a three-dimensional disturbance in boundary layer flow, which was found to amplify in the downstream direction as $x^{0.213}$. In this case the growth is not followed by viscous decay since the Reynolds number is increasing in the downstream direction.

Several numerical as well as physical experiments show that transient growth also occur for spatially developing channel flows. One example is the experiment by Klingmann 1992 who investigated growing three-dimensional disturbances in plane Poiseuille flow at subcritical Reynolds numbers. She used a point-like disturbance which developed into streaky structures. The energy of the structure first increased linearly, whereupon, depending on the strength of the initial disturbance, it either decayed or gave rise to a turbulent spot. This scenario seems to be close to what is described by the temporal analysis. Henningson, Lundbladh & Johansson 1993 made direct numerical simulations of the same flow with a localized disturbance which further corroborated the transient growth mechanism. It is noteworthy that one old transition experiment has recently been re-evaluated and evidence for the existence of transiently growing disturbances was found (see Mayer & Reshotko 1997). In the analysis the temporal development was converted to a spatial development by using the propagation velocity of the disturbance.

Another interesting scenario where transient growth is one of the major components is the so called oblique transition which was first suggested by Schmid & Henningson 1992. The starting point is the introduction of two oblique waves of small but finite amplitude. The wave-pair can be characterized by $(\omega_0, \pm \beta_0)$, where ω_0 is their angular frequency and $\pm \beta_0$ their spanwise wave numbers. They may interact non-linearly and the first generation interaction will, among others, give rise to a $(0, \pm 2\beta_0)$ mode, which corresponds to a stationary, spanwise periodic disturbance. It was found by Schmid & Henningson that the $(0, \pm 2\beta_0)$ mode initially reach high amplitudes through transient growth. Experimentally this has

been verified in plane Poiseuille flow by Elofsson & Alfredsson 1995 1998, whereas Berlin, Lundbladh & Henningson 1994 carried out direct numerical simulations of oblique transition in a Blasius boundary layer flow (i.e. the initial disturbance was two oblique waves) and found that after an initial growth of the streaky structures a rapid growth of modes with nonzero ω followed.

The secondary instability of transiently growing streaks has recently been investigated by Reddy et al. 1998 through direct numerical simulations and stability calculations. Their results indicate that the secondary instability mainly is due to spanwise inflectional profiles which occur through the transient growth of the streaky structures. A similar analysis were made by Hamilton, Kim & Waleffe 1995 and Waleffe 1995 who investigated streak breakdown in Couette flow. In these studies streak breakdown was one part of a process describing self-sustained turbulence near walls.

1.2 Instabilities associated with streamwise vortices. Wall bounded flows which are affected by body forces normal to the wall, such as flow over curved surfaces or curved channels, flows undergoing system rotation or flows affected by buoyancy may develop streamwise oriented vortices (see for instance the review on Görtler vortices by Saric 1994). These vortices will at first grow exponentially and this development can be well predicted through linear stability theory assuming the principle of exchange of stability to be valid. However, the vortices will give rise to streamwise streaks of high and low velocity which are susceptible to secondary instability in the form of travelling wave disturbances. This may be quite similar to the transition scenario developing after transiently growing streaks have been established.

Swearingen & Blackwelder 1987 investigated the detailed breakdown process of counter-rotating streamwise vortices generated on a concave wall via the centrifugal or Görtler instability mechanism. Their study was focused on the travelling wave type instability which takes place on the streaks just prior to the vortex breakdown. Flow visualization showed two types of secondary instability, one sinuous and one varicose. Their hot-wire measurement studied the sinuous instability which was manifested by the presence of a two-peak structure in the u_{rms} distribution. These peaks are located on the sides of low-speed regions. Both naturally occurring and forced disturbances were measured. They concluded that the maximum disturbance amplitude was found in regions of high spanwise shear and that the spanwise inflectional profiles were responsible for the secondary instability.

Masuda, Hori & Matsubara 1995 showed for a boundary layer developing on a flat plate subjected to system rotation (in this case the Coriolis force takes the role of the centrifugal force) that the mode selection (sinuous or varicose) depends on the initial spanwise wavelength of the vortex structure, a small wavelength is

more susceptible to the sinuous mode whereas a large wavelength gives rise to the varicose mode. Theoretical analysis by Bottaro & Klingmann 1996 for Görtler flow has shown that it is the sinuous mode that becomes unstable first. They also gave an expression for the most unstable frequency of the sinuous instability, which correlated well with some of the experimental findings by Swearingen & Blackwelder. Other theoretical/numerical investigations can be found in Yu & Liu 1991 and Liu & Domaradzki 1993.

In curved channel flow Matsson & Alfredsson 1994 investigated naturally occuring travelling waves which formed on top of the primary Dean vortex structure. The same flow was also investigated through numerical simulations by Finlay, Keller & Ferziger 1988. An experiment in a rotating plane channel was made by Matsubara & Alfredsson 1997 where both the primary vortex structure as well as the secondary instability was triggered in a controlled way (see also the numerical study of Finlay 1990). In the experiments both sinuous and varicose modes were forced but only the sinuous were found to have a positive growth rate. In this study the wave properties were accurately mapped, both the shape, growth and phase speed. Also here the inflectional spanwise profiles were found to be associated with the instability.

An experiment where the vortex structure was generated on a flat plate inside the boundary layer by means of longitudinal roughness elements was reported by Bakchinov *et al.* 1995 In that case wave disturbances were introduced into the boundary layer with a vibrating ribbon and the observed high-frequency instability was found to be similar to the sinuous mode observed in Görtler flow.

1.3 Tollmien-Schlichting wave transition.

1.3.1 Boundary layer flows

Traditionally the linear stability of two-dimensional wave-disturbances, known as Tollmien-Schlichting waves (hereafter, T-S wave) has been the starting point to investigate transition in boundary layer flows. Schubauer & Skramstad 1947 experimentally verified the existence of such waves whereas extensive investigations were conducted by Klebanoff & Tidstrom 1959 and Klebanoff, Tidstrom & Sargent 1962. It was then realized that before transition occurred the wave became three-dimensional and another instability developed. In their experiment primary disturbances were introduced using the vibrating ribbon technique and single strips of tape placed apart beneath the ribbon controlled the three-dimensionality of the flow. Measurements of the spanwise component detected an existence of longitudinal vortices, which were coupled to the peak-valley structure.

The peak-valley structure intensifies downstream and forms a local shear layer at the position corresponding to the *peak*. This breaks down into, so called, hairpin

eddies just prior to the transition, where time traces of the streamwise velocity exhibit spikes and subsequent high-frequency wave packets. This type of the breakdown process is called K-type after Klebanoff and is expected under reasonably large two-dimensional input intensities (order of $1 \% u'/U_{\infty}$), while for smaller amplitude of the T-S wave another type of the regime is detected. This interaction, which results in the staggered Λ -vortices visualized by Saric & Thomas 1984, has been observed experimentally in a transitional boundary layer by Kachanov *et al.* 1977 and Kachanov & Levchenko 1984. Later Corke & Mangano 1989 established the sub-harmonic interaction by simultaneous generation of controlled two- and three dimensional disturbances.

1.3.2 Plane Poiseuille flow

In plane Poiseuille flow transition to turbulence usually is observed at much lower Reynolds numbers than the linearly critical Re of 5772. In the flow visualizations by Carlson, Widnall & Peeters 1982 turbulent spots were observed for Re down to 1000. This subcritical transition belongs to the class of transition scenarios denoted bypass. However, Nishioka, Iida & Ichikawa 1975 showed a few characteristics of wave disturbances in plane Poiseuille flow which indicated that the waves develop according to linear stability theory, and later that work was extended by Elofsson & Alfredsson 1998 to also include results for oblique waves. Since the study of Nishioka $et\ al.$ numerical simulations have shown that transition follows the same steps as in boundary layers, although sub-harmonic breakdown is unlikely under unforced conditions.

1.4 Present work. The present study deals both with the transient growth of streaky structures, and their instability characteristics which lead to streak breakdown. The experiment has been conducted at sub-critical conditions in plane Poiseuille flow where the streamwise streaks have been forced. Both natural and forced secondary instabilities on the streaks have been studied, and instability characteristics such as growth rate, phase speed and amplitude distributions have been mapped. In §2 we describe the experimental setup and procedure. Section 3 contains experimental results and consists of three parts. The first part treats the development of the streaky structure, whereas the second and third parts deals with natural and forced secondary instability, respectively. Further discussion and concluding remarks are given in §4.

2 Experimental apparatus and procedure

2.1 Channel and traversing system. The experiments were conducted in an air-flow channel at the Department of Mechanics at the Royal Institute of Technology (KTH). The channel was originally used by Klingmann 1992 and later modified in part by Elofsson & Alfredsson 1998. The air was supplied by a centrifugal fan, running at constant speed via a silencer to two damping chambers. The flow rate was adjusted by a valve open to the atmosphere connected to the first of the damping chambers. The air coming to the channel is distributed through a perforated pipe and a high flow-resistance screen to the stagnation chamber via guide vanes and a package of three turbulence damping screens. Downstream the screen package a carefully polished 40:1 ratio contraction part leads the air to the 1.9 m long channel. The channel consists of two 10 mm thick parallel glass plates separated by 8.2 mm thick distance bars of aluminium. They are positioned to give a channel width of 830 mm, yielding an aspect ratio of 101 (see Figure 1).

The channel is equipped with static pressure taps and a total pressure probe for calibration and monitoring purposes. The total pressure probe can be inserted into the channel from its downstream end. It has a conical shape with its largest diameter equal to the channel width which automatically makes the pressure sensing opening to be located at the channel centreline.

2.2 Hot-wire measurements. The streamwise velocity component was measured with a constant temperature anemometer (AA-systems model 1003) using platinum single wire probes with a wire diameter and length of 2.5 μ m and 0.5 mm, respectively.

The traversing system for the hot-wire probe is automatic through the use of stepping motors in two directions, namely in the normal (y) direction with a step of 0.015 mm and in the spanwise (z) direction with a step of 0.05 mm. In the streamwise (x) direction it can be moved manually. In the spanwise and streamwise directions the probe is moved with two perpendicular guide systems. In the y-direction it is moved via a wedge-mechanism which makes the hot wire move along a circular arc. In this way it is possible to come close to both sides of the channel. Since the distance from the wire to the axis of rotation is 11.7 cm the variation in streamwise location of the wire is less than 0.1 mm when moved from the centre to the wall.

A Macintosh computer and a National Instruments plug-in board were used to control the stepping motors and the data acquisition.

Calibration of the hot wire was carried out against the parabolic velocity profile by means of traversing the probe in the wall-normal direction at a position

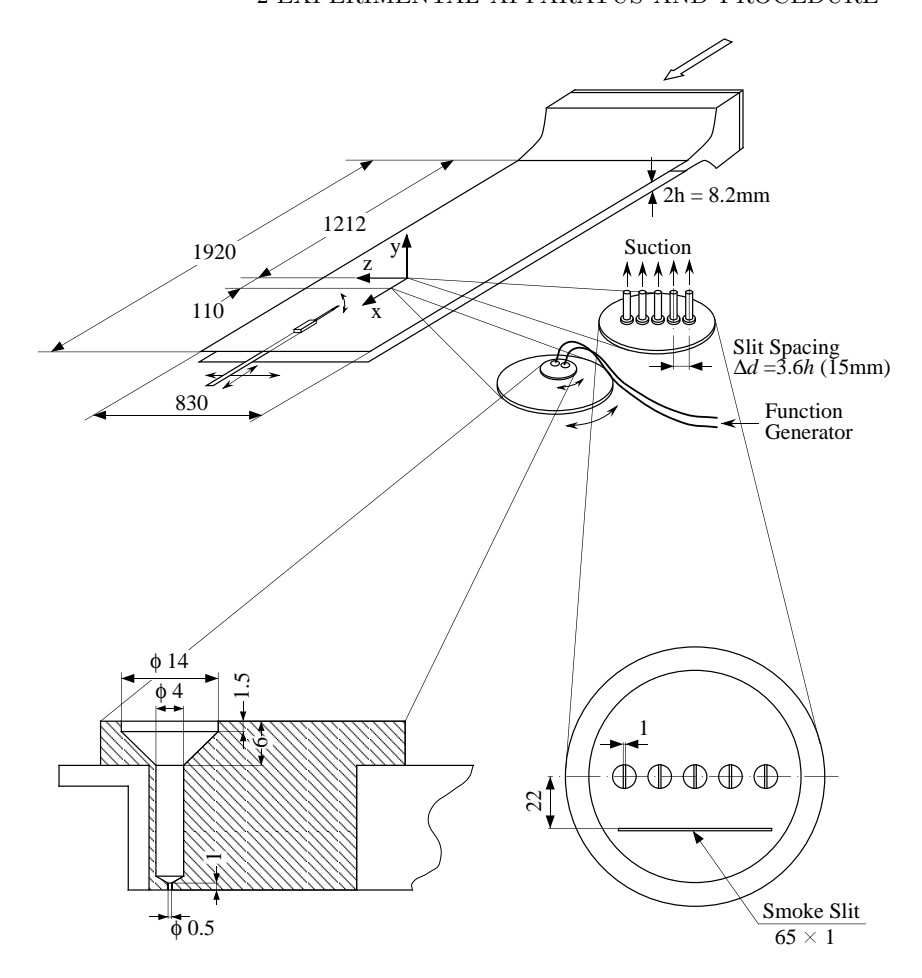


FIGURE 1. Experimental set-up. All measurements in mm.

296h downstream of the channel inlet. The calibration curve used was,

$$U = k_1 (E^2 - E_0^2)^{1/n} + k_2 (E - E_0)^{1/2},$$
(1)

where E is the anemometer voltage at the velocity U, E_0 the voltage at zero velocity and the coefficients k_1, k_2 and n are determined from a best fit of the data to the calibration function. Typically the calibration procedure resulted in an error less than 1% for all calibration points.

2.3 Flow visualization technique. For flow visualization, a smoke sheet was introduced through a transversely oriented slit at the upper channel wall (see Figure 1). Smoke was generated with a portable fog-generator and a small fan mounted to the smoke chamber made it possible to adjust the thickness of the

smoke layer. Photographs were taken from the lower side of the channel, using a flash mounted downstream of the channel exit. The flow visualization was made at unforced conditions for a fixed Reynolds number and streak amplitude.

2.4 Disturbance sources. In this study two types of disturbances are introduced through two 90 mm diameter aluminium plugs which can be rotated. The centres of the plugs are located at 296h and 323h downstream of the channel inlet. The upstream plug is used to generate a stationary disturbance and the downstream plug for a time-periodic secondary disturbance. The origin of the xyz coordinate system is at the centre of the upstream plug and half-way between the lower and the upper plate.

2.4.1 Primary disturbance

The primary disturbance, consisting of regularly spaced high and low velocity streaks, is generated by applying suction through five slits (1 mm wide and 10 mm long) in the upstream plug, which allows the streak amplitude as well as its wave length to be controlled. The slits are made in circular plugs with a diameter of 10 mm, and these plugs are mounted in the large plug with diameter 90 mm. Since both the large plug as well as the small slit-plugs can be rotated the streak spacing can be varied in the range from 0 mm to 15 mm, and still have the slits aligned in the streamwise direction. The slits are connected to plastic tubes which go together into a low-pressure tank connected to the inlet of a centrifugal fan. The suction rates at the five slits can be adjusted by clamps mounted around the tubes and are individually regulated to give a homogeneous sinusoidal spanwise profile for each streak amplitude case. Since the suction is applied at the upper channel wall the generated streaks are mainly confined to the upper half-channel. High velocity regions are centred at the slit positions and low velocity regions in between.

Experiments were made for different suction rates giving different streak amplitudes. Most of the measurements were conducted with a streak wave length of 15mm ($\approx 3.6h$). The flow field where only suction is employed is hereafter called the 'natural case' in contrast with the 'forced case' which will be described in the next section.

2.4.2 Secondary disturbance

The main aim of this experiment was to study the development of a time-dependent secondary instability on the primary streaky disturbance. Phase controlled disturbances were introduced downstream the slits at the second large plug through two small holes (diameter 0.5 mm) 6 mm apart. As for the slit disturbances a

combination of two circular plugs made it possible to position the outlet holes at various spanwise positions without changing the spacing between them. The outlets were made in a 30 mm diameter Plexiglass plug and two earphones were glued in cavities made in the plug with the same diameter as the earphones. This gave an area contraction of 64:1 between the earphone chamber and the outlet hole.

The earphones were driven by a sinusoidal signal from a function generator and were either driven out-of-phase or in-phase according to the desired forcing mode. The movement of the earphone membranes gives rise to an alternate injection and suction through the holes at the wall. For the input voltages used the measured rms of the streamwise velocity filtered at the forcing frequency was less than 0.6 % of the laminar centreline velocity close to the forcing. The response of the disturbance generator in a frequency band ranging from 10 Hz to 500 Hz showed a monotone decrease of the energy output to the flow, i.e. there is no resonance for the forcing system within this frequency range.

Since the hot-wire signal and the output from the function generator are sampled simultaneously, phase information for the signals were obtained.

2.5 Data presentation. In the presentation of data all lengths and velocities are scaled by the channel half-height (h) and the laminar centreline velocity (U_{CL}) , respectively. The Reynolds number is defined as $Re = U_{CL}h/\nu$, where ν is the kinematic viscosity. The experiment is conducted at sub-critical Reynolds numbers in the range of Re = 2000 to Re = 2900. For those Reynolds numbers measurements of the laminar centreline velocity U_{CL} across the channel show a deviation of less than $\pm 0.5\%$ in the spanwise direction $(-16 \le z \le 16)$ and $\pm 0.4\%$ in the streamwise direction $(0 \le x \le 120)$. The maximum background disturbance level was found to be 0.3% of U_{CL} .

To describe the measurement results we decompose the velocity field U(x, y, z, t) in a time averaged part \overline{U} and a fluctuating part u,

$$U(x, y, z, t) = \overline{U(x, y, z)} + u(x, y, z, t).$$
(2)

For the stationary disturbance field we use U_d defined as

$$U_d(x, y, z) = \overline{U(x, y, z)} - \frac{1}{z_1 - z_0} \int_{z_0}^{z_1} \overline{U(x, y, z)} \, dz, \tag{3}$$

where z_0 and z_1 are the spanwise limits of the measurement region. However, as a direct measure for the streak amplitude we will rather use $\Delta U(x)$, which is defined as the peak-to-peak value of \overline{U} in the spanwise direction. The reason for the use of two measures is that the initial sine-shape of the spanwise profiles of \overline{U} will change at large amplitudes or large x, and the narrower shape of the low velocity regions will result in a non-symmetric distribution of U_d .

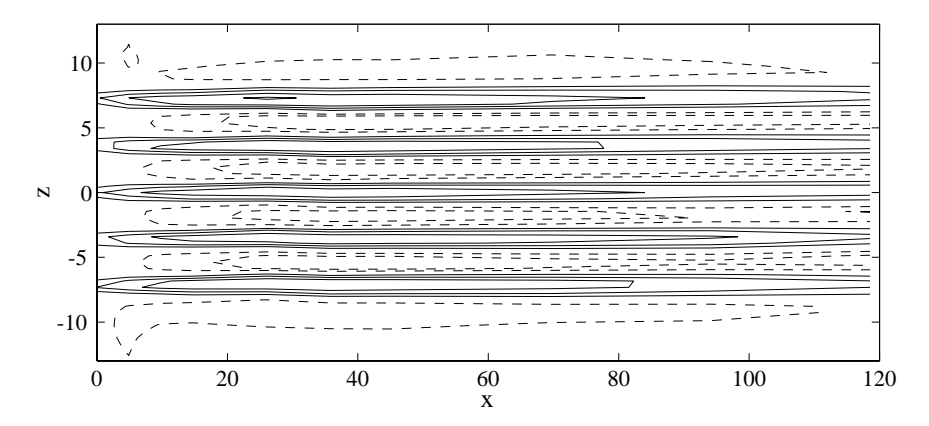


FIGURE 2. Contours of U_d in an xz-plane at y=0.6 for Re=2000 and $\Delta U_{max}=0.40$. The figure is based on measurements in a plane spanned by 10 streamwise and 57 spanwise positions. Contours are $\pm 6\%$, $\pm 12\%$, ... Negative contours are dashed.

To characterize time dependent disturbances rms measures will be used, either the total rms, u_{rms} , or a value filtered in a narrow band around the frequency f_i , u_{rms,f_i} . The forcing frequency will be denoted the fundamental or first harmonic frequency and represented by f_1 .

3 Experimental results

3.1 Induced streaky structure. The streaky structure is triggered by suction at the upper channel wall through five slits which are oriented in the streamwise direction. The streak spacing (λ_z) and the Reynolds number are in the following, if not otherwise stated, fixed at 3.6h and 2000, respectively. This corresponds to a spanwise wavenumber $\beta = 2\pi h/\lambda_z = 1.75$. In the upper half of the channel suction draws high momentum fluid toward the wall, resulting in a stationary streaky structure which consists of alternating high and low velocity regions in the spanwise direction. Figure 2 shows a contourplot of U_d in an xz-plane at y=0.6 obtained with a relatively low suction flow rate for a Reynolds number of 2000. At the given conditions ΔU reach a maximum value of about 0.4 after which the streak amplitude decays. In this case breakdown does not occur. The development of the streaky structures in this figure (i.e. first a rapid growth followed by a slow decay) is similar to what is to be expected for a transiently growing disturbance.

The streamwise elongated structure gives rise to two types of inflectional velocity profiles, one in the wall-normal direction at the centre of the low velocity

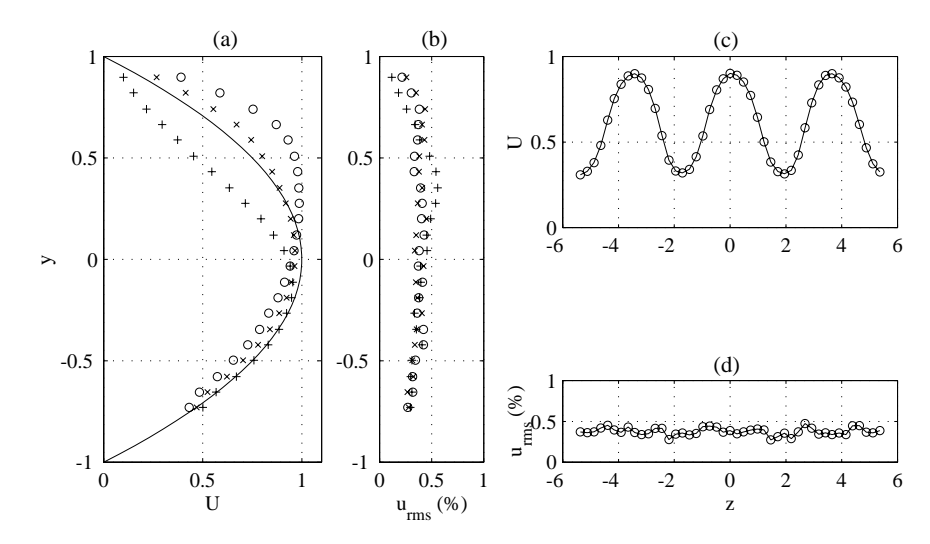


FIGURE 3. Wall-normal profiles of (a) \overline{U} and (b) u_{rms} at x=45 for three different spanwise positions: \circ , z=0; \times , z=-0.75; +, z=-1.7. Solid line in (a) shows the parabolic profile. Spanwise profiles at y=0.63 of (c) \overline{U} and (d) u_{rms} .

region and the other in the spanwise direction. This is illustrated in Figure 3 which shows velocity profiles obtained at the same Reynolds number as in the previous figure but for a larger streak amplitude. Figure 3(a) and (b) shows wall-normal profiles of \overline{U} and u_{rms} respectively for three different spanwise positions. The profiles with u_{rms} look similar at the different spanwise stations whereas the \overline{U} -profiles show a changing behaviour, which is clearly seen in the spanwise profile displayed in Figure 3(c). One can further note that despite the fairly large amplitude of the stationary disturbance structure ($\Delta U \approx 0.6$), u_{rms} is only about 0.5% [Figure 3(d)].

The initial growth of the streaky structures can be seen in Figure 4. The figure shows the development of ΔU for small x at five different suction rates (giving rise to maximum streak amplitudes in the range between 37% and 71%). For all cases it seems that the initial growth of the amplitude is linear in x. This further strenghten the hypothesis that the streaks are undergoing transient growth.

The overall evolution in the streamwise direction of ΔU and u_{rms} is plotted in Figure 5(a,b), respectively. These figures contain the results from several suction flow rates resulting in streak amplitudes of up to 78% of U_{CL} . The data in the figures represent the maxima in each cross-stream plane. The streak amplitude displays a rapid growth followed by a slow decay, and as can be seen in Figure 5(b) the value of u_{rms} remains constant with x for most initial streak amplitudes.

However, for the two largest streak amplitudes u_{rms} shows a significant growth for the most downstream positions. The threshold in the streak amplitude for a growth of u_{rms} was found to be approximately 70% of U_{CL} .

3.2 Secondary instability at unforced conditions. As observed in Figure 5(b) the rms level starts to grow if the streak amplitude is high enough. Figure 6 shows contour plots of U_d (a,c) and u_{rms} (b,d) for two Reynolds numbers (Re=2000 and Re=2500). The contour lines for u_{rms} are plotted with logarithmic increments, which for an exponentially growing disturbance would give rise to equal spacing between neighbouring contours.

At Re=2000 [Figure 6(a,b)] the suction was set to get $\Delta U_{max} = 78\%$, which is large enough to give rise to disturbance growth. The negative regions of the streaky structure is quite persistent in the downstream direction whereas the positive regions are less so. The rms distribution shows that the disturbances first are observed in the region between the high and low speed regions. The spacings of the logarithmic contour lines do show that the disturbance growth is close to exponential.

Figure 6(c,d) show similar results for Re=2500 where the maximum streak amplitude was 81% which results in transition to turbulence at the downstream end of the channel. High values of u_{rms} can be observed at both sides of the low velocity regions and the transition sets in earlier at regions with negative U_d than

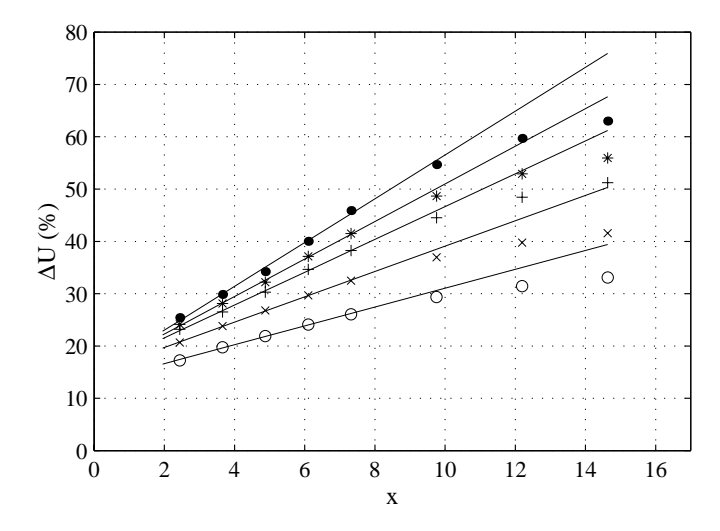


FIGURE 4. Initial transient growth of streak amplitude ΔU . Different symbols represent the variation in the initial streak amplitude.

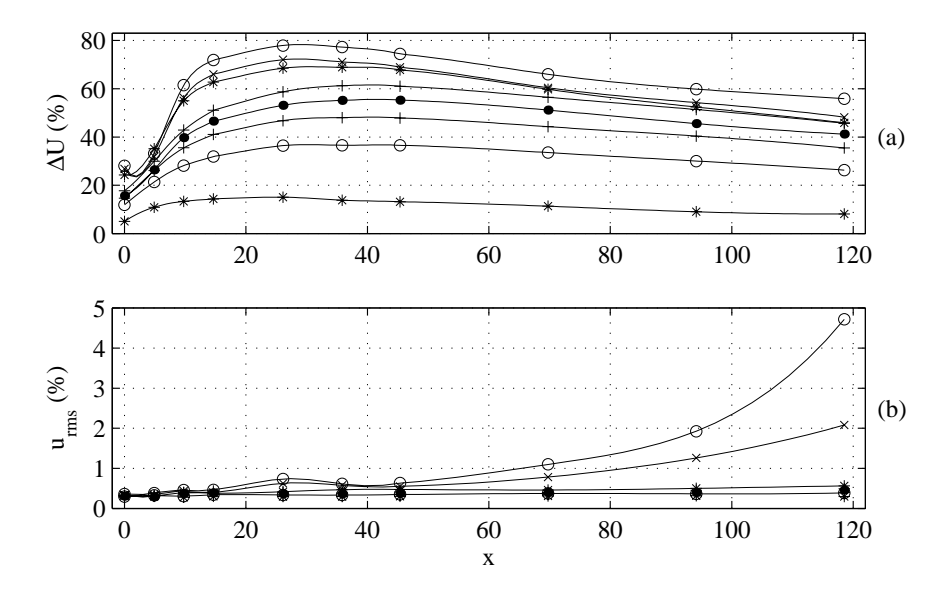


FIGURE 5. Evolution of (a) streak amplitude ΔU and (b) u_{rms} for Re=2000.

for areas of positive U_d . For $Re=2500~u_{rms}$ reach values of about 13% before transition sets in at $x \approx 95$.

In Figure 7 contours of various disturbance measures are shown in cross-stream planes for two streamwise positions, x = 26 and x = 70. The top figures (a,f) shows contours of the time average of the total velocity (\overline{U}) whereas Figure 7(b,g) shows U_d . From the figures it is observed that the effect of the suction applied at the upper wall is concentrated to the upper channel half (y > 0). The u_{rms} (c,h) have the largest values at regions which correspond to spanwise gradients of U_d , and at x = 70 there is a clear two-peak structure in u_{rms} centred around each low velocity region. To further investigate the relation between the positions of peaks in u_{rms} and the time-averaged velocity field derivatives of \overline{U} were calculated. Before the derivatives were evaluated the measured velocity field was interpolated using cubic splines. Contours of $\partial \overline{U}/\partial z$ are shown in Figures 7(d,i) and the corresponding gradients in the wall-normal direction, $\partial \overline{U}/\partial y$ are shown in (e,j). When comparing the absolute value of the gradients with the u_{rms} distributions it seems clear that large time-dependent disturbances appear mainly at regions with large spanwise gradients in the time-averaged field. However, one should note that the y-positions for the maxima in u_{rms} and $|\partial \overline{U}/\partial z|$ are not identical.

Figure 8 shows a flow visualization picture of the flow in an xz-plane near the upper wall of the channel. In the figure the flow is from left to right and the grid

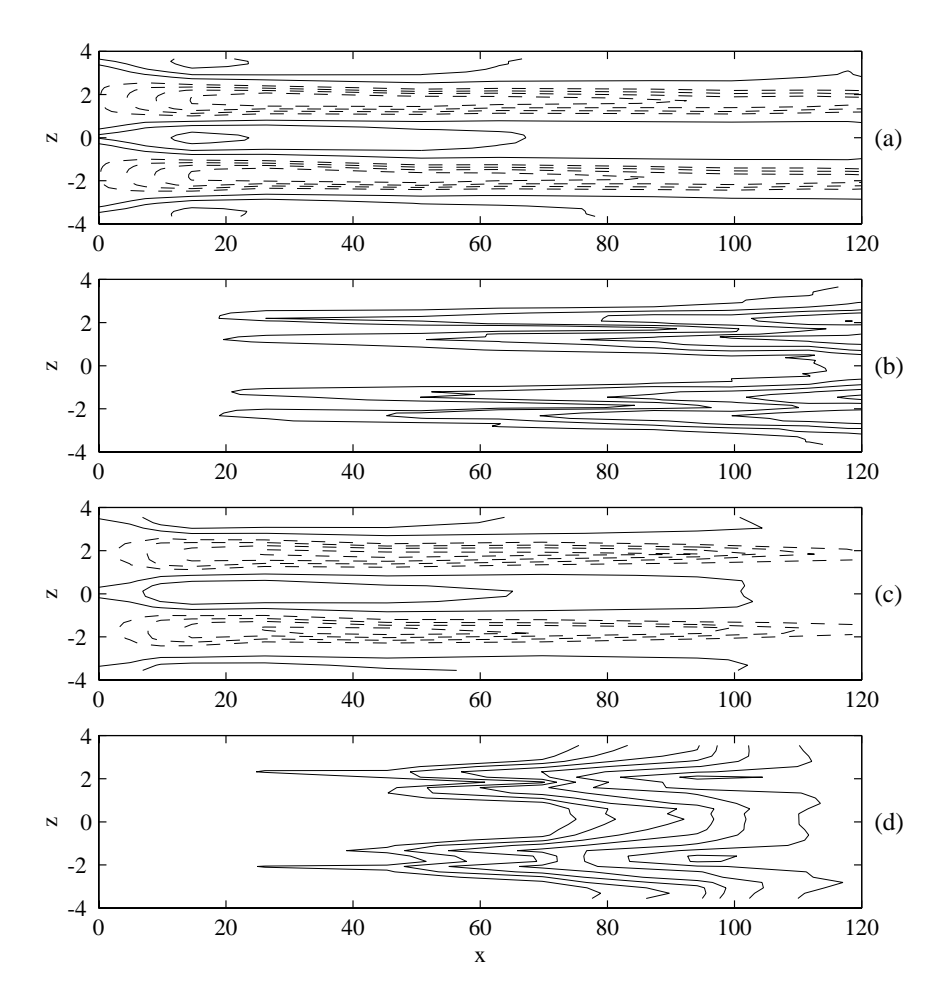


FIGURE 6. Contours of (a,c) perturbation velocity U_d and (b,d) u_{rms} in an xz-plane at y=0.63. (a,b) Onset of natural instability for $Re{=}2000$ and (c,d) turbulent transition for $Re{=}2500$. Each figure is based on measurements in a plane spanned by 11 streamwise and 61 spanwise positions. Contours are $\pm 10\%, \pm 20\%, \ldots$ for U_d , logarithmic 0.6%, 1%, 1.6%, 2.7%, ... for u_{rms} . Negative contours are dashed.

lines have a spacing of 50 mm in the streamwise direction. The most left-hand side vertical line corresponds to x=150 mm ($\approx 37h$) and the horizontal grid line represents z=0. Due to a circular brass-plug mounted in the lower glass

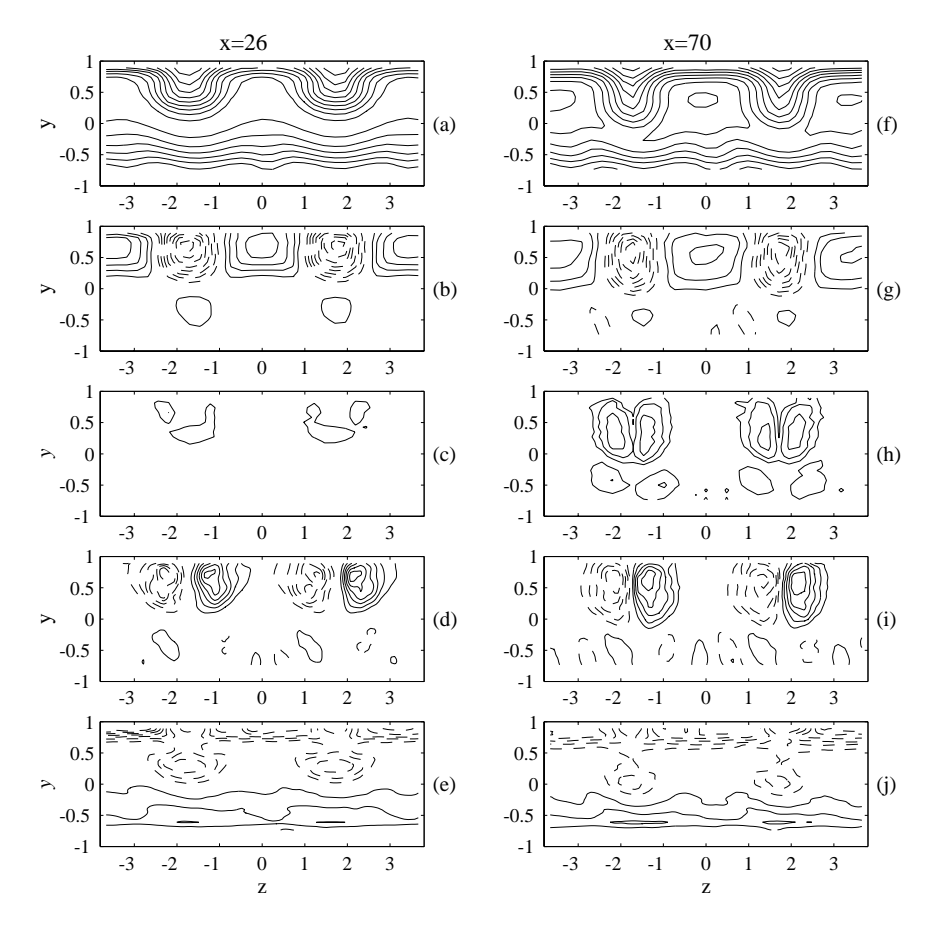


FIGURE 7. Contours of (a,f) \overline{U} , (b,g) U_d , (c,h) u_{rms} , (d,i) spanwise- and (e,j) wall-normal velocity gradients in yz-planes at (a-e) x=26 and (f-j) x=70 for the natural disturbance case. Each figure is based on measurements in a plane spanned by 22 wall-normal and 31 spanwise positions. Contours are $10\%, 20\%, \ldots$ for \overline{U} , $\pm 6\%, \pm 12\%, \ldots$ for U_d , logarithmic 0.6%, 1%, 1.6% for $u_{rms}, \pm 0.5, \pm 1, \ldots$ for $\partial \overline{U}/\partial z$ and $\pm 0.15, \pm 0.3, \ldots$ for $\partial \overline{U}/\partial y$. Negative contours are dashed.

plate (used in a previous experiment), information is lacking in the region near $x=300~\mathrm{mm}.$

The homogeneous smoke layer from the spanwise slit becomes concentrated to four distinct smoke lines just downstream of the smoke slit and each of them indicates the centre of a low speed region located in between the suction holes.

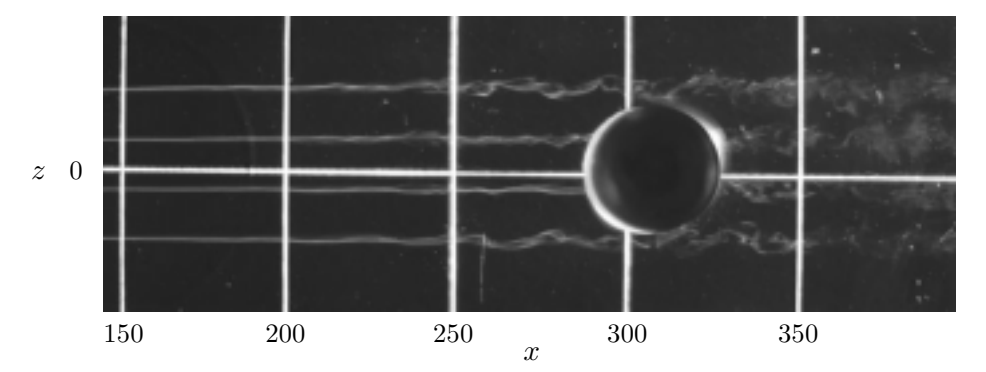


FIGURE 8. Smoke visualization of the flow near the upper wall. Smoke is accumulated in the low velocity regions. All positions are expressed in mm.

Initially the streaks are fairly stable and show no distortion up to $x \approx 200$ mm. Around x = 220 mm the streaks start to oscillate in the spanwise direction and breakdown sets in near x = 320 mm. It is clearly seen from the photograph that the sinuous mode is the dominating one. An estimated streamwise wave length (λ_x) for the streak oscillations is approximately 20 mm, which corresponds to a streamwise wavenumber $\alpha = 2\pi h/\lambda_x \approx 1.3$. However, for the hot-wire measurements streak breakdown is observed to take place further downstream. One explanation for this might be that the small momentum inflow associated with the smoke introduction make the transition to turbulence more rapid.

As discussed in the introduction, there are mainly two different secondary instability modes: the anti-symmetric (or sinuous) and the symmetric (or varicose). The flow visualization indicates the dominance of the sinuous mode, and in order to further investigate which of the modes that will occur at unforced conditions simultaneous measurements using two hot-wire probes were made. The left part of Figure 9(a) shows time signals obtained simultaneously from two hot-wire probes, which were positioned at two neighbouring peaks in u_{rms} (i. e. peaks on each side of a low velocity region) as illustrated on the right hand side of the figure. As can be seen the two signals are distinctly out of phase, indicating the dominance of the anti-symmetric mode.

Figure 9(b) shows correlation coefficients obtained from measurements where one of the hot-wire probes (positioned at y=0.23 and z=-1.3) was traversed in the streamwise direction while the other was fixed at x=95 and z=-2.3. From the calculated correlation coefficients it is found that the wave disturbance is travelling with a phase velocity of approximately 67% of the laminar centreline velocity.

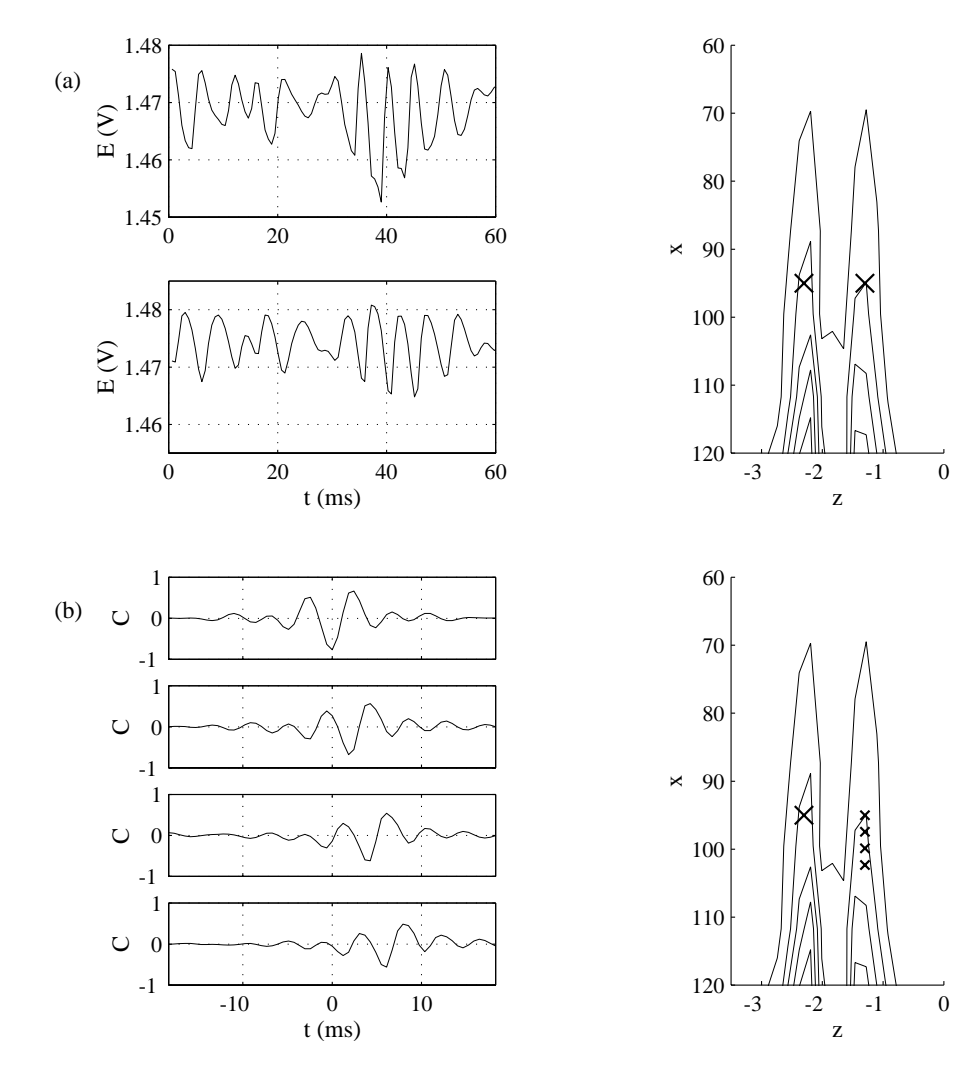


FIGURE 9. (a) Time-traces of simultaneous velocity fluctuations at $x=95,\ y=0.23$ and: $z{=}-2.3$ (top), $z{=}-1.3$ (bottom). (b) Correlation coefficient C between z=-2.3 (x=95) and z=-1.3 (from top to bottom, x=95,97.5,100,102.5). Probe positions are indicated in the contourplots of u_{rms} .

In Figure 10 the results from FFT analysis are shown for two different streak amplitudes. For each streak amplitude two power spectra are shown, one spectrum obtained from measurements at the centre of a low velocity region and one from a region with a large spanwise gradient. For the low streak amplitude [Figure 10(a)]

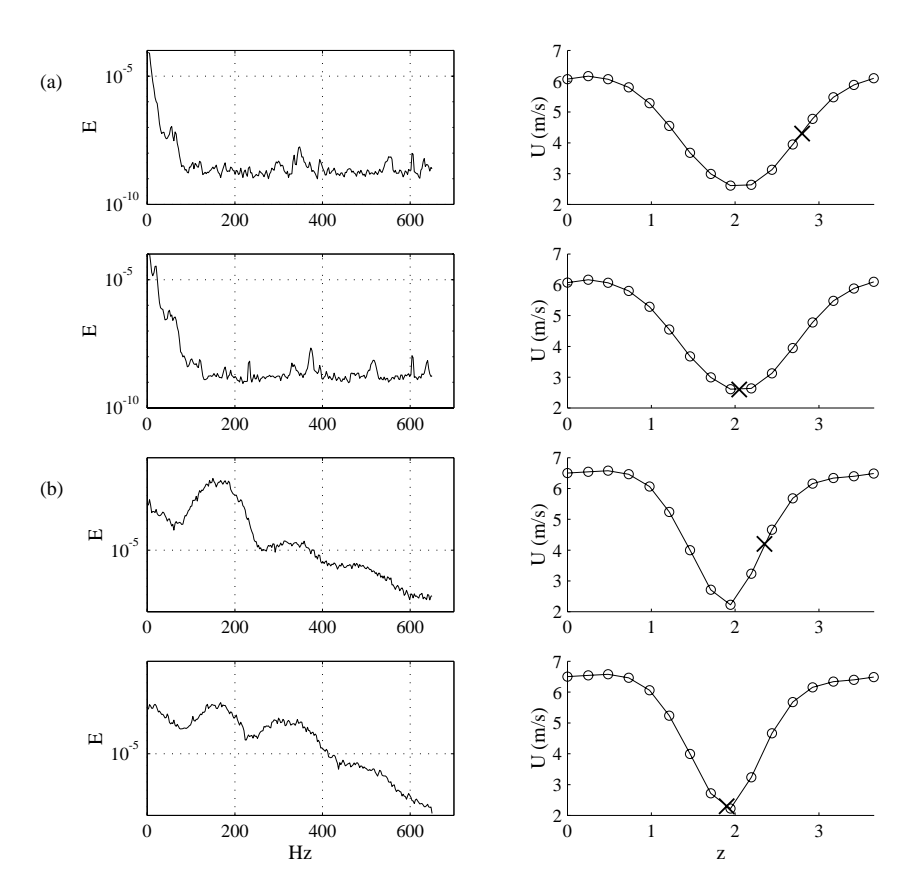


FIGURE 10. Power spectra at streak-amplitudes ΔU_{max} of (a) 59% and (b) 78% of U_{CL} taken at two z-positions corresponding to spanwise high shear (top) and centre of low velocity region (bottom) for natural case, x=95, y=0.2. (The figures to the right show spanwise profiles of \overline{U} in which the measurement positions are indicated.)

the spectra look similar to each other with most of the energy in low frequencies. Figure 10(b) displays results for the case with a higher streak amplitude. A power spectrum obtained in the region of high gradient (top) indicates a broad band

peak centred at approximately 180 Hz and for the corresponding spectrum in the low velocity region a second broad band peak is also observed around f=360 Hz. The appearance of the second harmonic in the region with negative U_d further indicates that the anti-symmetric mode is the preferred one.

It should be noted that the peak frequency depends not only on the streak spacing but also on the streamwise position. An increase in x or a decrease in the streak spacing results in a higher peak frequency. Since the spanwise velocity profile shows a more narrow low velocity region downstream, the increasing frequency in the two cases can probably be explained by an increase in $|\partial \overline{U}/\partial z|$.

3.3 Secondary instability at forced conditions. In this section the secondary instability operating on the streaks is triggered by phase-controlled periodic disturbances, which were introduced through orifices downstream the slits producing the streaky structures. The forcing station x=27 is close to the streamwise position where the streak amplitude reaches its maximum. Two different configurations were used, one which utilizes a single earphone and another configuration in which the use of two earphones allowed the direct forcing of both symmetric and anti-symmetric modes.

3.3.1 Forcing conditions

At unforced conditions the maximum u_{rms} is known to appear in regions with large spanwise gradients (section 3.2). In the case where the secondary instability is directly triggered by the disturbance source in the downstream plug we investigated at which spanwise position it was most efficient to apply the forcing. This was done by rotating the two plugs to move one of the earphones over one spanwise wavelength of \overline{U} (from z=0 to 3.6) while the response was measured with the hot-wire probe at x=100. The results are displayed in Figure 11(a) which shows u_{rms} obtained at two spanwise positions, one corresponding to a position close to the position of strongest spanwise gradient and one the centre of a low velocity region. The maximum u_{rms} occurs when the earphone is positioned at z=1 or z=2.4. When relating these z-positions to the spanwise \overline{U} -profile shown in Figure 11(b) it is clear that the optimum forcing position is where the spanwise gradient is large. All results in the following with this streak spacing were obtained with the earphones positioned at z=1 and 2.4, and for the case when forcing with a single earphone the one centred at z=1 was used.

The dependence on the initial amplitude of the secondary disturbance is shown in Figure 12(a), where the N-factor $(\ln(u/u_0))$ is plotted against the streamwise coordinate for initial amplitudes ranging from u_{rms} =0.12% to 0.6%. It can be observed that the growth rate is independent of the forcing for amplitudes displaying exponential growth.

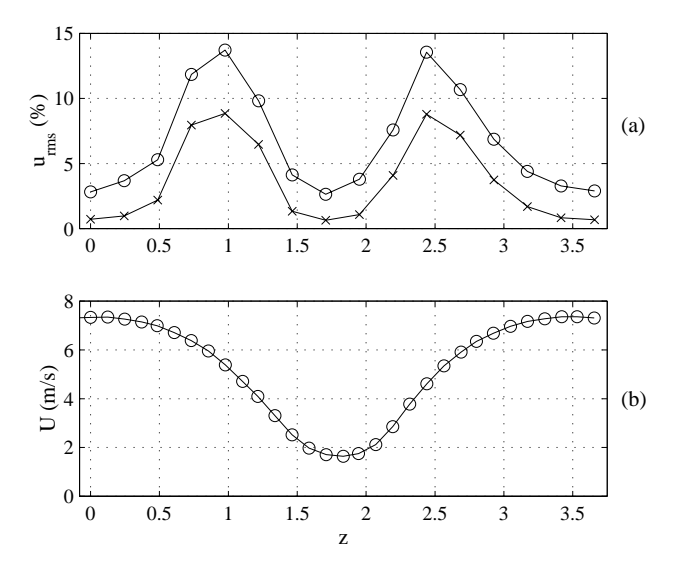


FIGURE 11. (a) The dependence of u_{rms} on forcing positions in the spanwise direction. The values of u_{rms} were measured at x=100,y=0.27 and at fixed z-positions: \circ , spanwise high shear; \times , low velocity region. (b) Spanwise profile of \overline{U} at x=26, y=0.63 (the x-position where the forcing is applied) is shown for reference.

Figure 12(b) shows the dependence of the growth-rate, $\gamma = N/(x_1-x_0)$, on the streak amplitude for three different Reynolds numbers. The measurements were all made using $f{=}250$ Hz and the growth rates were found from graphs similar to Figure 12(a) where a line was fitted to the straight part in the region of exponential growth between $x_0 = 36$ and $x_1 = 69$. The figure shows several interesting features. First there exists a threshold in the streak amplitude of approximately 0.7 below which all time periodic disturbances decay. Secondly it seems to exist a linear relation between the streak amplitude and growth rate. Thirdly it is found that the growth rate is independent of the Reynolds number. The implication of the latter two features is clearly that the instability is of an inviscid, inflectional type.

The growth rate at different angular frequencies ω (=2 $\pi fh/U_{CL}$) is shown in Figure 12(c). Also here the growth rate is obtained from measurements of the amplitude between x=36 and 69, except for ω which showed negative growth where the straight part was shorter. As can be seen a fairly wide range of frequencies gives rise to a positive growth, however the most amplified frequency differs from the frequency found to contain most energy in the unforced case (see §3.2). In

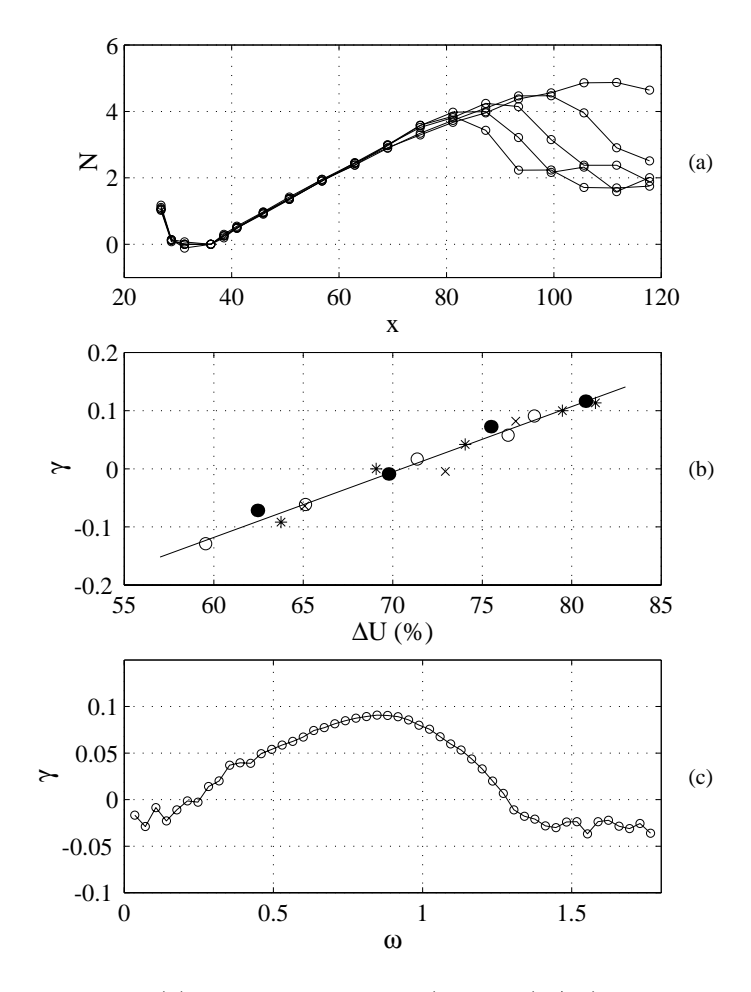


FIGURE 12. (a) Amplitude growth $(N = \ln(u/u_0))$, where u_0 is measured at x=36) for different forcing amplitudes. (b) The dependence of γ on ΔU_{max} for three different $Re: 0, 2000; \bullet, 2500; \star, 2900.$ (c) The dependence of γ on forcing frequency ω . Growth rates were determined between x=36 and x=69.

that case the frequency containing the most energy is a result from the combined effect of the background spectrum and the streamwise variation of the growth rate for the individual frequencies.

In the following a forcing amplitude of u_{rms} =0.24% was chosen which eventually resulted in turbulent transition inside the channel for a forcing frequency of 250 Hz and a streak amplitude $\Delta U = 78\%$.

3.3.2 Mode

The energy growth in the forcing frequency and its first harmonics is shown in Figure 13(a-c) for the three types of forcing, i. e. one-earphone forcing and forcing of the symmetric and the anti-symmetric modes with the use of two earphones. In the figure, energy in a frequency component is defined as the square of the normalized Fourier coefficient corresponding to that frequency, i. e. $E = |\hat{u}_f|^2$.

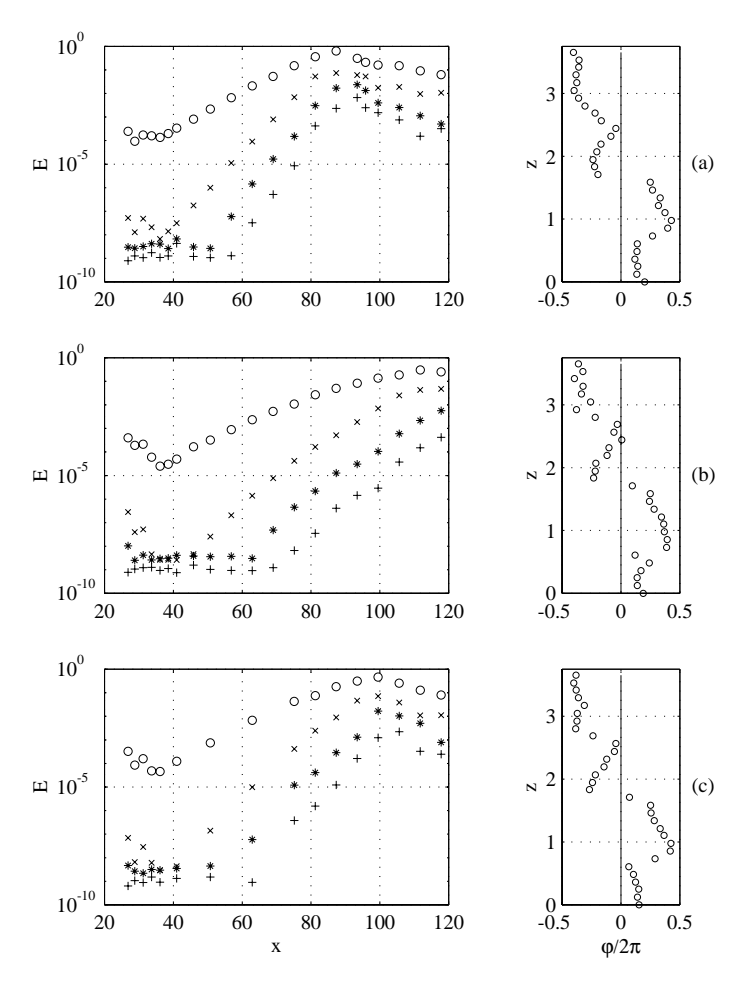


FIGURE 13. Amplitude growth for different forcing modes, (a) anti-symmetric, (b) symmetric, (c) one-earphone forcing : \circ , f_1 ; \times , $2f_1$; *, $3f_1$; +, $4f_1$. Right figures show spanwise phase profiles.

Measurements were made at the spanwise position where each frequency component had its maximum value. The streak amplitude was the same for all cases. However, one should note that the initial disturbance energy is not the same for the one earphone forcing as for the forcing with two, since in both cases the earphones were operated with the same voltage. Although the growth rates of higher harmonics are relatively larger than that of the fundamental frequency, the amplitude of the harmonics never exceed the fundamental one in the whole region.

For all three modes of forcing it is found that the anti-symmetric mode will be detected further downstream and dominate up to the point of transition. This is seen in the right part of Figure 13, where spanwise profiles of the phase for the fundamental frequency are shown. The profiles have been measured at streamwise positions just upstream of the position with the largest energy, and a phase shift of 180° across the low velocity region is observed for all forcing cases.

One should emphasize that even in the case of a symmetric mode forcing the energy growth is due to the evolution of the anti-symmetric mode. Even though the total energy of the secondary disturbance is lower in the one earphone case [Figure 13(c)] than for the symmetric forcing [Figure 13(b)] the forcing with one earphone will result in earlier transition. This is probably due to an initial suppression of the growth of the anti-symmetric mode by the symmetric forcing.

In the following only results from the use of a two earphone anti-symmetric forcing will be described.

3.3.3 Higher harmonics

Contours of U_d and u_{rms} in cross-stream planes are plotted in Figure 14(a) and (b), respectively. The figures show two low velocity streaks of the primary disturbance. Forcing of the secondary instability is only applied to the streak centred at z=1.7 whereas no direct forcing is applied to the streak centred at z=-1.9. When comparing with the natural case as well as the unforced side in the present figures it can be concluded that although the forcing enhances the growth of the instability the basic structure has not been changed.

The maximum value of U_d decays slowly downstream while the maxima in u_{rms} grow and appear at positions where $|\partial \overline{U}/\partial z|$ is large. The u_{rms} distribution at x=87 is characterized by a widened spacing at the centre of the channel and a narrowed one near the upper channel wall, which seems to follow a similar development of the unforced flow field.

At x = 106 the low velocity region on the upper side become unstable and breaks down and it seems that new low velocity regions with corresponding high values of u_{rms} appear near the upper channel wall between the original ones.

To further illustrate the variation in frequency content with the spanwise position, Figure 15 shows time traces and spectra both from strong shear and low velocity regions from measurements at two x-positions. Figures (a,c) show data from a position with large gradients in the spanwise direction, whereas data in (b,d) was obtained at the centre of regions with negative U_d . From the figures the fundamental frequency (f_1) is seen to dominate at the spanwise inflectional point, and in the low velocity region the frequency band around the second harmonic $(2f_1)$ has the largest amplitude. Also, the third harmonic $(3f_1)$ reach high amplitude at the same positions as the fundamental and in the same way, the distribution of the fourth harmonic is similar to the second harmonic.

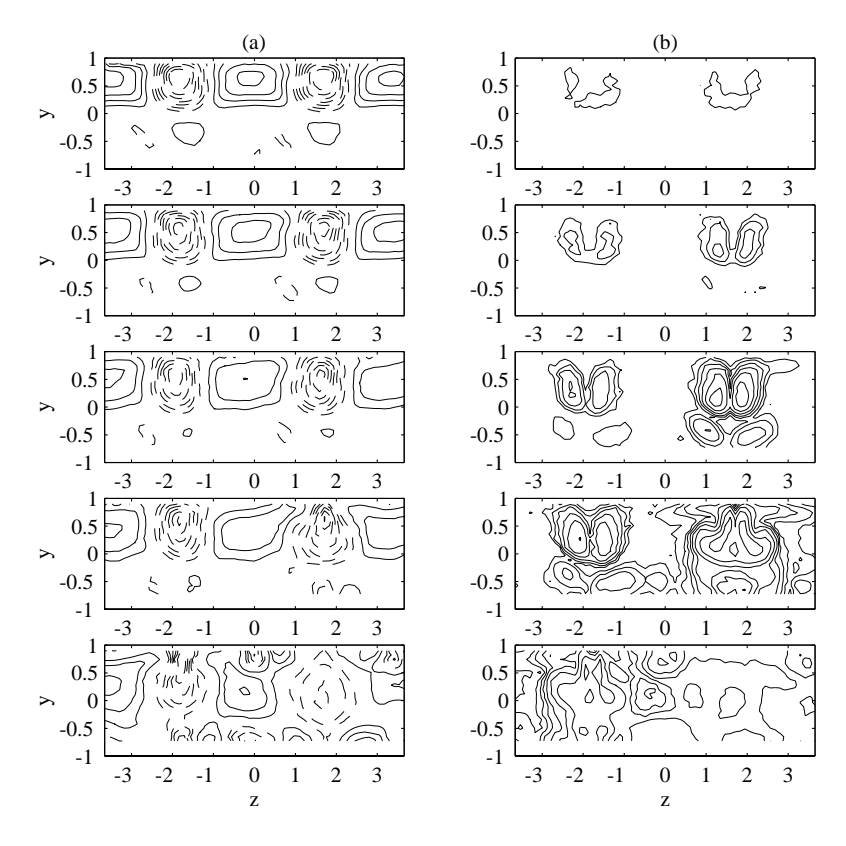


FIGURE 14. Contours of (a) U_d and (b) u_{rms} in yz-planes at x=36,58,75,87&106 (from top to bottom). Forcing with $f_1=250~{\rm Hz}$ at z=1 and z=2.4. Each figure is based on measurements in a plane spanned by 22 y- and 61 z-positions. Contours are $\pm 6\%, \pm 12\%, \ldots$ for U_d , logarithmic 0.67%, 1%, 1.5%, 2.2%, ... for u_{rms} . Negative contours are dashed.

Further evidence for the relation between the frequency components is presented in Figure 16, which in addition to contours of U_d and u_{rms} shows u_{rms} filtered around the forcing frequency and its higher harmonics. One can clearly observe that the maxima corresponding to the odd modes $(f_1 \text{ and } f_3 = 3f_1)$ occur where the spanwise gradient of the mean velocity is large (g), whereas the maxima of the even modes $(f_2 \text{ and } f_4)$ are connected to the centre of the low velocity region (h).

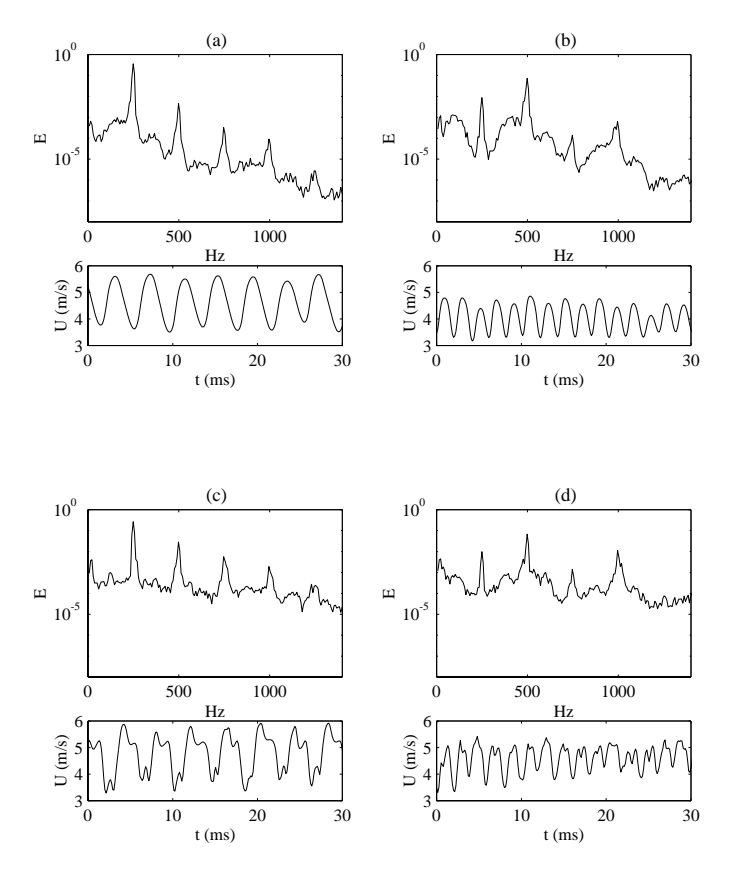


FIGURE 15. Time-traces and spectra at (a,b) x=81 and (c,d) x=93. Spanwise positions correspond to (a,c) strong spanwise shear and (b,d) the centre of the low velocity region at y=0.2.

Figure 17 shows the same frequency decomposition as in the previous figure but now in a streamwise-spanwise plane at y = 0.2. As in Figure 16 it is seen that all maxima of the respective modes appear in the same regions (i. e. odd modes

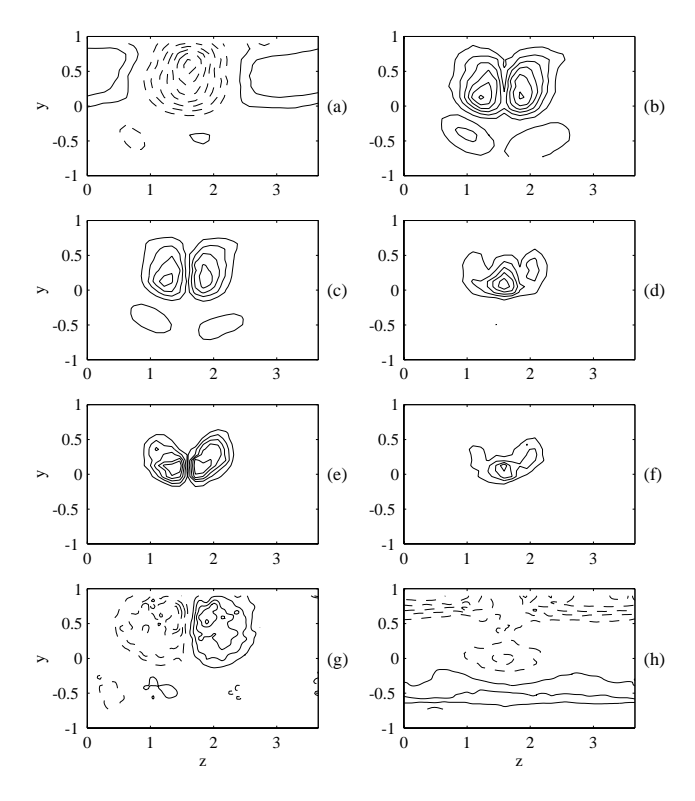


FIGURE 16. Contour plots in a yz-plane at x=75 of: (a) U_d , levels are $\pm 6\%, \pm 12\%, \ldots$; (b,c) u_{rms} and u_{rms,f_1} , spacing is 1%; (d) $u_{rms,2f_1}$, spacing is 0.2%; (e) $u_{rms,3f_1}$, spacing is 0.02%; (f) $u_{rms,4f_1}$, spacing is 0.01%; (g,h) $\partial \overline{U}/\partial z$ and $\partial \overline{U}/\partial y$, levels are $\pm 0.3, \pm 0.6, \ldots$ The figures are based on measurements in a plane spanned by 22 y- and 31 z-positions for a forcing with $f_1=250~{\rm Hz}$ at $z=1~{\rm and}~z=2.4$.

are related to the spanwise gradient and even modes are connected with the low velocity regions).

Wall-normal profiles of u_{rms} at the fundamental frequency (u_{rms,f_1}) and the second harmonic $(u_{rms,2f_1})$ are shown in Figure 18. These profiles were measured at spanwise positions corresponding to a region of strong spanwise gradient (fundamental) and the centre of a low velocity region (second harmonic).

Initially the peak in u_{rms,f_1} is located around the position where $|\partial \overline{U}/\partial z|$ is maximum $(y \approx 0.6)$. However, its amplitude decays downstream [as can also be seen in Figure 13(c)], while the second maxima at the position close to the

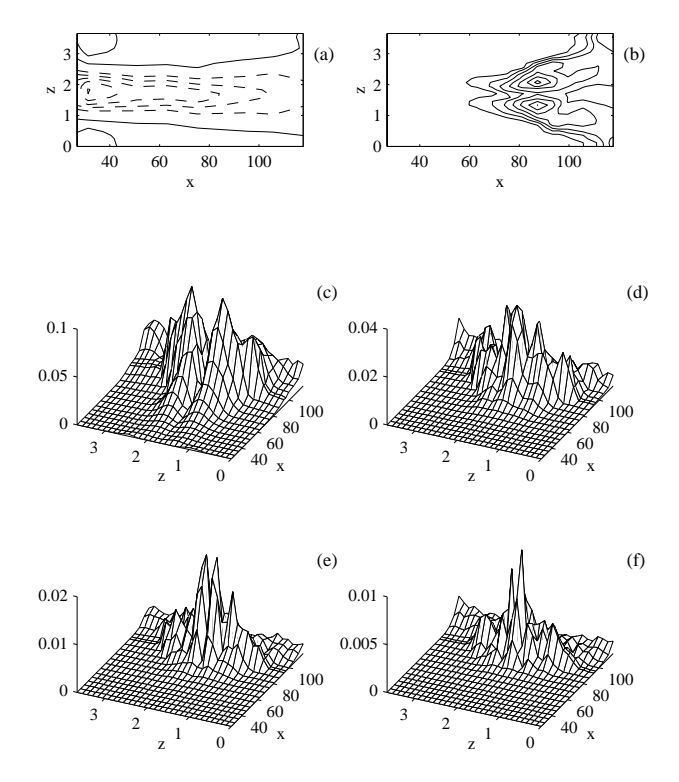


FIGURE 17. Contours of (a) U_d and (b) u_{rms} in an xz-plane at y=0.2, obtained for a forcing with $f_1=250$ Hz at z=1 and z=2.4. Contours are $\pm 10\%, \pm 20\%, ...$ for U_d and 2%, 4%, ... for u_{rms} . Three-dimensional plots of u_{rms} for the harmonic components: (c), f_1 ; (d), $2f_1$; (e), $3f_1$ and (f), $4f_1$. Each figure is based on measurements in a plane spanned by 21 x- and 31 z-positions.

centreline ($y \approx 0.25$) grows continuously. This maximum takes the place of the largest one between the measuring stations at x=34 and x=41, and its y-position moves closer to the centreline in the downstream direction. There is also another peak which evolves in the lower channel half and at x=93, in spite of a much lower streak amplitude (less than 10%), this peak has reached almost the same amplitude as the upper maximum.

For $u_{rms,2f_1}$ the wall-normal distribution is initially uniform and a peak, located near y=0.1, appears first at x=51. As for u_{rms,f_1} the peak position moves closer to the centreline with increasing x. However, at x=93 the largest peak is observed closer to the channel wall (near y=0.5, note that the scale is

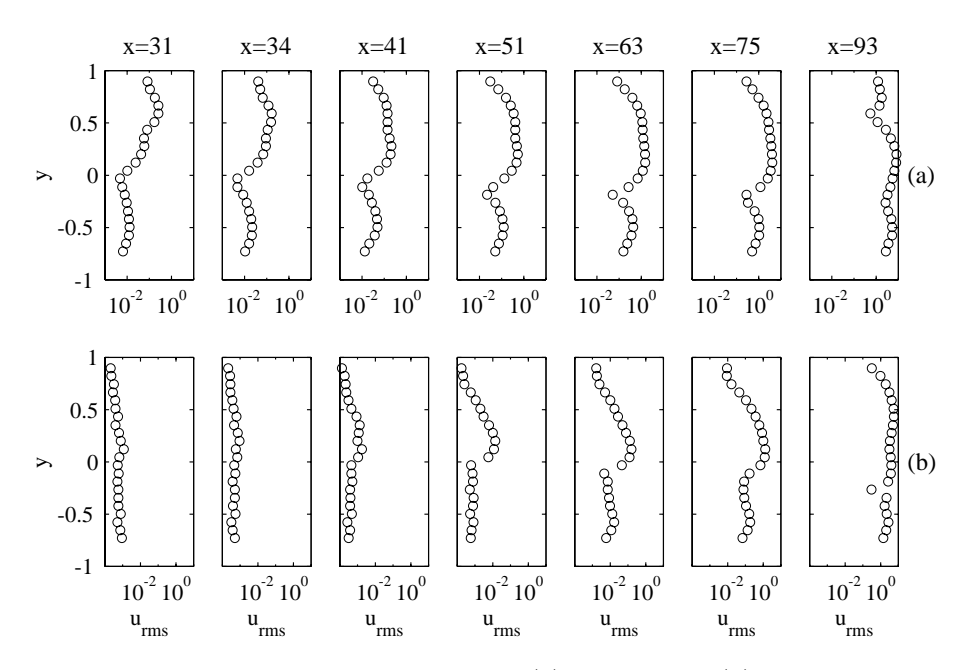


FIGURE 18. Wall-normal profiles of (a), u_{rms,f_1} and (b), $u_{rms,2f_1}$ measured at z-positions corresponding to strong spanwise shear and a low velocity region, respectively.

logarithmic). This can be explained with the distortion of the streaky structure seen at x = 87 in Figure 14(b).

3.3.4 Instantaneous structure

Since controlled secondary disturbances were used, phase-averaged information was easily obtained with the use of the reference signal from the function generator, which makes it possible to describe the instantaneous structure.

Figure 19 shows contours of the phase-averaged disturbance velocity in zt-planes obtained at four different streamwise positions. In the figure the time axes are reversed so the flow is from left to right. The time-resolved data verifies the existence of the wavy type instability (anti-symmetric mode). It is noteworthy that there is a phase discrepancy between the centre and the side of the low velocity region [seen in Figure 19(b)], which cause a subsequent deformation of the low speed streak (x=93) followed by breakdown (x=112).

Figure 20 displays a time sequence of the total velocity in a yz-plane where one period of the oscillation is shown at x=87, which is a streamwise position just upstream of the streak breakdown. As can be seen the area with low velocity is

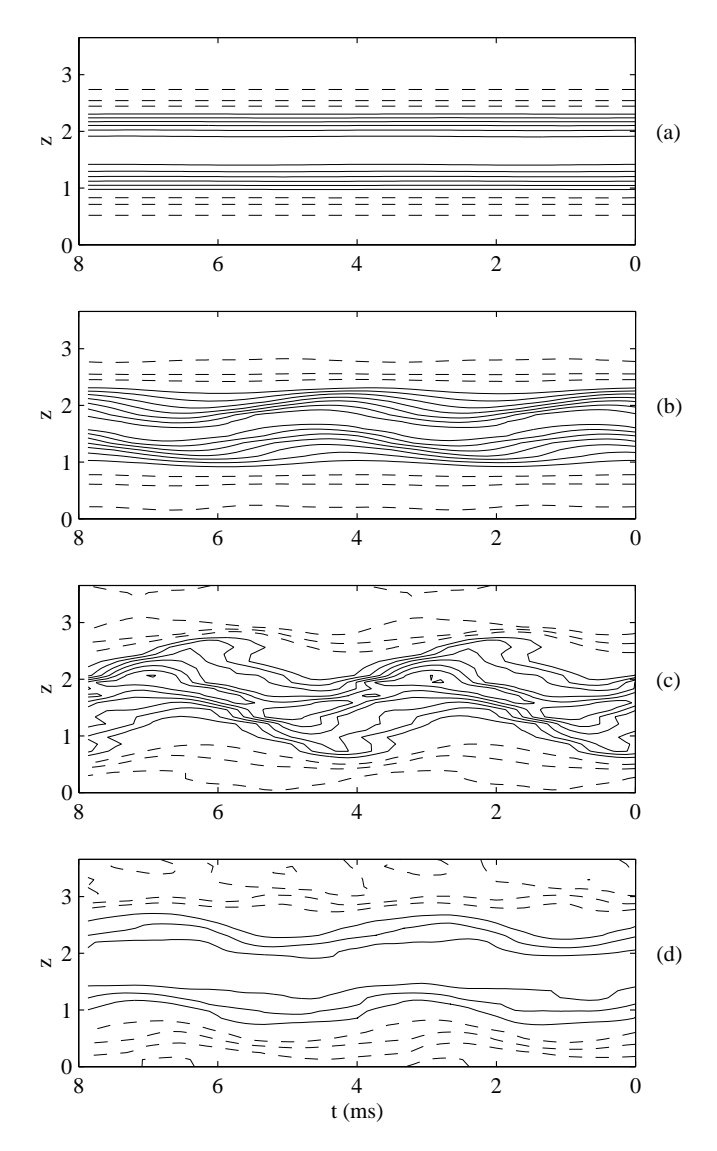


FIGURE 19. Contours of the phase averaged velocity field with the spanwise average subtracted. The zt-planes are measured at y=0.2 and: (a), x=36; (b), x=75; (c), x=93; (d), x=112 at 31 spanwise positions. The contour levels are \pm 5%, \pm 10%,... with positive contours shown as dashed lines.

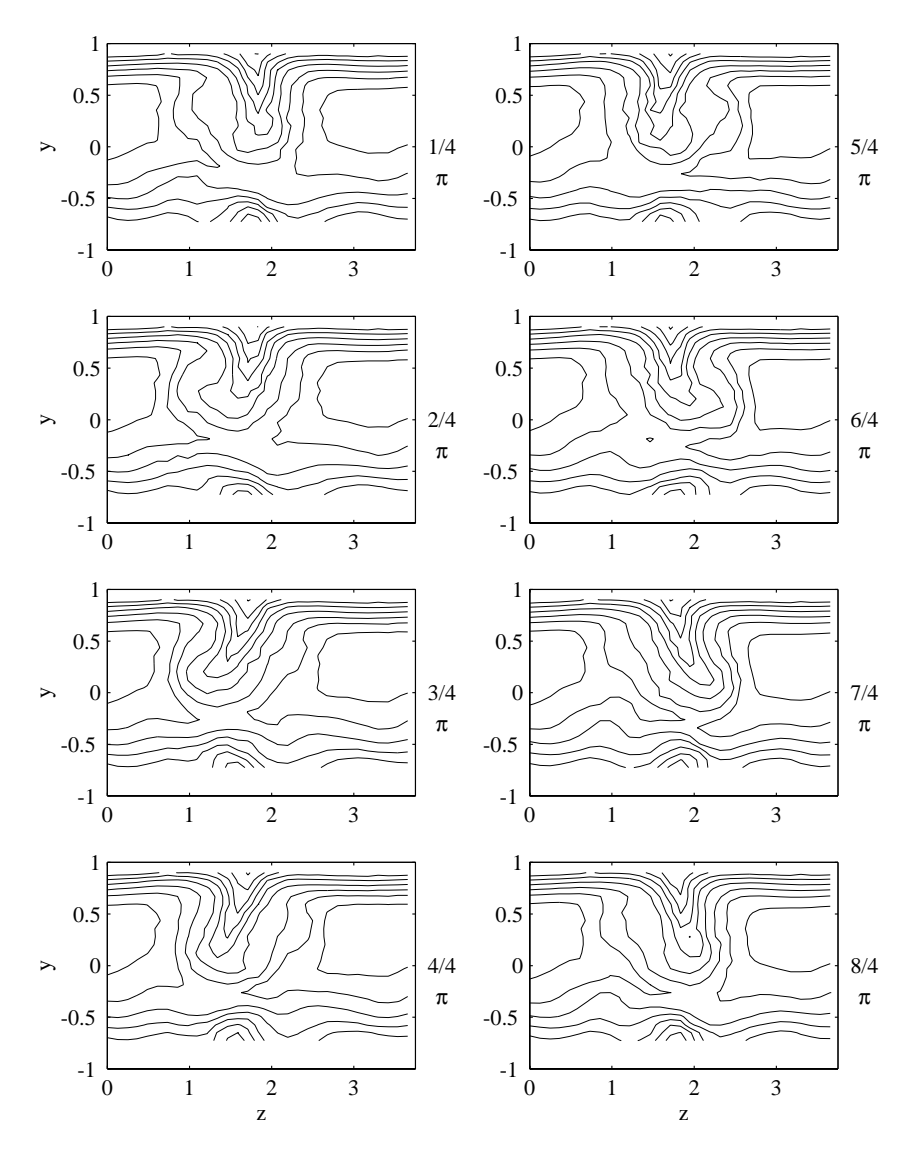


FIGURE 20. Time sequence of the phase averaged velocity (U) in a yz-plane at x=87. The phase increases from top to bottom and left to right by $\frac{1}{4}\pi$. Each figure is based on measurements in a plane spanned by 22 y- and 31 z-positions. The contour spacing is 10%.

confined to a narrow region and its top part oscillates with a larger amplitude than the bottom part. Also, the oscillation of the top part precedes that of the bottom part by less than $\pi/2$.

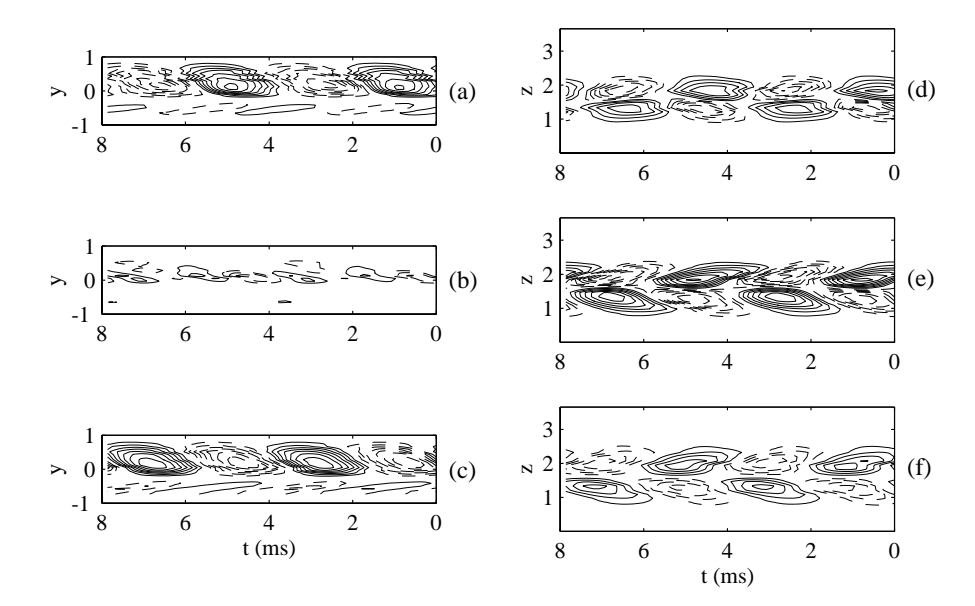


FIGURE 21. Contours of the phase averaged velocity with \overline{U} subtracted. Measurements at x=75 and: (a), z=1.35; (b), z=1.6; (c), z=1.85; (d), y=0.03; (e), y=0.28; (f), y=0.59. The contour levels are \pm 1%, \pm 2%,... with negative contours shown as dashed lines.

Figure 21 shows yt and zt-planes measured at x=75. In these figures the time averaged velocity have been subtracted, so that the phase relation can be easily observed. The yt-planes are measured at three spanwise positions, where (a) and (c) show positions with strong spanwise gradients on each side of the centre of a low velocity region (b). When comparing the yt-planes from regions of strong gradients the anti-symmetric mode is clearly recognized. Evidence for this is also given in (b) where the second harmonic is found to dominate near y=0. The inclination of the instantaneous structure in Figure 21(a,c) is due to the phase delay between the top and the bottom of the streak as discussed above. Figure 21(d-f) show zt-planes from three y-positions in the upper half of the channel. The phase difference between the centre and the side of the low velocity region, that was earlier observed in Figure 19(b), is here seen in the form of oblique regions in (e,f).

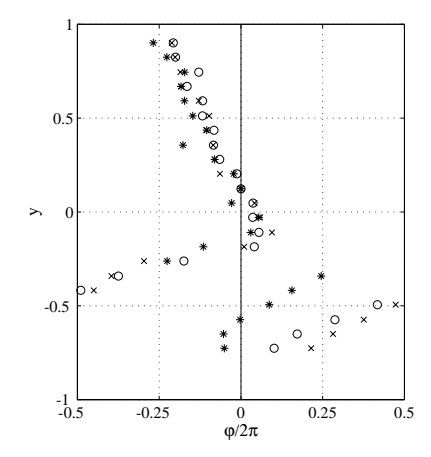


FIGURE 22. Variation of the wall-normal phase distribution with the x-position. φ is the change in phase relative to that observed at y=0.12 for: \times , x=58; \circ , x=75; *, x=87. The measurements were made at z=1.83.

3.3.5 Phase velocity and wavenumber

Figure 22 shows that although there exists a phase difference between the top of a streak and its bottom, that difference will neither increase nor decrease in the x-direction, which means that the phase velocity is constant in the y-direction. To determine the phase speed it is therefore sufficient to study the phase evolution at a constant height. Figure 23(a) displays the results from measurements of the phase evolution at y=0.26 for different forcing frequencies, f, in the range from 150Hz to 350Hz. The phase velocity at a given frequency can then be determined from the slope of the line with the streamwise evolution of the phase as,

$$c = 2\pi f \frac{\Delta x}{\Delta \varphi}. (4)$$

Figure 23(b) shows that the phase velocity has an almost constant value of 0.69 U_{CL} which is near the values obtained at unforced conditions. As a reference, the local velocities at peak u_{rms} positions are also plotted and they are found to be in close correspondence with the phase velocity.

In Figure 24 the streamwise wavenumber α of the secondary instability is plotted against the spanwise wavenumber β based on the streak wave length λ_z . The streamwise wavenumber was calculated as

$$\alpha = \frac{2\pi fh}{c}. (5)$$

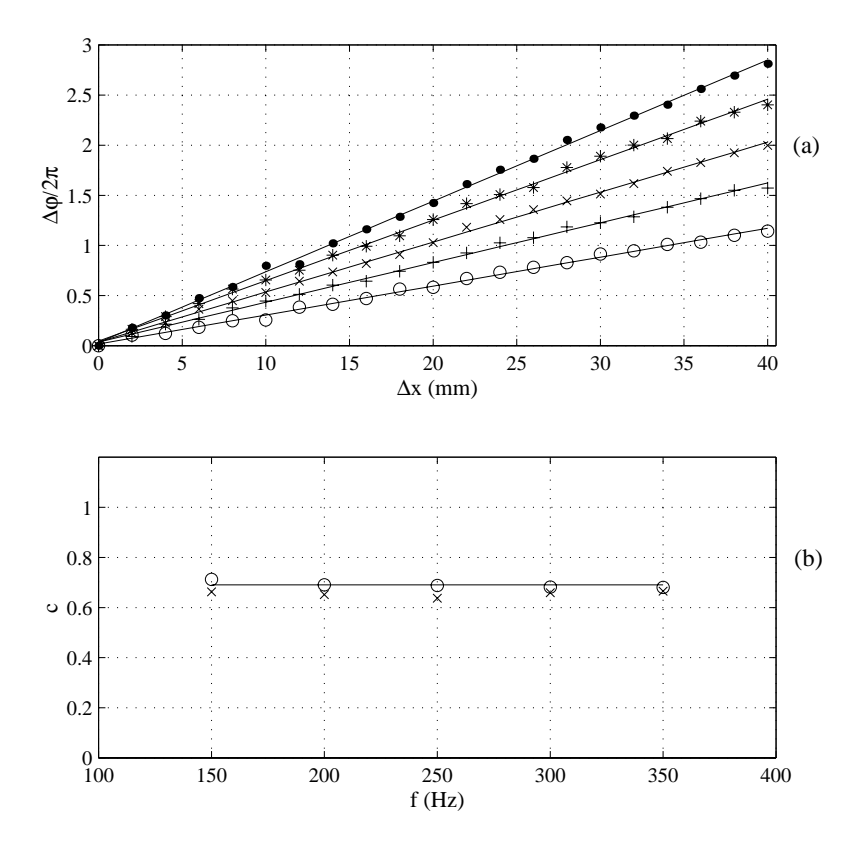


FIGURE 23. (a) Phase evolution for various forcing frequencies: \circ , 150 Hz; +, 200 Hz; ×, 250 Hz; *, 300 Hz; •, 350 Hz. (b) Comparison between (\circ) the phase velocity obtained from the measurements of the phase evolution and (\times) the local velocity at positions corresponding to the peaks in the u_{rms} distribution. The line represents c=0.69.

Here, f is the frequency which yields the maximum growth rate for each λ_z and it generally increases with a smaller λ_z , whereas the phase velocity c is constant. Different spanwise wavenumbers are obtained by rotating the first plug at the same time as the individual inserts are rotated to align the suction slits with the x-axis. As can be seen an increase of β results in larger α , which is interpreted as narrowing the streak spacing gives rise to a secondary instability of a shorter wave length.

4 Summary and discussion

Growth of streaky structures, i.e. regions of low and high velocity, appear under many circumstances in wall bounded shear flows, such as flows over concave surfaces, flows disturbed by localized roughness elements or free stream turbulence of moderate amplitude etc. (see e.g. Alfredsson & Matsubara 1996). All these flows may undergo a secondary instability in the form of travelling waves which develop on top of the streaky stucture. These could be either varicose or sinuous depending on the flow parameters. In the present study we have experimentally investigated the secondary instability operating on streaks in plane Poiseuille flow at subcritical Reynolds numbers. The streaks are introduced by constant suction through narrow slits at one wall, making it possible to control both the initial streak amplitude and their spanwise spacing. The secondary instability is found to develop both under unforced and forced conditions and its characteristics have been determined. The use of controlled forcing made it possible to determine the instantaneous structure of the secondary instability as well as its growth rate and phase speed.

The primary disturbance was introduced through suction through slits at the wall and this gives rise to high velocity regions at the slits and low velocity regions in between. The streaks are confined to the same side of the channel as where the suction is applied. These regions were found to initially grow linearly in amplitude whereupon they saturate and decay slowly. This is what is to be expected from a transiently growing disturbance at subcritical Re which finally decays by the

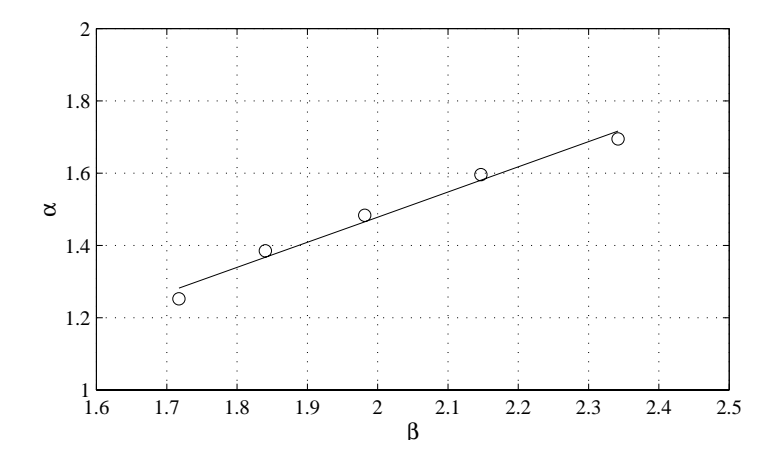


FIGURE 24. Relation between streamwise- and spanwise wavenumbers. The indicated line is $\alpha = 0.70\beta + 0.087$.

action of viscosity (see e.g. Gustavsson 1991). Although the spanwise distribution of the disturbance initially is close to sinuous, i.e. the low and high velocity regions are equally wide, the disturbance deforms as it grows and the low velocity region narrows. A similar narrowing was observed in curved channel flow by Matsson & Alfredsson 1992 for the low velocity regions between the counter-rotating vortices set up through a centrifugal instability.

In the present experiments a secondary instability was found to develop when the streaks reached a certain (high) threshold amplitude. In case of Re=2000, $\beta=1.75$ the threshold amplitude, measured as the velocity difference between the high and low velocity regions, is approximately 70% of U_{CL} . In the unforced case the instability was first observed in the regions of strong shear in between the low and high velocity streaks. The measurements also showed that the initial growth of the rms level increased exponentially. Two-probe spatial correlations also revealed that the instability was in the form of the wavy (anti-symmetric) mode.

From the experiments using controlled forcing of the secondary instability, it was clear that the sinuous mode was the dominating one. If the varicose mode was forced it was damped and the sinuous mode started to grow instead. It was also found that the growth rate of the sinuous mode initially is exponential and that above the threshold the growth rate increased linearly with the streak amplitude. The growth rate was also found to be independent of Reynolds number (within the range 2000-2900). These findings strongly indicate that the instability is of an inflectional nature.

Contour plots of u_{rms} as well as u_{rms,f_1} show a two peak structure and those shapes are quite similar to that of $|\partial \overline{U}/\partial z|$, implying the significance of the spanwise velocity distribution. The wall-normal position where the largest maximum of $|\partial \overline{U}/\partial z|$ appears is, however, much closer to the channel wall than that of u_{rms} . In addition the phase velocity of the secondary instability (69% of U_{CL}) does not agree with the local velocity at the position of the maximum $|\partial \overline{U}/\partial z|$ (41% of U_{CL}), which indicates that the secondary instability is not directly driven by the $|\partial \overline{U}/\partial z|$ -maxima. However to expect a direct correspondence between $|\partial \overline{U}/\partial z|$ and the distribution of u_{rms} would be an oversimplification, since the basic flow is strongly three-dimensional. It was also pointed out by Reddy et al. 1998 that a normal shear in addition to the spanwise shear reduces the growth of this type of instability. Since the normal shear is strongest close to the wall this may explain why the disturbance distribution is located further from the wall.

The streak threshold amplitude for growth of secondary instability is around 70% of U_{CL} . Similar amplitudes are found for streaks initiated by a centrifugal instability in curved channel flow (see e.g. Matsson & Alfredsson 1992) or Coriolis induced instabilities in rotating channel flow (Matsubara & Alfredsson 1997). Also

the numerical study by Reddy et al. 1998 gives similar amplitudes for secondary instability to occur.

A simple model of the instability may be obtained by assuming that the spanwise velocity profile has a one-dimensional form written as $\Delta U \cos \beta z$. From the stability analysis of this inviscid flow Waleffe 1995 gives the imaginary part of the phase speed (\sim growth rate) as¹

$$c_i = i \frac{|\alpha \Delta U|}{\sqrt{2}} \left(\frac{\beta^2 - \alpha^2}{\beta^2 + \alpha^2} \right)^{1/2} \tag{6}$$

A positive growth of the disturbance is, hence, obtained for $0 < \alpha < \beta$. In the experiments it was found that the most amplified α was around 70% of β . It was also found that for high enough frequency (i.e. α) the growth rate was negative. If this frequency is converted to a wave number using the phase speed it was just slightly larger than the spanwise wave number, thus supporting the analysis above. In the DNS and linear stability analysis by Reddy $et\ al.$ 1998 the maximum growth rate occur when α is close to β .

Another streak instability occurs during the so called oblique transition scenario (Schmid & Henningson 1992, Berlin, Lundbladh & Henningson 1994, Elofsson & Alfredsson 1995, 1998). During this scenario two oblique waves interact to form zero frequency streaky structures, which increase in amplitude through transient growth. Elofsson & Alfredsson 1998 showed that for high enough streak amplitudes ($\approx 40\%$) breakdown occurred. The lower threshold amplitude in that case may be due to a higher noise level. For the oblique transition case this noise comes in the form of the initial oblique waves ($\omega_0, \pm \beta_0$) and their harmonics. Another plausible explanation for the lower threshold might be the fact that in the oblique transition scenario the streaks are formed in both channel halves.

The numerical study of Berlin *et al.*1994 was made for a flat plate boundary layer. In that case the secondary instability occurred in the form of the varicose mode. If this was due to the spanwise wavelength of the primary disturbance or because of another type of flow field is still an open question.

Acknowledgements

This work was supported by the Swedish Research Council for Engineering Sciences (TFR). The stay of M. Kawakami at KTH was supported by the Axel och Margaret Ax:son Johnsons stiftelse. Masaharu Matsubara contributed with valuable advices concerning the experiments, which are gratefully acknowledged. Discussions with Dan Henningson, Satish Reddy and Peter Schmid are also acknowledged. We also like to thank Prof. Y. Kohama of the Institute of Fluid Sciences, Tohoku University, Sendai for taking the initiative to this co-operation.

¹This also indicates that the growth rate is linear with the streak amplitude.

References

- ALFREDSSON, P. H. & MATSUBARA, M. 1996 Streaky structures in transition. In Proc. Transitional Boundary Layers in Aeronautics, pp. 373–386, Royal Netherlands Academy of Arts and Sciences. Elsevier.
- Bakchinov, A. A., Grek, G. R., Klingmann, B. G. B. & Kozlov, V. V. 1995 Transition experiments in a boundary layer with embedded streamwise vortices. *Phys. Fluids* **7**, 820–832
- Berlin, S., Lundbladh, A. & Henningson, D. S. 1994 Spatial simulations of oblique transition in a boundary layer. *Phys. Fluids* 6, 1949–1951.
- Boberg, L. & Brosa, U. 1988 Onset of turbulence in a pipe. Z. Naturforsch. 43 a, 697–726.
- BOTTARO, A. & KLINGMANN, B. G. B. 1996 On the linear breakdown of Görtler vortices. Eur. J. Mech., B/Fluids 15, 301–330.
- Butler, K. M. & Farrell, B. F. 1992 Three-dimensional optimal perturbations in viscous shear flow. Phys. Fluids A 4, 1637–1650.
- Carlson, D. R., Widnall, S. E. & Peeters, M. F. 1982 A flow visualization study of transition in plane Poiseuille flow. *J. Fluid Mech.* 121, 487–505.
- CORKE, T. C. & MANGANO, R. A. 1989 Resonant growth of three-dimensional modes in transitional Blasius boundary layers. *J. Fluid Mech.* **209**, 93–150.
- Ellingsen, T. & Palm, E. 1975 Stability of linear flow. Phys. Fluids 18, 487-488.
- ELOFSSON, P. A. & ALFREDSSON, P. H. 1995 Experiments on nonlinear interaction between oblique Tollmien-Schlichting waves. In *Laminar-Turbulent Transition* (Kobayashi, R., editor), pp. 465–472, IUTAM Symposium, Sendai 1994, Springer.
- ELOFSSON, P. A. & ALFREDSSON, P. H. 1998 An experimental study of oblique transition in plane Poiseuille flow. J. Fluid Mech. 358, 177–202.
- FINLAY, W. H. 1990 Transition to oscillatory motion in rotating channel flow. *J. Fluid Mech.* **215**, 209–227.
- FINLAY, W. H., KELLER, J. B. & FERZIGER, J. H. 1988 Instabilities and transition in curved channel flow. *J. Fluid Mech.* **194**, 417–456.
- Gustavsson, L. H. 1991 Energy growth of three-dimensional disturbances in plane Poiseuille flow. J. Fluid Mech. 224, 241–260.
- HAMILTON, J. M., KIM, J. & WALEFFE, F. 1995 Regeneration mechanisms of near-wall turbulence structures. J. Fluid Mech. 287, 317–348.
- Henningson, D. S. 1995 Bypass transition and linear growth mechanisms. In $Advances\ in\ Turbulence\ V$ (Benzi, R., editor), pp. 190–204, Kluwer.
- Henningson, D. S., Lundbladh, A. & Johansson, A. V. 1993 A mechanism for bypass transition from localized disturbances in wall bounded shear flows. *J. Fluid Mech.* **250**, 169–207.

- Kachanov, Y. S., Kozlov, V. V. & Levchenko, V. Y. 1977 Nonlinear development of a wave in a boundary layer. *Izv. Akad. Nauk SSSR, Mekh. Zhid. Gaza.* **3**, 49–53. (in Russian, English transl. 1978 in *Fluid Dyn.* **12**, 383–390).
- Kachanov, Y. S. & Levchenko, V. Y. 1984 The resonant interaction of disturbances at laminar turbulent transition in a boundary layer. J. Fluid Mech. 138, 209–247.
- Klebanoff, P. S. & Tidstrom, K. D. 1959 Evolution of amplified waves leading to transition in a boundary layer with zero pressure gradient. NASA TN D-195.
- Klebanoff, P. S., Tidstrom, K. D. & Sargent, L. M. 1962 The three-dimensional nature of boundary layer instability. *J. Fluid Mech.* 12, 1–34.
- KLINGMANN, B. G. B. 1992 On transition due to three-dimensional disturbances in plane Poiseuille flow. J. Fluid Mech. 240, 167–195.
- LANDAHL, M. T. 1980 A note on an algebraic instability of inviscid parallel shear flows. J. Fluid Mech. 98, 243–251.
- Liu, W. & Domaradzki, J. A. 1993 Direct numerical simulation of transition to turbulence in Görtler flow. J. Fluid Mech. 246, 267–299.
- Luchini, P. 1996 Reynolds-number-independent instability of the boundary layer over a flat surface. J. Fluid Mech. 327, 101–115.
- MASUDA, S., HORI, D. & MATSUBARA, M. 1995 Secondary Instability Associated with Streamwise Vortices in a Rotating Boundary Layer. In *Laminar-Turbulent Transition* (KOBAYASHI, R., editor), pp. 69–76, IUTAM Symposium, Sendai 1994, Springer.
- MATSSON, O. J. E. & ALFREDSSON, P. H. 1992 Experiments on instabilities in curved channel flow. *Phys. Fluids A* **4**, 1666–1676.
- MATSSON, O. J. E. & ALFREDSSON, P. H. 1994 The effect of spanwise system rotation on Dean vortices. J. Fluid Mech. 274, 243–265.
- MATSUBARA, M. & ALFREDSSON, P. H. 1998 Secondary instability in rotating channel flow. *J. Fluid Mech.* (in press).
- MAYER, E. W. & RESHOTKO, E. 1997 Evidence for transient disturbance growth in a 1961 pipe-flow experiment. *Phys. Fluids* **9**, 242–244.
- Nishioka, M., Iida, S. & Ichikawa, Y. 1975 An experimental investigation of the stability of plane Poiseuille flow. J. Fluid Mech. 72, 731–751.
- REDDY, S. C., SCHMID, P. J., BAGGETT, J. S. & HENNINGSON, D. S. 1998 On stability of streamwise streaks and transition thresholds in plane channel flows. *J. Fluid Mech.* (in press).
- SARIC, W. S. 1994 Görtler vortices. Ann. Rev. Fluid Mech. 26, 379-409.
- Saric, W. S. & Thomas, A. S. W. 1984 Experiments on the subharmonic route to turbulence in boundary layers. In *Turbulence and chaotic phenomena in fluids* (Tatsumi, T., editor), pp. 117–122, North-Holland.
- SCHMID, P. J. & HENNINGSON, D. S. 1992 A new mechanism for rapid transition involving a pair of oblique waves. Phys. Fluids A 4, 1986–1989.
- Schubauer, G. B. & Skramstad, H. K. 1947 Laminar boundary layer oscillations and the stability of laminar flow. *J. Aero. Sci.* 14, 69–78.
- SWEARINGEN, J. D. & BLACKWELDER, R. F. 1987 The growth and breakdown of streamwise vortices in the presence of a wall. *J. Fluid Mech.* **182**, 255–290.
- Trefethen, L. N., Trefethen, A. E., Reddy, S. C. & Driscoll, T. A. 1993 Hydrodynamic stability without eigenvalues. *Science* **261**, 578–584.
- Waleffe, F. 1995 Hydrodynamic stability and turbulence: Beyond transients to a self-sustaining process. Stud. Appl. Math. 95, 319–343.
- Yu, X. & Liu, J. T. C. 1991 The secondary instability in Görtler flow. Phys. Fluids A 3, 1845–1847.